BOLU ABANT İZZET BAYSAL UNIVERSITY

INSTITUTE OF GRADUATE STUDIES
Department of Chemical Engineering

DETERMINATION OF AIR POLLUTANT SOURCES BY PHYSICAL AND CHEMICAL CHARACTERIZATION OF ATMOSPHERIC PARTICULATE MATTER: FIELD APPLICATION IN BOLU PROVINCE.

MASTER OF SCIENCE

ABILMANSUR YESHMURATOV

ACADEMIC SUPERVISOR
Prof.Dr. Turgay Pekdemir

BOLU, JULY - 2024

APPROVAL OF THE THESIS

DETERMINATION OF AIR POLLUTANT SOURCES BY PHYSICAL AND CHEMICAL CHARACTERIZATION OF ATMOSPHERIC PARTICULATE MATTER: FIELD APPLICATION IN BOLU PROVINCE submitted by **Abilmansur Yeshmuratov** and defended before the Examining Committe Members listed below in partial fulfillment of the requirements for the degree of **Master of Science** in **Department of Chemical Engineering Institute of Graduate Studies of Bolu Abant Izzet Baysal University in 29.07.2024** by

Examining Committee Members	**Signature**
Supervisor Prof.Dr. Turgay PEKDEMİR Bolu Abant Izzet Baysal University	.....
Member Prof.Dr. Fatma ÖZTÜRK Bolu Abant Izzet Baysal University	.....
Member Assistant Prof.Dr. Ebru KOÇAK Aksaray University	.....

Prof. Dr. İbrahim KÜRTÜL

Director of Instıtute of Graduate Studies

ETHICAL DECLARATION

In this thesis dissertation that was properly prepared according to the Thesis Writing Rules of Bolu Abant İzzet Baysal University of the Institute of Graduates Studies, I hereby declare that;

- All data, information, and documents presented in the thesis were obtained in accordance with the academic and ethical rules,
- All data, documents, assessments, and results were presented in accordance with the scientific ethical and moral rules,
- All works that were benefitted in the thesis were appropriately cited,
- No alteration was made in the data used,
- Study presented in this thesis is original,

  Otherwise, I declare that I accept the loss of all my rights in case any contradiction that may arise against me.

The similarity rate obtained by using the Turnitin program, a plagiarism detection software, is within the limits approved by the University Senate.

_____

Abilmansur YESHMURATOV

ABSTRACT

DETERMINATION OF AIR POLLUTANT SOURCES BY PHYSICAL AND CHEMICAL CHARACTERIZATION OF ATMOSPHERIC PARTICULATE MATTER: FIELD APPLICATION IN BOLU PROVINCE
MASTER OF SCIENCE
ABILMANSUR YESHMURATOV
BOLU ABANT IZZET BAYSAL UNIVERSITY
INSTITUTE OF GRADUATE STUDIES
DEPARTMENT OF CHEMICAL ENGINEERING
SUPERVISOR: PROF.DR. TURGAY PEKDEMİR

BOLU, JULY 2024
Number of pages xv + 117

Air pollution is responsible for several million deaths worldwide every year. Particulate matter (PM) is one of the air pollutants and its constituents such as organic carbon (OC), elemental carbon (EC), and mineral dust are known as short life climate forcers (SLCFs) due to their climate forcing effect. Nor only chemical composition but also size of PM in the air is important parameter for health concern. In order to take appropriate measures to keep the air clean to protect public health and to combat with climate change, it is important to know the sources of PM. This study examined the chemical composition and sources of size segregated particulate matter (PM) in Bolu City center (40.73° N–31.60° E and 741 m asl), Türkiye, to enhance regional air quality data and inform decision-making strategies. Size-segregated PM samples (>7.2, 3.0-7.0, 1.5-3.0, 0.95-1.5, 0.49-1.5, <0.49 μm) were collected using a High Volume Cascade Impactor (HVCI) with a 96-hour continues sampling period between February 2021 and March 2022 (about once in a week). The collected samples were analyzed in terms of OC and EC by using thermal-optical analyzer.

The research revealed high average OC/EC ratios (10.84 for $PM_{2.5}$ and 11.15 for $PM_{10)}$, while typical urban environment is around 6.6 on average. It surpasses those of many urban areas and indicating significant secondary organic aerosol (SOA) formation. Notably, secondary organic carbon (SOC) constituted up to 98% of OC in the $PM_{2.5}$ fraction in Winter, despite lower photochemical activity, due to high concentration of precursors from domestic heating activities. Meteorological factors, particularly atmospheric pressure and wind speed, showed significant correlations with SOC levels. These findings highlight Bolu City's unique air quality challenges, emphasizing the need for tailored management strategies addressing both primary emissions and SOC precursors.

Based on these results, the study recommends establishing a network of sampling sites across Bolu City, conducting more detailed source apportionment studies, and investigating specific mechanisms driving year-round SOA formation in the region. This research contributes valuable data to inform air quality planning and strategy development by local decision-makers and implementers, while also identifying critical areas for future investigation.

KEYWORDS: Particulate Matter, Elemental Carbon, Organic Carbon, Secondary Organic Carbon, OC/EC, Cascade Impactor

ÖZET

ATMOSFERİK PARTİKÜL MADDE FİZİKSEL VE KİMYASAL KAREKTERİZASYONU İLE HAVA KİRLETİCİ KAYNAKLARININ TESPİTİ: BOLU İLİ SAHA UYGULAMASI.
YÜKSEK LİSANS TEZİ
ABILMANSUR YESHMURATOV
BOLU ABANT İZZET BAYSAL ÜNİVERSİTESİ
LİSANSÜSTÜ EĞİTİM ENSTİTÜSÜ
KİMYA MÜHENDİSLİĞİ BÖLÜMÜ
TEZ DANIŞMANI: PROF.DR. TURGAY PEKDEMİR

BOLU, TEMMUZ - 2024
Sayfa sayısı xv + 117

Hava kirliliği dünya çapında her yıl milyonlarca ölüme neden olmaktadır. Partikül madde (PM), hava kirleticilerinden biridir ve organik karbon (OK), elemental karbon (EK) ve mineral toz gibi bileşenleri, iklim üzerindeki etkileri nedeniyle kısa ömürlü iklim etkileyicileri olarak bilinir. PM'nin kimyasal bileşimi ve boyutu sağlık açısından önemlidir. Halk sağlığını korumak ve iklim değişikliğiyle mücadele etmek için PM kaynaklarını bilmek önemlidir. Bu çalışma, Bolu şehir merkezinde (40.73° K–31.60° D ve 741 m rakım) boyutlarına göre ayrılmış PM'nin kimyasal bileşimini ve kaynaklarını incelemiştir. Boyutlarına göre ayrılmış PM örnekleri (>7.2, 3.0-7.0, 1.5-3.0, 0.95-1.5, 0.49-1.5, <0.49 μm) Şubat 2021 ile Mart 2022 arasında 96 saatlik sürekli örnekleme periyoduyla (haftada bir kez) Yüksek Hacimli Kaskat İmpaktör (YHKİ) kullanılarak toplanmıştır. Örnekler termal-optik analizör kullanılarak OK ve EK açısından analiz edilmiştir.

Araştırma, yüksek ortalama OK/EK oranları ($PM_{2.5}$ için 10.84 ve PM_{10} için 11.15) ortaya koyarken, benzer çalışmalarda ortalama 6.6 civarında olduğu tespit edilmiştir. Bu oranlar birçok kentsel alanı aşmakta ve önemli ikincil organik aerosol (İOA) oluşumuna işaret etmektedir. Kışın, $PM_{2.5}$ fraksiyonundaki OC'nin %98'ini ikincil organik karbon (SOK) oluşturmuştur. Meteorolojik faktörler, özellikle atmosfer basıncı ve rüzgar hızı, SOK seviyeleriyle önemli korelasyonlar göstermiştir. Bu bulgular, Bolu'nun hava kalitesi sorunlarını vurgulamakta ve birincil emisyonlar ile SOK öncüllerini ele alan stratejilerin gerekliliğini ortaya koymaktadır.

Çalışma, Bolu genelinde örnekleme ağı kurulmasını, daha detaylı kaynak belirleme çalışmaları yapılmasını ve bölgedeki yıl boyu İOA oluşumunu araştırmayı önermektedir. Bu araştırma, yerel karar vericiler için hava kalitesi planlamasına katkıda bulunurken gelecekteki araştırmalar için kritik alanları belirlemektedir.

ANAHTAR KELİMELER: Partikül Madde, Elemental Karbon, Organik Karbon, İkincil Organik Karbon, OK/EK, Kaskat İmpaktör

TABLE OF CONTENTS

Page

APPROVAL OF THE THESIS ..... **iii**

ETHICAL DECLARATION ..... **iv**

ABSTRACT ..... **v**

ÖZET ..... **vi**

TABLE OF CONTENTS ..... **vii**

LIST OF FIGURES ..... **ix**

LIST OF TABLES ..... **xii**

LIST OF ABBREVIATIONS AND SYMBOLS ..... **xiii**

1. INTRODUCTION **1**

2. LITERATURE REVIEW **4**

2.1 Global Air Quality Research and Particulate Matter 4
2.2 Composition and Sources of Particulate Matter 6
2.3 Health and Environmental risks of PM 8
2.4 PM research in Mediterranian region 10
2.5 Gaps in PM research in Türkiye, Bolu 11

3. MATERIALS AND METHODS **13**

3.1 Sampling Site Location 13
3.2 Sampling 14
3.3 Preparation of Filter Samples 15
3.4 OC/EC Analyses of the Filter Samples 18
3.4.1 What is TOA Protocol? 19
3.4.2 Advantages of NIOSH 870 Protocol 20
3.4.3 OC/EC Analysis Procedure 22
3.5 Quality Assurance/Quality Control 24
3.5.1 Identification of Uncertainty Sources 25
3.6 Secondary organic carbon 30
3.7 Correlation Factor 31
3.8 Meteorology at the Sampling Site 32
3.9 Sattelite Images and Data. 36
3.9.1 MODIS Aqua and Terra 36
3.9.2 CALIPSO Sattelite 37
3.10 HYSPLIT Trajectory Modelling 38

4. RESULTS AND DISCUSSION **40**

4.1 PM Summary Statistics 40
4.2 Carbonatious Species 43
4.2.1 OC Concentrations 48
4.2.2 EC Concentrations 50
4.2.3 CC Concentrations 52

4.3 Literature Comparison to Other Locations 55
4.4 Seasonal Variations of PM and Carbonaceous Species 59
4.4.1 Seasonal variation of PM 59
4.4.2 OC Seasonal Variations 60
4.4.3 EC Seasonal Variaton 61
4.4.4 CC Seasonal Variations 61
4.4.5 TC Seasonal Variations 63
4.5 SOC Calculation and Seasonal Variations 64
4.6 OC/EC Ratios, Correlations and Seasonal Variations 69
4.7 Case Studies of high PM, CC and OC/EC 72
4.7.1 Case Study of high PM in July 2021. 72
4.7.2 Case Studies of high CC peaks, Possible Dust Episodes 74
4.7.3 Case Study of Increasing OC in the end of August 2021. 85
4.7.4 Case Studies of OC/EC Ratios for Different Sources 86
5. CONCLUSIONS AND RECOMMENDATIONS 93
6. REFERENCES 96
7. APPENDICES 108

LIST OF FIGURES

Page

Figure 1.1. Comparison of the PM_{10} and PM2.5 sises.[15] 1
Figure 2.1. Schematical representation of the sources of the $PM_{2.5}$ and the ability of PM penetrate deeper into the respiratory system.[24] 9
Figure 2.2. Source apportionment of Organic Aerosols (OA) and Black Carbon (BC) in $PM_{2.5}$ in Eastern Mediterranian region (Nicosia; Cyprus).[74] 11
Figure 2.3. Composition of PM_{10} and PM_1 above Mediterranian Sea between summer 2012 and 2013.[75] 12
Figure 3.1. Map of the sampling site 14
Figure 3.2. HVCIs mounted on elevation on the sampling site. 15
Figure 3.3. Standalone HVCI sampler.[85] 16
Figure 3.4. Discicator for conditioning of samples 16
Figure 3.5. Example of collected filters after sampling. 17
Figure 3.6. Weights used for weighting samples. 17
Figure 3.7. Schematics of OC/EC analyzer.[84] 19
Figure 3.8. Example of NIOSH protocol thermogram 22
Figure 3.9. OC/EC analyser from Sunset Laboratories 23
Figure 3.10. The process of sample cut and load into the OC/EC analyzer 23
Figure 3.11. Graph of quality assurance cata with standart deviations 24
Figure 3.12. Variation of flowrate of the high volume sampler during the field campaign 26
Figure 3.13. Variation of meteorological data during field campaign. Red lines represent days of sample extraction, the sampling was continuous for 4 days prior to extraction. Date format: MM.DD.YYY. 33
Figure 3.14. Wind speed distribution by derection through whole sampling period 33
Figure 3.15. Topography of the city.[95] 1 cm on original website map is 1 km, zoom = 13 34
Figure 3.16. Wind speed distribution during Summer (April 2021 – October 2021) 35
Figure 3.17. Wind speed distribution during Winter. (February 2021 – March 2021; November 2021 – March 2022) 35
Figure 4.1. PM mass concentration over time with temperature and humidity on one timeline. 41
Figure 4.2. Cumulative particle size distribution 42
Figure 4.3. Particle size distribution of PM mass concentration 43
Figure 4.4. Temporal variation of TC concentration with respect to size fraction with Relative Humidity and Temperature data on one timeline. 44
Figure 4.5. Cumulative particle size distribution of TC 45
Figure 4.6. Particle size distribution of TC concentration 45
Figure 4.7. Temporal variation of OC concentration with respect to size fraction, with Relative Humidity and Temperature 49
Figure 4.8. Cumulative particle size distribution of OC 49
Figure 4.9. Particle size distribution of OC concentration 50
Figure 4.10. Temporal variation of EC concentration with respect to size fraction 51

Figure 4.11. Cumulative particle size distribution of EC 52
Figure 4.12. Particle size distribution of EC concentration 52
Figure 4.13. Temporal variation of CC concentration with respect to size fraction 53
Figure 4.14. Cumulative particle size distribution of CC 54
Figure 4.15. Particle size distribution of CC concentration 54
Figure 4.16. Seasonal distribution of PM mass concentration with respect to particle size fraction 59
Figure 4.17. Seasonal variation of OC concentration with respect to particle size fraction 60
Figure 4.18. Seasonal variation of EC concentration with respect to particle size fraction 61
Figure 4.19. Seasonal variation of CC concentration with respect to particle size fraction 62
Figure 4.20. Seasonal variation of TC concentration with respect to particle size fraction 64
Figure 4.21. SOC values across all fractions during sampling period and meteorological data. 65
Figure 4.22. Temporal variation of SOC concentration with respect to size fraction 65
Figure 4.23. Particle size distribution of SOC concentration 66
Figure 4.24. Correlation heatmap for SOC and atmospheric conditions. 67
Figure 4.25. Fraction of SOC and OC_{pri} in Total OC in % 68
Figure 4.26. Positive correlation between temperature and SOC fraction. 68
Figure 4.27. OC/EC values for each individual fraction with meteorology data of RH and Temperature and Wind speed on one timeline. 70
Figure 4.28. OC/EC for PM_3 and PM_{10} fractions with standart deviations. 71
Figure 4.29. Correlation heatmap between atmospheric conditions and OC/EC ratio 72
Figure 4.30. CALIPSO satellite LIDAR data on Aerosol Subtypes in different locations on 4th July 2021[144], arrow indicates coordinates of interest. 73
Figure 4.31. 12.04.2021/09.04.2021 (CC peak Date/ Image Date) CALIPSO images from NASA[147], arrows indicate coordinates of interest (Türkiye). Backscatter image (upper panel), Aerosol Subtype image (lower panel). 77
Figure 4.32. 28.04.2021/ 27.04.2021 (CC peak Date/ Image Date) CALIPSO images from NASA[147], arrows indicate coordinates of interest (Türkiye). Backscatter image (upper panel), Aerosol Subtype image (lower panel). 78
Figure 4.33. 08.09.2021/ 05.09.2021 (CC peak Date/ Image Date) CALIPSO images from NASA[147], arrows indicate coordinates of interest (Türkiye). Backscatter image (upper panel), Aerosol Subtype image (lower panel). 79
Figure 4.34. 06.01.2022/ 06.01.2022 (CC peak Date/ Image Date) CALIPSO images from NASA[147], arrows indicate coordinates of interest (Türkiye). Backscatter image (upper panel), Aerosol Subtype image (lower panel). 80
Figure 4.35. HYSPLIT trajectory model from 09.04.2021 – 12.04.2021, for CC peak on 12.04.2021 81

Figure 4.36. HYSPLIT trajectory model from 25.04.2021 – 28.04.2021, for CC peak on 28.04.2021 82
Figure 4.37. HYSPLIT trajectory model from 05.09.2021 – 08.09.2021, for CC peak on 08.09.2021 83
Figure 4.38. HYSPLIT trajectory model from 03.01.2022 – 06.01.2022, for CC peak on 06.01.2022 84
Figure 4.39. 28.08.2021 CALIPSO images from NASA[147], arrows indicate coordinates of interest (Türkiye). Aerosol Subtype image. 85
Figure 4.40. HYSPLIT trajectory model from 24.08.2021 – 27.08.2021, for OC peak on 27.08.2021 86

LIST OF TABLES

Page

Table 3.1. Temperature steps and durations of NIOSH, IMPROVE_A and EUSAAR_2 protocols.[88] 20
Table 3.2. NIOSH870 protocol thermal profile.[86] 21
Table 3.3. Accuracy and precision values of measured standarts 25
Table 3.4. Summary statistics of meteorological parameters during field campaign 36
Table 4.1. Summary statistics of PM mass concentrations (Concentration Unit: $\mu g/m^3$) 40
Table 4.2. Summary statistics of carbonaceous aerosol mass concentrations (Concentration Unit: $\mu g/m^3$) 47
Table 4.3. Summary statistics of carbonaceous aerosol mass concentrations (Concentration Unit: $\mu g/m^3$) (continued) 48
Table 4.4. Characteristics of locations from literature 56
Table 4.5. Literature comparison of measured parameters 57
Table 4.6. Summary of statistic for every fraction for best fitting percentile. 64
Table 4.7. Aqua and NPP images from NASA[146] 75
Table 4.8. Sources and OC/EC values for different locations 87
Table 1.1 PM fractionated concentrations data 108
Table 1.2 OC, EC, TC fractionated concentrations data 111
Table 1.3 OC, EC, TC fractionated concentrations data 116

LIST OF ABBREVIATIONS AND SYMBOLS

AQG : Air Quality Guideline
BAP : Benzo[a]pyrene
BB : Biomass Burning
BC : Black Carbon
CDFFP : California Department of Forestry and Fire Protection
CCN : Cloud Condensation Nuclei
CLOUD : Cosmics Leaving Outdoor Droplets
D100 : Dual Carriage Intercity Road
EC : Elemental Carbon
EPA : Environmental Protection Agency
EU : The European Union
EUSAAR2 : European Supersites for Atmospheric Research
FID : Flame Ionization Detector
FFs : Fossil Fuels
HULIS : Humic-like Substances
HVCI : High Volume Cascade Impactor
IMPROVE : Interagency Monitoring of Protected Visual Environments
IN : Ice Nuclei
IPCC : The Intergovernmental Panel on Climate Change
LAD : Leaf Area Density
LA : Los Angeles
MEF : Mutagenic Equivalent Factor
NAAQS : National Ambient Air Quality Standards
NIOSH : National Institute for Occupational Safety and Health
NPF : New Particle Formation
OA : Organic Aerosols
OC : Organic Carbon
PAHs : Polycyclic Aromatic Hydrocarbons
PM : Particulate Matter
SARS-CoV-2 : Severe acute respiratory syndrome coronavirus 2
SOA : Secondary Organic Aerosols
SOC : Secondary Organic Carbon

TEM	: Trans-European Motorway
TC	: Total Carbon
TOA	: Thermal Optical Analysis
USA	: United States of America
VOCs	: Volatile Organic Compounds
WHO	: World Health Organization
WSOA	: Water-Soluble Organic Aerosols
WSOC	: Water-Soluble Organic Carbon

ACKNOWLEDGEMENTS

The author wishes to express his deepest gratitude to his supervisor Prof. Dr. Turgay PEKDEMİR and Prof. Dr. Fatma ÖZTÜRK for their guidance, advice, criticism, encouragements, and insight throughout the research.

Gratitutes to Assistant Prof.Dr. Ebru KOÇAK for advises and recommendations.

The technical assistance of Mr. Emre Dikmen and Dr. Eda Sagirli are gratefully acknowledged.

Gratitudes to authors parents for their support: Aiman Yeshmuratova and Arman Yeshmuratov

This study was supported by Scientific and Technological Research Council of Türkiye (TUBITAK) under the Grant Number 119Y256. The authors thank to TUBITAK for their supports.

1. INTRODUCTION

The EPA recognizes 6 types of main pollutants air pollutants of primary hazards to human health and the environment. The concentration of those pollutants determines air quality. Those are: ground-level ozone, particulate matter, carbon monoxide, sulfur dioxide, nitrogen oxides, and lead. The EPA regulates the level of those pollutants according to National Ambient Air Quality Standards (NAAQS).[13, 50] The standards are set up[4] based on research on the effects of exposure to the criteria pollutants on different kinds of populations: elderly, children, and people with respiratory diseases or other special conditions.[13]

Particulate matter (PM) is a complex mixture of tiny particles and liquid droplets suspended in the air, originating from natural and anthropogenic sources.[1] PM_{10} (particles ≤10 μm in diameter) and $PM_{2.5}$ (particles ≤2.5 μm in diameter) have gained significant attention due to their detrimental effects on human health, environmental quality, and climate.[10] In Figure 1.1, it is possible to understand the difference in scale between different PM sises and their toxicity levels, with finer particles having higher surface area and, consequently – toxicity.[15]

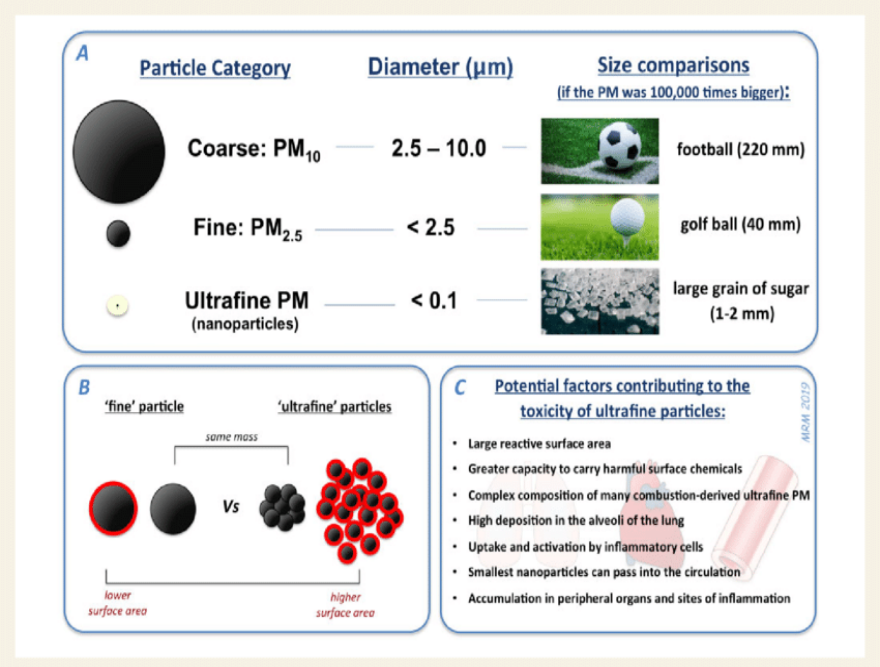


Figure 1.1. Comparison of the PM_{10} and PM2.5 sises.[15]

According to the World Health Organisation, 99% of the global population breathes air that exceeds WHO air quality limits, leading to approximately 4.2 million fatalities annually in recent years.[9,10] $PM_{2.5}$ is considered more hazardous than PM_{10} due to its ability to penetrate deeper into the respiratory system,[17,18] potentially causing severe health issues such as asthma, cancer, and increased non-accidental deaths.[40,41] The composition of PM includes organic carbon (OC), elemental carbon (EC), volatile organic compounds (VOCs), polycyclic aromatic hydrocarbons (PAHs), and various inorganic elements.[21,22] The EU and USA have set annual limits for $PM_{2.5}$ at 25 $\mu g/m^3$ and 15 $\mu g/m^3$, respectively. At the same time, the WHO recommends that annual $PM_{2.5}$ concentrations should not exceed 5 $\mu g/m^3$.[47,48,49] Understanding the sources, composition, and impacts of PM is crucial for effective air quality management and the development of targeted pollution control strategies.[12, 31, 114]

Bolu City, Türkiye, faces challenges associated with PM pollution due to its urbanization, industrial activities, and climatic conditions. However, specific studies focusing on the detailed chemical composition, seasonal variation, and source apportionment of PM in Bolu City are limited.[2]

The scope of the thesis is to investigate air pollution due to PM with particular emphasis on the carbonaceous fraction of particulate matter and identify its sources in urban areas. The research spans one year, from February 2021 to March 2022, details on location of sampling site are provided in Section 3.1 – "Sampling Site Location" of this work.

This research focus is on Bolu City, Türkiye, with specific attention on the formation and prevalence of secondary organic aerosols and analyzes the impact of local meteorological conditions on air pollution levels and composition.

Specific aims include:

1. To quantify the mass concentrations of PM in various size fractions, focusing on PM_{10} and $PM_{2.5}$.
2. To determine the concentrations of OC and EC in different PM size fractions and calculate their ratios.

3. To assess the temporal variability of PM concentrations and composition, including seasonal patterns.

4. To investigate the relationship between meteorological parameters and PM characteristics.

5. To estimate the contribution of secondary organic carbon to the total organic carbon in PM.

6. Compare the PM characteristics in Bolu City with those of other locations to contextualize the findings within the broader field of atmospheric research.

7. To provide insights into potential PM sources in Bolu City based on the chemical composition and OC/EC ratios.

8. To contribute to the limited research on PM pollution in Bolu City and similar urban environments in Türkiye.

9. To inform policymakers and environmental managers about the unique aspects of PM pollution in Bolu City, facilitating the development of targeted air quality improvement strategies.

2. LITERATURE REVIEW

This section aims to analyse available literature to indicate gaps that this study can fill with data. The rapidly developing Türkiye with fast urbanization process[115] lacks on air quality data, especially PM.

2.1 Global Air Quality Research and Particulate Matter

While global air quality concerns have been extensively studied, for example on Scince Direct website (Elsever publisher), there is 153000 articles on "Particulate Matter" (in quotemarks) search, with about 11000 articles annually for last three years. However, among those if we will add “Türkiye” and “Bolu” and filter only “Research articles” only 15 studies will remain. When “PM” is used instead "Particulate Matter", there is 31 studies availiable. Among them only 3 take measurement in outdoor in Bolu, those studies will be reviewed further.

The relationship between PM and climate change has emerged as a critical area of research. The IPCC “Special Report on Global Warming of 1.5°C”[116] underlines the complex relationship between aerosols and climate change. While some PM components, such as black carbon, contribute to warming, others may have a cooling effect. However, the net impact of these interactions in specific urban environments, particularly in regions like Türkiye that are vulnerable to climate change, remains poorly understood.[116]

PM play’s role in cloud formation[38, 53, 55], Fan et al.[117] demonstrated that PM can significantly affect cloud dynamics and precipitation, but these effects can vary greatly depending on local conditions. “PM” “Cloud” and “Precipitation” keywords with “Türkiye” in title, and filtered only research articles on Elsever publisher website, gives 18 results. One of such research is produced by Tuna Tuygun & Elbir in 2020[163]. They conducted an analysis of the relationships between planetary boundary layer height (PBLH), surface PM_{10}, and aerosol optical depth (AOD) in Mersin, a coastal city in southern Türkiye, from 2008-2016. This study is particularly relevant for understanding air quality dynamics in Türkiye's urban coastal regions. The authors utilized ground-based PM_{10} measurements from Türkiye's Ministry of Environment and Urbanization, MODIS satellite data, AERONET ground-based measurements from the Erdemli station, and MERRA-2

PBLH data. Their analysis revealed distinct seasonal patterns in Türkiye's southern coast, with PM_{10} peaking in winter and AOD and PBLH reaching maximum values in summer. The study found a weak overall correlation between hourly PM_{10} and PBLH, but noted significant seasonal variations influenced by Türkiye's unique geography and regional air pollution patterns. By analyzing the PM_{10}/AOD ratio, the authors accounted for transported aerosols, which are significant in Türkiye due to its proximity to the Sahara and Middle Eastern deserts.[163] This research utilizes data on PM_{10} concentration, thus providing the data on PM concentration and sources could support such studies in the future.

The health impacts of PM have been well-documented globally[9,10,15, 45], but region-specific studies are still needed, for Türkiye there is only one study about mortality rate due to PM that appears on keywords "PM", "Health" and "Türkiye". Aksoy et al. (2021)[164] conducted a comprehensive study examining the health impacts and costs of road traffic-based air pollution in Türkiye for the period 2020-2030. The research compared five different policy scenarios, ranging from business-as-usual (BAU) to more ambitious policies promoting cleaner vehicles and removing older, polluting ones. The authors employed COPERT software to calculate emissions of air pollutants (PM_{10}, $PM_{2.5}$, NO_2, SO_2) for each scenario, used a box model to convert emissions to concentrations, and estimated health impacts using exposure-response functions from the EVA (Economic Valuation of Air Pollution) software. Health costs were monetized using benefit transfer methods to adapt values from other studies to Türkiye.[164]

The study's findings revealed that the most ambitious scenario (SCE-4) could lead to significant reductions in emissions by 2030 compared to BAU, with up to 27% for PM_{10}, 41% for $PM_{2.5}$, and 27% for NO_2. This scenario could potentially prevent up to 19,396 premature deaths and save 803,328 years of life lost (YOLL) over the 2020-2030 period. The economic benefits were substantial, with potential health cost savings ranging from 112 billion TL (most conservative scenario) to 252 billion TL (most ambitious scenario) over the 11-year period. Additionally, significant reductions in various illnesses were projected, including restricted activity days, hospital admissions, and cases of bronchitis.[164]

Pope and Dockery[118] provided a seminal review of health effects of fine particulate air pollution but noted that the specific components of PM responsible for these effects are not fully understood. This work on PM, carbonatious species and its sources could significantly enhance studies like Aksoy et al.'s (2021)[164] by providing more detailed insights into the nature and sources of emissions. It could lead to more accurate modeling in software like COPERT, enabling the development of more specific exposure-response functions for different PM components. This underscores the need for detailed chemical characterization of PM in different urban environments.[118]

2.2 Composition and Sources of Particulate Matter

The composition and sources of particulate matter have been the subject of numerous studies, revealing a complex mixture of organic and inorganic components.[25, 26, 74] However, the specific composition can vary significantly depending on the location, season, and local emission sources, highlighting the need for region-specific studies.[118]

OC and EC have been identified as crucial components of PM[27, 28], significantly influencing air quality and health impacts. Thangavel et al. (2022)[35] and Xue et al. (2019)[36] found that elements such as S, Cu, Pb, and Zn are typically found in higher concentrations in $PM_{2.5}$, often linked to anthropogenic activities.

The OC/EC ratio is a valuable indicator for distinguishing between different pollution sources. High OC/EC ratios, typically greater than 2, suggest significant contributions from secondary organic formations[73]. This ratio is particularly important in understanding particle origins and transformations in the atmosphere, yet studies specifically examining this ratio in Turkish urban environments are limited, and Even more limited when the Bolu city is in focus. Search on Elsever website by keywords “Bolu, Türkiye, PM, OC” provide 19 articles in Environmetal Science section, if only research articles in focus, number of papers is 14, with only 10 related to outdoor air quality and only 9 related to Türkiye. Among them only 2 collects data in Bolu.

The study of Lang-Yona et al., (2020)[119] examined the relationships between airborne microbiome composition (which are organic materials), meteorology, and

particulate matter chemistry in northwestern Türkiye. Air samples collected in Bolu during summer 2017 and winter 2018 were analyzed for microbial content, chemical composition, and antibiotic resistance genes. Microbial communities differed significantly between seasons, with bacterial compositions correlating with PM_{10} and air trajectories, while fungal communities were mainly associated with PM_{10} levels. Summer samples exhibited higher bacterial diversity and abundance, particularly Proteobacteria. The fungal phylum Ascomycota was more prevalent in summer, correlating with dust markers and suggesting long-range transport. The study demonstrates how integrating chemical, meteorological, and microbiome data can provide insights into atmospheric microbial transport and distribution. It highlights the contribution of distant sources to summer microbial composition and local anthropogenic sources in winter.[119] This approach allows for improved evaluation of air quality and potential health risks under varying atmospheric conditions in a previously understudied region.[119]

Another study that collected data in Bolu is work of Bayramoğlu Karşı et al., (2020)[165], and was focused on the correction and source apportionment of vehicle emission factors obtained from the Bolu Mountain Highway Tunnel in Türkiye.[165] This comprehensive research analyzed total suspended particulate (TSP) samples collected at the tunnel's entrance and exit, examining 35 major and trace metals, 11 water-soluble anions and cations, and organic and elemental carbon concentrations. The resulting average OC/EC ratio of approximately 1.14 during one week period (July 23 to July 29, 2018)[165], which is typical for traffic emission (Table 4.8). Through factor analysis and factor analysis-multiple linear regression techniques, the researchers identified five primary emission sources: road dust re-suspension, road cover material and tire wear abrasion, brake pad solid lubricants, diesel combustion emission, and gasoline-LPG combustion emission. Surprisingly, non-exhaust sources dominated the particulate matter composition, accounting for 69.1% of the total variance, with road dust re-suspension alone explaining 33.4%.[165]

Secondary Organic Carbon (SOC) formation has been recognized as a significant contributor to PM, especially in urban areas. The oxidation of volatile organic compounds in the atmosphere leads to SOC production, which can make up a significant proportion of biogenic emissions globally[72]. Natural sources of PM,

including sea salt, airborne soil and dust, pollen, and volcanic eruptions, contribute significantly to overall PM levels[59]. Anthropogenic sources, such as vehicle emissions, industrial processes, and biomass burning, have been well-documented in various urban studies[56, 57, 63,65]. Recent research has also highlighted the importance of secondary inorganic formation in urban PM pollution. In Los Angeles, for instance, this process accounts for 42% of the total fine PM[69]. However, similar comprehensive studies in Turkish cities are lacking there is only one study (by 29.08.2024) that was focused on OC and SOC in Bolu, leaving a significant gap in our understanding of PM formation and dynamics in this region. This study is from researchers Öztürk & Keleş (2016)[101], this wintertime study in Bolu, Türkiye found elevated concentrations of OC in $PM_{2.5}$, with an average of 59.9 ± 50.4 μg/m^3, the study compared it to Kanpur, India where reported concentration was 29 μg/m^3 in $PM_{2.5}$, which is about 6 times higher than WHO standart[3]. Analysis revealed that primary OC and SOC contributed 60% and 40% respectively to total OC over the study period (December 2014 to February 2015). SOC contribution increased up to 74% during periods of stable atmospheric conditions characterized by low temperatures, low wind speeds, and reduced mixing heights. The researchers linked this to enhanced condensation of semi-volatile organic compounds onto existing particles under these stagnant conditions. The high OC/EC ratio of 10.1 found in Bolu was notably higher than most other wintertime urban studies (for example 7.5 in Kanpur), which the authors suggested was due to increased emissions from residential heating combined with the lower mixing heights observed.[101]

2.3 Health and Environmental risks of PM

$PM_{2.5}$ has been identified as more hazardous than PM_{10} due to its ability to penetrate deeper into the respiratory system[40,41]. Long-term exposure to $PM_{2.5}$ has been linked to increased risks of respiratory diseases, cardiovascular problems, and cancer.[23, 24] The schematics of $PM_{2.5}$ danger is depicted on Figure 2.1.

The composition of PM plays a crucial role in its health effects.[20, 35, 39, 58] Polycyclic Aromatic Hydrocarbons (PAHs), particularly Benzo[a]pyrene (BAP), have been recognized as significant contributors to the mutagenic activity of PM[42,43,44,68]. Jahedi et al. (2021)[37] found that PAH concentrations are typically

higher in PM_{10} than in $PM_{2.5}$. However, studies examining the specific PAH content in PM samples from Turkish urban environments are limited, for example by searching "Bolu", "Türkiye", "PAH", "PM" there were found 0 studies, leaving a gap in our understanding of potential health risks. Since PAHs are also organic – OC value can indirectly provide information on hazard level of the air.[33]

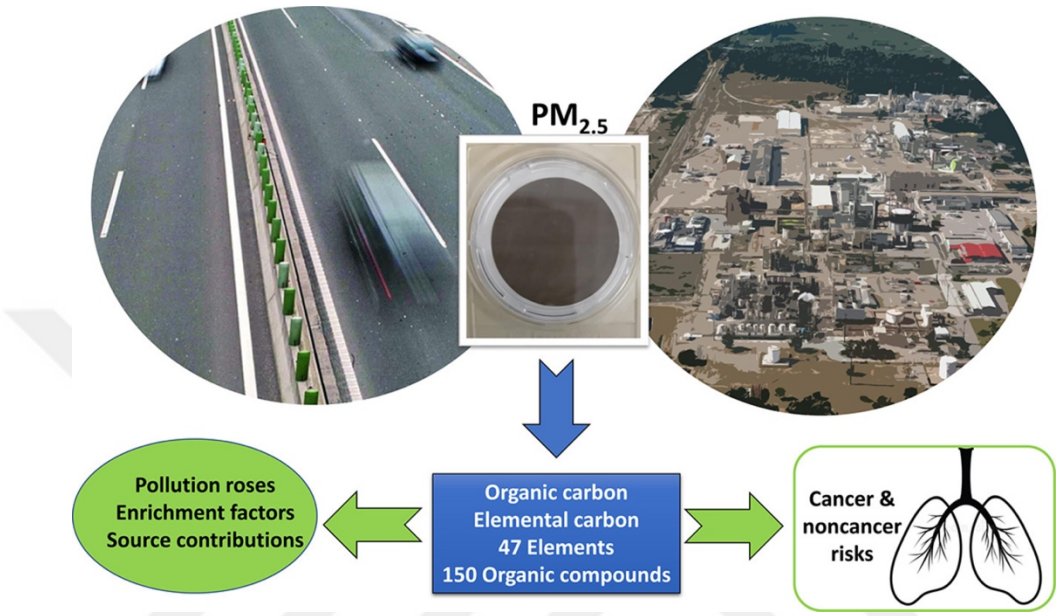


Figure 2.1. Schematical representation of the sources of the $PM_{2.5}$ and the ability of PM penetrate deeper into the respiratory system.[24]

The environmental impacts of PM extend beyond direct health effects. PM has been shown to affect vegetation, particularly in areas with high Leaf Area Density (LAD)[51]. The impact of PM on global warming is complex and not fully understood[52]. While some components of PM, such as Black Carbon, contribute to warming, others may have a cooling effect by scattering solar radiation.[67, 71, 76, 79] The net impact can vary depending on the specific composition of PM, which can differ significantly between urban environments.[34, 52, 66]

Recent research has highlighted the potential role of PM as a vector for biological contaminants, including viruses like SARS-CoV-2[46]. This finding underscores the importance of studying PM not just as a pollutant itself, but as a potential carrier of other health hazards. Kayalar et al., (2021)[166] collected particulate matter samples from 13 sites across 10 Turkish cities, in Bolu, samples were collected from an urban site and an urban background site using SKC Filter

Pack Samplers to collect TSP on Teflon filters. The sampling was conducted from May 14 to May 22, 2020, during a period of high COVID-19 prevalence in Türkiye. However, the study found that all analyzed samples from Bolu, both from the urban and urban background sites, were negative for the presence of SARS-CoV-2 RNA.[166] This result contrasts with some other cities in the study, such as Istanbul, Tekirdağ, and Zonguldak, where positive samples were detected, particularly near hospitals. The negative results in Bolu could be due to various factors, including lower COVID-19 prevalence in the area, meteorological conditions, or air quality parameters. However, the study did not provide specific details on these factors for Bolu.[166] Despite results being negative, it diesnt nescessary mean that air of Bolu was completely free of SARS-CoV-2 RNA due to limited sampling period. Also, the discovery of persistent antibiotic resistance genes in urban air samples across seasons highlights the need for closer examination of local anthropogenic sources and their potential impact on public health.[64, 119]

2.4 PM research in Mediterranian region

Studies in the Mediterranean region have shown high levels of PM that often exceed WHO guidelines. For instance, research conducted in Jordan between May 2018 and March 2019 found average 24-hour PM_{10} levels of about 64 $\mu g/m^3$ and $PM_{2.5}$ levels of 47 $\mu g/m^3$, with $PM_{2.5}$ constituting about 80% of PM_{10}[73]. These levels are higher than most Mediterranean countries but lower than some Middle Eastern nations.[73]

The composition of PM in the Mediterranean region has been found to vary significantly. In the Eastern Mediterranean (Nicosia, Cyprus), OC accounted for 81% of the $PM_{2.5}$ carbonaceous fraction, with an annual average of 2.8 ± 1.2 $\mu g/m^3$.[74] EC showed strong seasonality, with higher concentrations during colder months. This seasonality in PM composition has not been thoroughly investigated in Turkish urban environments, representing a crucial knowledge gap. One of the few studies that studied seasonal variation of the OC and EC shown 2-4 and 3-6 times exceedance of OC in Istanbul in comparison to USA and Europe.[120]

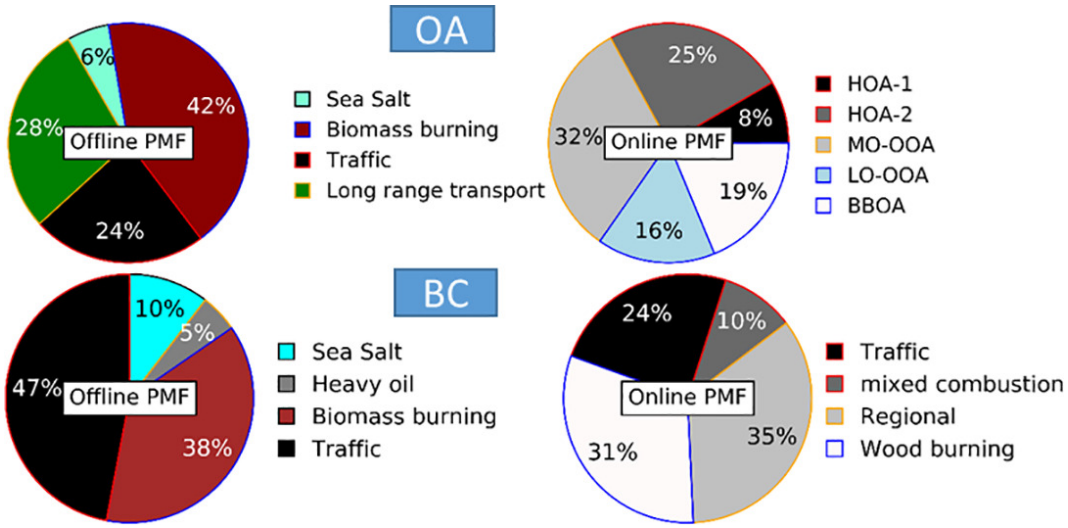


Figure 2.2. Source apportionment of Organic Aerosols (OA) and Black Carbon (BC) in $PM_{2.5}$ in Eastern Mediterranian region (Nicosia; Cyprus).[74]

This figure illustrates the complex source apportionment of PM in the Eastern Mediterranean. Research in the Mediterranean Sea has revealed significant contributions of organic matter to both PM_{10} and PM_1 [75]. The study found that organic matter contributed 30% to PM_{10} in 2012 and 33% in 2013, while for PM_1, it contributed 41% in 2012 and 38% in 2013. These findings highlight the importance of studying organic aerosols in the region.

The Mediterranean region is also significantly affected by long-range transport of dust, particularly from the Sahara. A study by Rodríguez et al. [121] found that North African dust can contribute up to 20-25 $\mu g/m^3$ to the annual mean PM_{10} in the Eastern Mediterranean.[121] Given Türkiye's geographical location, understanding the contribution of long-range transported dust to urban PM levels is crucial, yet understudied.

Climate change is expected to have significant impacts on PM dynamics in the Mediterranean region.[77, 78] The IPCC report (2022)[10], which is latest report on impacts on climate change, identifies the region as a global hotspot, warming more rapidly than the global mean. This warming trend, combined with decreasing near-surface moisture levels, is likely to affect PM concentrations and composition.

2.5 Gaps in PM research in Türkiye, Bolu

There is a notable lack of long-term, comprehensive PM monitoring data in many Turkish cities. As of 2019, the Turkish Ministry of Environment and Urbanization had been operating an air quality monitoring station in Bolu city center since 2006, but it only monitored SO_2 and PM_{10} concentrations[80]. This limited monitoring scope fails to capture the full spectrum of PM pollution, particularly the crucial $PM_{2.5}$ fraction.

Some studies provide information on the chemical composition of PM in terms of metals and carbonaceous material for Bolu city center, these have been limited to wintertime observations (Dec. 2014 – Feb. 2015)[80]. The lack of year-round data hinders our understanding of seasonal variations in PM composition and sources. Current research, covering a full year from February 2021 to March 2022, fills this critical gap in seasonal PM characterization.

There is a lack of studies examining the relationship between local meteorological conditions and PM characteristics in Turkish cities. Given Türkiye's diverse climate and the Mediterranean region's vulnerability to climate change[10], understanding these relationships is crucial. Current investigation into the influence of temperature, humidity, wind speed, and atmospheric pressure on PM concentrations and composition in Bolu City fills this critical research gap.

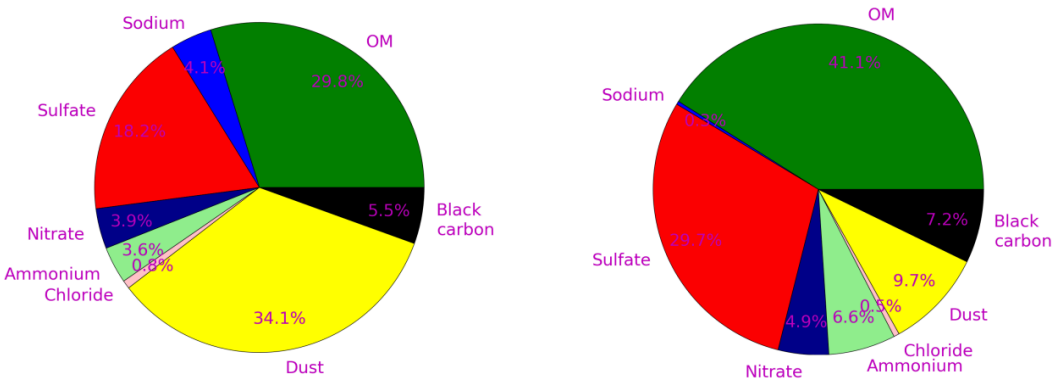


Figure 2.3. Composition of PM_{10} and PM_1 above Mediterranian Sea between summer 2012 and 2013.[75]

Figure 2.3 provides valuable insights into PM composition over the Mediterranean Sea, comparable data for Turkish urban atmospheres, particularly in inland cities like Bolu, is lacking.

3. MATERIALS AND METHODS

This study employed a High-Volume Cascade Impactor (HVCI) to collect size-segregated PM samples. The sampling location and materials used for sample collection and methods are described in detail, followed by the methods and procedures employed for sample preparation, OC/EC analysis, and data reduction and analysis.

3.1 Sampling Site Location

Air samples were collected at a location in Bolu city, Türkiye, with coordinates 40.7330°N, 31.6017°E. The sampling site is situated at a meteorological station and is exposed to wind and traffic. The location can be characterized as distanced from highways and close to daily traffic inside the city. Bolu City Centre is pierced through by a network of 2 and 1 laned roads that limit traffic in comparison to highways. The site is elevated by approximately 743 m above sea level.

Map on the Figure 3.1 provides data on elevation and location and types of areas of the Bolu city. The city of Bolu is located in Türkiye's western Black Sea region, with 64% of its territory covered by forests. 56% of its landmass consists of mountains that reach heights up to 2500 meters. There are no heavy industry facilities in the city and outskirts; however, there is one highway called Trans-European Motorway (TEM) and one dual carriage intercity road (D100).[82] According to Google Maps the distances between sampling site and mentioned roads are approximately 490 meters and 3.2 kilometer respectively.

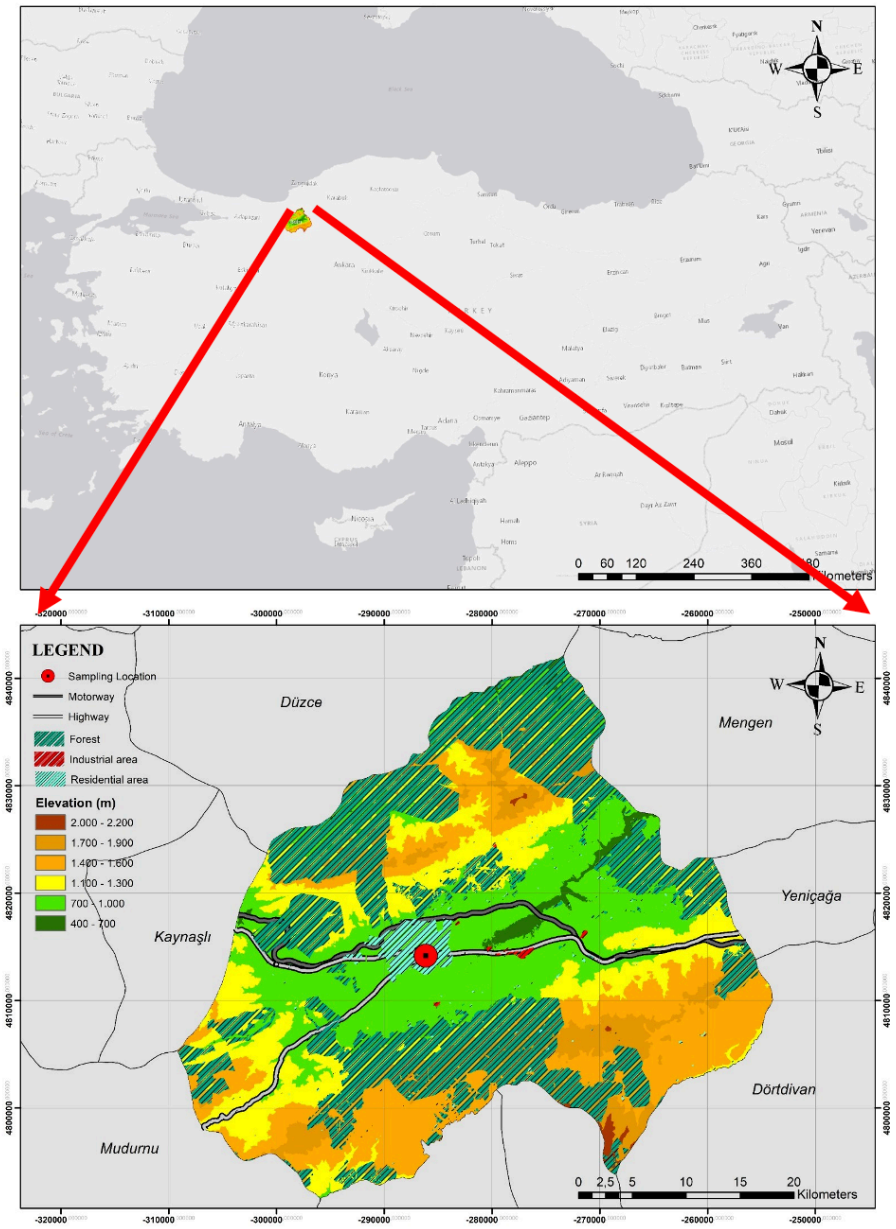


Figure 3.1. Map of the sampling site

3.2 Sampling

Samppling Period was from 17th February of 2021 to 10th March 2022, sampling period – 96 hours. This time frame covered all four seasons.

High Volume Cascade Impactors (HVCI) are widely used for sampling particulate matter (PM) in environmental monitoring and pharmaceutical industry applications. These devices operate based on the principle of inertial impaction, allowing for the collection and categorization of particles by size. The design parameters of HVCI, such as the number of stages, cut-off diameters, flow rate, and physical configuration, can be adapted to suit the expected sizes of PM. HVCIs are

useful for collecting large amounts of particles onto relatively small surfaces without the need for adhesives, making particle recovery through aqueous extraction easier[81]. Additionally, HVCIs can collect a high volume of air and provide a representative sample of PM, although their size and weight may limit their suitability for short-term sampling.[81] Mounting the HVCIs on an elevation, as shown in Figure 3.2, can help mitigate the issue of uneven airflow distribution from the narrow outlet of the inlet to the top stage of the impactor during initial operation.[83] By elevating the HVCIs, the air intake is less likely to be affected by ground-level turbulence or obstructions, which can contribute to the maldistribution of the flow profile. This setup ensures a more consistent and representative sampling of particulate matter across the different stages of the impactor.[81]



Figure 3.2. HVCIs mounted on elevation on the sampling site.

3.3 Preparation of Filter Samples

The samples were collected using a series of quartz filters in the High-Volume Cascade Impactor (The sampler's model is: 1-TSP-AND-PM10 from Tisch Environmental) with size fractions: >7.2, 3.0-7.2, 1.5-3.0, 0.95-3.0, 0.49-1.5, <0.49 µm. Figure 3.3 shows a standalone HVCI sampler of this model. The volumetric flow rate was set to 40 cfm, and the air pumping time was 96 hours. The sampling period was from February 2021 to March 2022.



Figure 3.3. Standalone HVCI sampler.[85]

Before being placed into the sampler, quartz filters were burned in an oven at 550°C for 3 hours to remove possible carbon contaminants and conditioned in a desiccator for 24 hours. After conditioning, the filters were weighed immediately before installation into the impactor. Figure 3.4 illustrates the desiccator used for conditioning the samples.



Figure 3.4. Disciicator for conditioning of samples

The weight balance used was Precisa 360 ES (Figure 3.6).

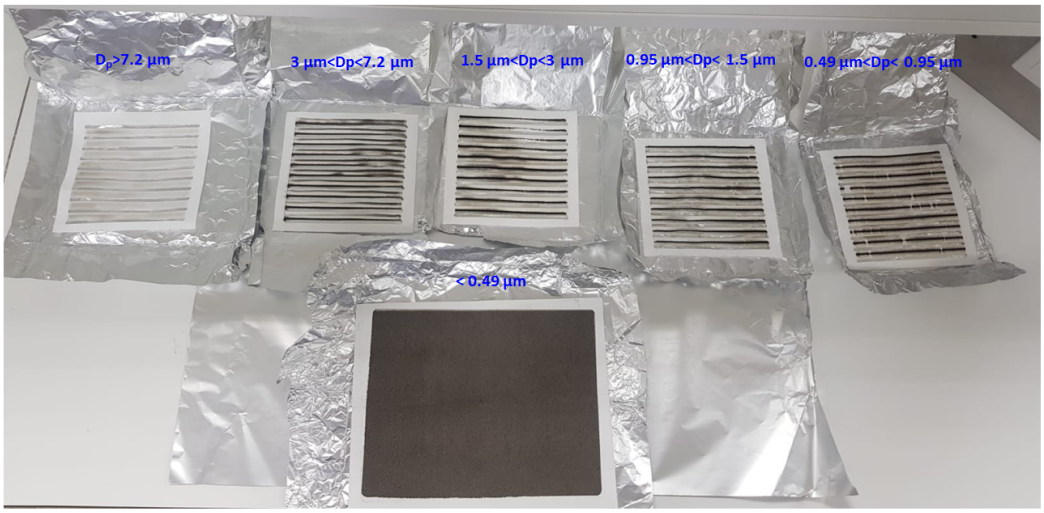


Figure 3.5. Example of collected filters after sampling.



Figure 3.6. Weights used for weighting samples.

Two types of filters were used: one for the first five fractions and another for the finest (<0.49 µm) fraction. Figure 3.5 shows an example of collected filters after sampling.

The difference in filter masses before and after sampling provides the mass of each fraction accumulated in the air. By dividing this mass by the total volume of air that passed through the filters, the concentration of each fraction in the air can be calculated. The exact models of the filters used were TE-230-QZ from Tisch Environmental for >7.2, 3.0-7.2, 1.5-3.0, 0.95-1.5, 0.49-1.5 µm fractions and PALLFLEX Membrane Filters type: TISSUQUARTZ 2500QAT-UP for the <0.49 µm fraction.

After collecting the filters from the impactor, they were conditioned in the desiccator for 24 hours and weighed. Following the weighing process, each filter was cut into 4 pieces, and each piece was weighed again.

3.4 OC/EC Analyses of the Filter Samples

Thermal Optical Analysis (TOA) has become the standard method for detecting OC and EC in PM in Europe and the US. This method is also suitable for the quartz filters used in the current study, according to the US EPA. TOA involves a series of heating steps in inert (usually pure Helium) and oxidizing (usually a mixture of Helium and Oxygen) atmospheres. In the inert atmosphere, the Organic Carbon sample is heated up in several steps, following a specific protocol (for example, NIOSH870 or EUSAAR2). During this process, OC is oxidized to CO_2 without affecting EC. The produced CO_2 is then converted to methane (CH_4) and detected by a flame ionization detector (FID), as shown in the schematics of an OC/EC analyzer in Figure 3.7. FID works by burning the methane and measuring the output ions, which are used to calculate the OC concentration. After oxidizing OC, the atmosphere switches to the oxidizing atmosphere, where EC oxidizes to CO_2, and the conversion to CH4 and detection process is repeated[84].

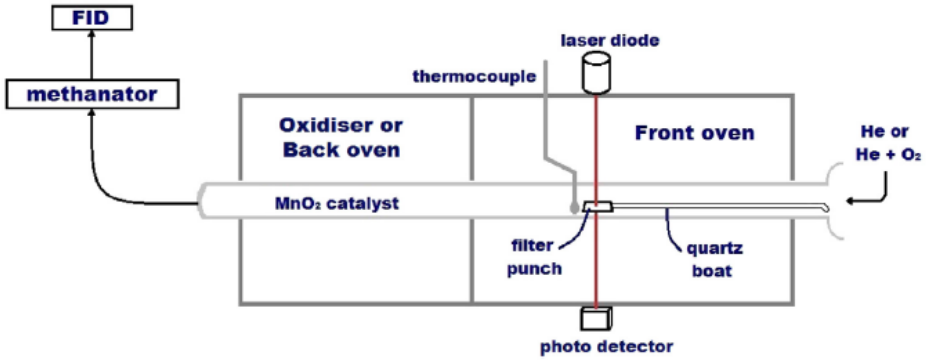


Figure 3.7. Schematics of OC/EC analyzer.[84]

However, inorganic carbons, such as carbonates, can produce CO_2 during heating in the inert atmosphere, potentially affecting OC results. Carbonates are part of natural mineral dust that can be raised into the air by wind or originate from construction sites that use carbonates like calcium carbonate ($CaCO_3$). To avoid this error, samples can be conditioned in an HCl atmosphere before the analysis. The reaction with acid decomposes carbonates and removes CO_2, eliminating the error and ensuring that the CO_2 produced during the analysis is solely from the oxidation of OC.[86]

3.4.1 What is TOA Protocol?

TOA protocols, such as the Interagency Monitoring of Protected Visual Environments (IMPROVE), the National Institute for Occupational Safety and Health (NIOSH), and the European Supersites for Atmospheric Aerosol Research (EUSAAR2), are standardized procedures used to determine the quantity of OC and EC in particulate samples. As shown in Table 3.1, each protocol has specific temperature steps and durations for the analysis. The IMPROVE protocol uses laser reflectance for measurements, while the NIOSH protocol, suitable for samples with high levels of EC, uses laser transmittance. The EUSAAR2 protocol, designed for consistency across different laboratories in the EU[87], utilizes both laser reflectance and transmittance. Reflectance refers to the light reflected off the sample surface during the heating process, while transmittance measures light passing through the sample. The formation of pyrolytic carbon can cause inaccuracies for both methods.

Table 3.1. Temperature steps and durations of NIOSH, IMPROVE_A and EUSAAR_2 protocols.[88]

Step	NIOSH T(°C), duration (s)	IMPROVE_A T(°C), duration (s)	EUSAAR_2 T(°C), duration (s)
OC1	310, 80	140, 150-580	200, 120
OC2	475, 60	280, 150-580	300, 150
OC3	615, 60	480, 150-580	450, 180
OC4	870, 90	580, 150-580	650, 180
EC1	550, 45	740, 150-580	500, 120
EC2	625, 45	840, 150-580	550, 120
EC3	700, 45		700, 70
EC4	775, 45		850, 80
EC5	850, 120		
EC6	870, 120		

Pyrolytic carbon, an undesirable product for TOA analysis, is formed by the pyrolysis of OC to EC in an oxygen-free atmosphere. It affects OC and EC results, leading to a lack of OC and an excess of EC in the results. Pyrolytic carbon can be observed as visible darkening of the sample.[87] The transmittance measurement in the NIOSH protocol is less influenced by the physical properties of the sample, such as particle size and shape, resulting in more reliable results. This well-established and widely accepted protocol ensures credible and comparable results with other studies. The NIOSH 870 protocol is designed to minimize the formation of pyrolytic carbon. Karanasiou et al. (2011)[86] conducted a study to identify and quantify atmospheric carbonate carbon (CC) by thermal-optical analysis using three different temperature protocols, including a modified NIOSH-like protocol. The study found that high recoveries of CC were achieved by all the thermal protocols, including the NIOSH 870 protocol.

3.4.2 Advantages of NIOSH 870 Protocol

The thermal protocols NIOSH870 and IMPROVE are both widely used for analyzing organic carbon (OC) and elemental carbon (EC). However, they use

different temperature ramps and times and apply different methods to correct for the charring of OC. While both methods can accurately measure total carbon (TC) concentrations, they differ when it comes to OC and EC. The IMPROVE protocol tends to underestimate OC levels due to its lower peak temperature in the inert mode; thus, the NIOSH870 protocol was chosen for the current study[89].

Table 3.2. NIOSH870 protocol thermal profile.[86]

Analyses Steps	Gas	Retention Time (sec)	Retention Temperature (°C)
OC_1	He	60	310
OC_2	He	60	475
OC_3	He	60	615
OC_4	He	90	870
	He	Cooling 50	
EC_1	He /O_2	45	550
EC_2	He /O_2	45	625
EC_3	He /O_2	45	700
EC_4	He /O_2	45	775
EC_5	He /O_2	45	850
EC_6	He /O_2	120	870

Table 3.2 shows the NIOSH870 protocol thermal profile. The heating steps of the NIOSH870 protocol for the inert atmosphere (100% He) are as follows: 310, 475, 615, and 870 °C. These steps are used for OC determination and are referred to as OC1, OC2, OC3, and OC4, respectively. After that, the oven switches to a 2% Oxygen and Helium atmosphere and repeats the heating with the following steps for EC analysis: 550, 625, 700, 775, 850, and 870 °C. Each heating step provides a corresponding peak, so the protocol provides 4 peaks for OC and 6 peaks for EC, which are referred to as EC1, EC2, EC3, EC4, EC5, and EC6, respectively.[86]

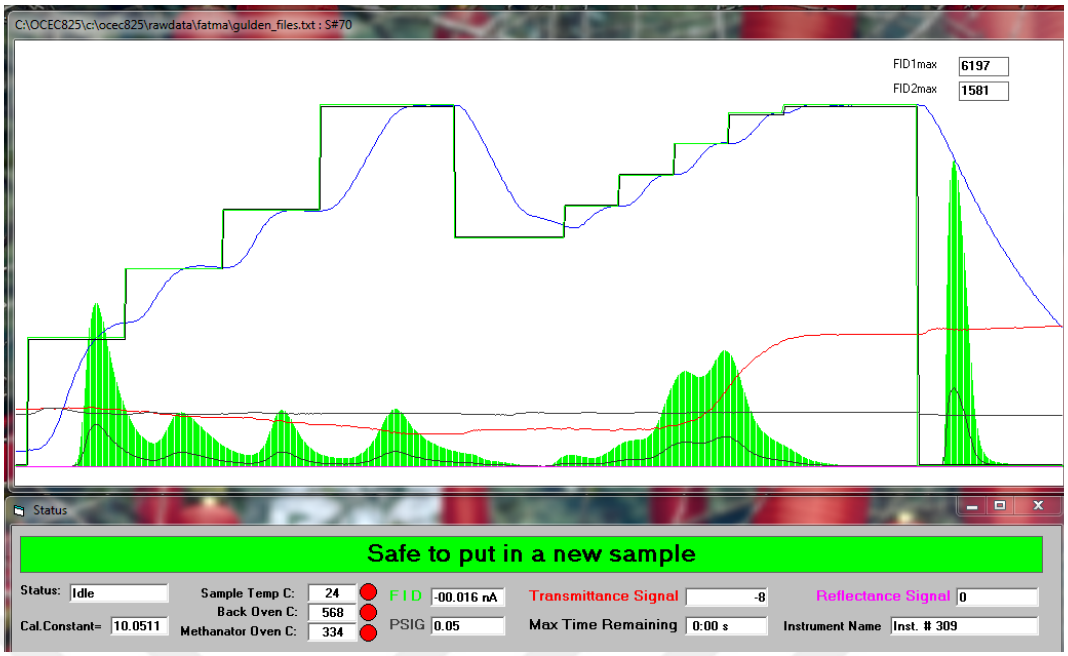


Figure 3.8. Example of NIOSH protocol thermogram

Figure 3.8 shows an example of a NIOSH protocol thermogram. The sum of EC1 (550 °C) + EC2 (625 °C) represents pyrolytic carbon, while soot, which is composed of submicron particles with strong light absorption characteristics, is equal to the sum of EC3 (700 °C) + EC4 (775 °C) + EC5 (850 °C) + EC6 (870 °C).[90]

The total OC species is equal to the sum of OC1 + OC2 + OC3 + OC4 + PC (Pyrolytic Carbon). OC4 is usually associated with secondary organic carbon, while OC1-3 are of primary origin.[91]

3.4.3 OC/EC Analysis Procedure

For the OC/EC analysis, a 1.5 cm^2 portion from each filter was taken using a special punch that comes with the OC/EC analyzer from Sunset Laboratories (established in Oregon, USA) and weighed before analysis. Figure 3.10 illustrates the process of cutting the sample with the punch and loading it into the OC/EC analyzer.

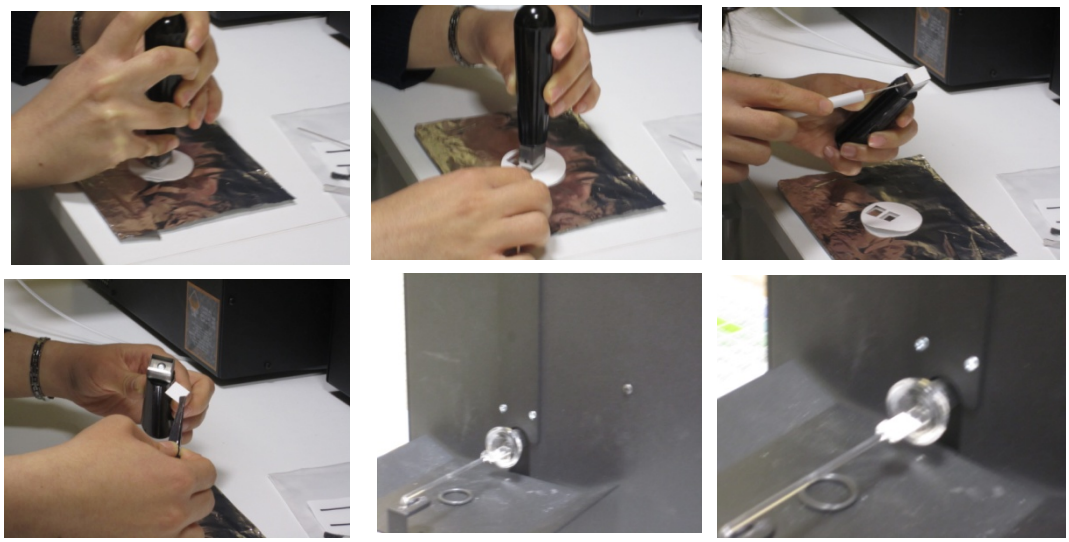


Figure 3.10. The process of sample cut and load into the OC/EC analyzer



Figure 3.9. OC/EC analyser from Sunset Laboratories

All samples were stored in the freezer at a temperature below -18 °C, covered by aluminum foil, and placed in zip-locked bags to prevent contamination and preserve their integrity.

The OC/EC analysis was performed using an analyzer from Sunset Laboratories, as shown in Figure 3.10. To ensure accurate results and maintain the instrument's performance, several quality control measures were implemented.

Before every sample run, a "Clean Oven" run was performed to eliminate any residual carbon components inside the instrument. Additionally, "Instrument Blank" samples, which are blank quartz filters identical to those used for sample analysis, were run to check the instrument's parameters, such as pressure, laser signal, heating procedure, and the FID signal during the calibration phase of analysis (FID1max). During the analysis of these blank samples, the EC should be zero, and the OC should be below 0.2 µg/cm^2, indicating that the instrument is functioning correctly and free from contamination.

3.5 Quality Assurance/Quality Control

To ensure the accurate performance of the OC/EC analyzer, a standard solution of sucrose with a concentration of 3.499 µg/µL was prepared for calibration. Each day, before analyzing the actual samples, 10 µL of the sucrose solution was applied to a clean, blank punch of quartz filter. The sucrose solution was then analyzed on the OC/EC analyzer until at least three consecutive results fell within the range of 34.99 µg/cm^2 ± 10% (represented by the corridor between the green lines in Figure 3.11), indicating proper equipment functioning. The software collected the results in a .txt file for further analysis. In cases where the OC4 peak of a sample was higher than the OC1 peak, suggesting possible contamination by carbonaceous dust, the analysis was repeated after conditioning the sample in an HCl atmosphere for 10 minutes, followed by a dry atmosphere for an additional 10 minutes. This extra step helped to remove any interfering carbonates and ensure the accuracy of the results.

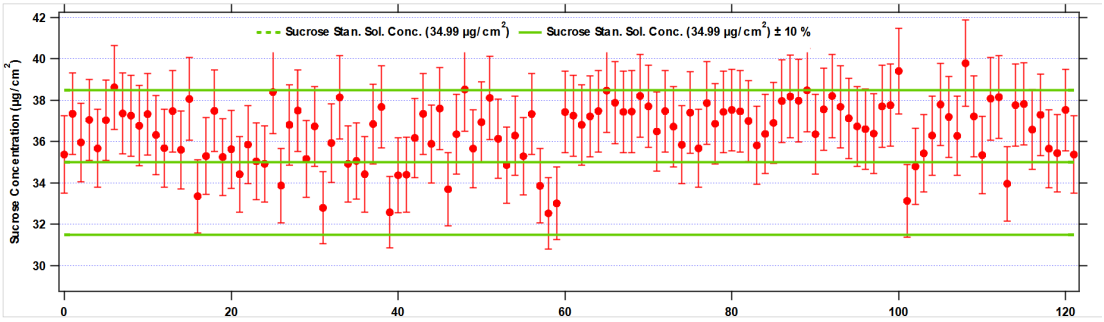


Figure 3.11. Graph of quality assurance cata with standart deviations

The calibration data were compiled, and standard deviations, accuracy, and precision were calculated. In addition to the daily calibration, standard

measurements were also performed, with the results presented in Table 3.3, showing deviations of less than 10%.

Table 3.3. Accuracy and precision values of measured standarts

Sample	OC (µg/cm²)	EC (µg/cm²)	TC (µg/cm²)	EC/TC Ratio
PES standard (Sunset Lab. Reported Value)	5.74±0.39	12.82±0.74	18.55±1.13	0.69
PES standard (BAİBU) 1	6.51±0.43	14.09+0.80	20.6±1.23	0.68
PES standard (BAİBU) 2	6.16±0.41	14.02+0.80	20.18±1.21	0.69
PES standard (BAİBU) 3	6.11±0.41	14.01+0.80	20.13±1.21	0.70
Average	*6.26*	*14.04*	*20.30*	*0.69*
Standard Deviation	*0.22*	*0.04*	*0.26*	*0.01*
Accuracy (%)	**9.13**	**9.55**	**9.44**	**0.11**
Precision (%)	**3.48**	**0.31**	**1.27**	**0.95**

3.5.1 Identification of Uncertainty Sources

The concentrations of carbonaceous aerosol parameters (OC and EC) in the filter samples expressed in µg/m^3 were calculated by using Equation 1[131]:

$$Carbonaceous\ Aerosol\ Concentration, C = \frac{(C_{filter\ sample} - C_{filter\ blank}) \times A_{filter}}{V_{air}} \cdots\cdots\cdots (Equation\ 1)$$

Where:

$C_{filter\ sample}$ is the carbonaceous aerosol concentration in the sample filter obtained from calibration curve in terms of µg/cm^2,

$C_{filter\ blank}$ is the carbonaceous aerosol concentration in the blank filter obtained from calibration curve in terms of µg/cm^2,

A_{filter} is the total area of the filter sampled in the field campaign in terms of cm^2, and

V_{air} is the amount of air sucked through the sample filter by the high volume sampler in terms of m^3

The following parameters were involved in the calculation of the concentrations of the carbonaceous aerosols in the samples collected on quartz filters[131]:

1. Volume of air
2. Calibration standard
3. Repeatability

3.5.1.1 Uncertainty due to High Volume Sampler (HVS)

Thus, the uncertainty in the concentrations is a combination of the uncertainties of each of the above-mentioned parameters. The combined uncertainty (in terms of relative uncertainty) can be calculated by using Equation 2[132]:

$$u_{rel}(C) = \sqrt{u_{rel}^2(CA) + u_{rel}^2(V_{air}) + u_{rel}^2(rep)} \cdots\cdots\cdots (Equation\ 2)$$

The flow of the instrument during sampling was depicted in Figure 3.12 below:

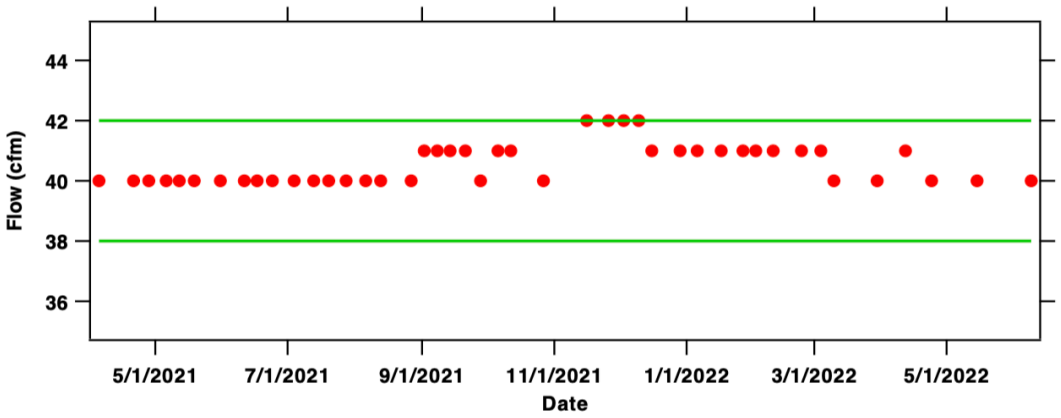


Figure 3.12. Variation of flowrate of the high volume sampler during the field campaign

The HVS was set at 40 cfm (67.96 m^3/h) in every sampling day. The standard deviation of flow rate during the sampling is 0.66 cfm (1.12 m^3/h). The

determination of air volume passed during the sampling period is calculated by using the Equation (3):

$$V_{air} = F \times t \cdots\cdots\cdots (Equation\ 3)$$

Where:

"F" is the flow of air in "m^3/hr" and "t" is the duration of sampling, 96 hours in this study. Once the flowrate of the high-volume sampler and duration of sampling were plugged into Equation 3, volume of air sucked through the filters is calculated as:

$$V_{air} = F \times t = 67.96\ \frac{m^3}{hr} \times 96\ hr = 6524.16\ m^3$$

Volume of air passed through the high volume of sampler at STP:

$$V_{air} = \frac{6524.16\ m^3 \times P_1 \times T_1}{P_2 \times T_2} = \frac{6524.16\ m^3 \times 745.65 \times 273}{(25 + 273.15) \times 760} = 5854.16\ m^3$$

Combined uncertainty due to high volume sampler is calculated using Equation 4[131]. The uncertainty values for time tracker recorded, ambient pressure measurement and temperature of the sire were assumed as 0.025, 0.3 and 1.5, respectively, at 95 % confidence level, by following the methodology used by Singh et al. (2011). In addition, the uncertainty of flow rate of HVS is 1.12/2=0.56 at 95 % confidence level and assuming normal distribution (k=2, type 'B' uncertainty). These values are plugged in Equation 4 and uncertainty due to flow is calculated as:

$$u(V_{air})^2$$
$$= \sqrt{(uncertainty\ in\ flow\ rate\ of\ HVS)^2}$$
$$+ \sqrt{(uncertainty\ in\ time\ tracker\ recorder)^2}$$
$$+ \sqrt{(uncertainty\ in\ ambient\ pressure\ measurement)^2}$$
$$+ \sqrt{(uncertainty\ in\ temperature\ of\ the\ site)^2} \cdots\cdots\cdots (Equation\ 4)$$

$$u(V_{air}) = \sqrt{(0.56)^2 + (0.025)^2 + (0.3)^2 + (1.5)^2} = 1.63\ m^3$$

3.5.1.2 Uncertainty due due to Calibration Standard

The calibration of the EC/OC analyzer was performed by using the sucrose solution prepared at a concentration of 3.489 µg carbon/µL. To prepare the calibration standard, the stock sucrose powder is used. The sucrose powder with an amount of 436 mg was weighed using microbalance and then transferred to 50 mL volumetric flask. The solution is transferred to the blank quartz filter by using micro pipette. The uncertainty due to calibration of the EC/OC analyzer can be calculated by considering the uncertainties due to volumetric flask (50 mL), microbalance and 50 µL micropipette.

The uncertainty associated with the use of the volumetric flask of 50 mL capacity at a temperature other than the calibration temperature (temperature difference) can be calculated by using Equation 5:

$$u(V_T) = V \times \Delta T \times 2.1 \times 10^{-4} \cdots\cdots\cdots (Equation\ 5)$$

The temperature effect describes the dispersion produced by a variation of liquid temperature through a rectangular distribution within ±3 ºC around the calibration temperature (EURACHEM/CITAC Guide, 2003)[170]. The uncertainty due to temperature variation on 50 mL volumetric flask:

$$u(V_T) = 50 \times 3 \times 2.1 \times 10^{-4} = 0.032$$

The standard uncertainty of volumetric flask $0.032/\sqrt{3}$=0.018 by assuming rectangular distribution. The volumetric calibration standard uncertainty associated with the 50 mL volumetric flask is 0.01. The combined uncertainty due to use of 50 mL volumetric flask is 0.021.

For the 50 µL micropipette, the standard uncertainty due to temperature variation is calculated similar to volumetric flask and found as 3.64×10^{-6}. The volumetric calibration standard uncertainty associated with the 50 µL micropipette is 0.01. The combined uncertainty due to use of 50 µL micropipette is 0.01.

Precisia 360 ES model microbalance was used in this study. The readability, repeatability and linearity of the microbalance given by the manufacturer are 0.1 mg, 0.02 mg and ± 0.1 mg, respectively. Uncertainty due to readability, repeatability and linearity of the microbalance is calculated as:

$$Uncertainty\ due\ to\ microbalance = \sqrt{(0.1)^2 + (0.02)^2 + (0.1)^2}$$
$$= 0.143\ mg$$

3.5.1.3 QA/QC and Uncertainty Analysis for OC/EC Measurements

The QA/QC of the OC/EC analyses are provided in this study. The standards provided by the Sunset Lab. (Oregon, USA) was analyzed in this study. Three standards were analyzed and repeatability for EC and OC was calculated as the relative standard deviation (RSD) of the analyses results. The uncertainty due to repeatability was calculated by dividing the RSD values of corresponding analysis results to the square root of the number of standards analyzed (n=3). Hence, the uncertainty due to repeatability for OC and EC were calculated as 2% and 0.18 %, respectively.

The relative combined uncertainty for OC parameter including the sampling flow rate, calibration curve and repeatability can be calculated as:

$$Relative\ Combined\ Uncertainty$$
$$= \sqrt{(1.63/5854.16)^2 + (0.021/50)^2 + (0.01/10)^2 + (0.143/436)^2 + (2/100)^2}$$
$$= 0.020$$

On the date of 17/2/2021, the OC in PM_{10} was measured as 20.05 µg/m^3, the standard combined uncertainty for this date for OC will be:

$$Standard\ Combined\ Uncertainty = 20.05 \times 0.020 = 0.40\ \mu g/m^3$$

Expanded uncertainty is calculated with k=2:

$$Expanded\ Uncertainty = 0.40 \times 2 = 0.80\ \mu g/m^3$$

Therefore, the PM_{10} OC for 17/2/2021 can be reported as 20.05± 0.80 $\mu g/m^3$. For EC, the same methodology can be followed. The relative combined uncertainty for EC is calculated as 0.0022. The PM_{10} EC for 17/2/2021 can be reported as 1.09± 0.01 $\mu g/m^3$.

The % of error can be calculated using standart measurments result:

Mean value of measurments is 6.26 for OC from Table 3.3.

$$Expanded\ Uncertainty\ For\ Stanandart = 6.26 \times 0.020 \times 2$$
$$= 0.2504\ \mu g/m^3$$

$$Error\ value\ in\ \% = \frac{0.2504}{6.26} \times 100\% = 4\%\ \mu g/m^3$$

For OC calculated Error is 4%, same way calculated Error for EC is 0.44%[131, 132]

The bank samples were pretreated same way as regular samples (burning in oven for 3 hours, and conditioning for 24). In total 11 blank analysis were run and as expected, the values for blanks for all analysis were 0.0. The deviation of results between two samplers was less than 10%.

3.6 Secondary organic carbon

There are several main approaches for estimating secondary organic carbon (SOC) based on the ratio of organic carbon to elemental carbon (OC/EC). The first approach involves determining the minimum OC/EC value and using it as the primary OC/EC ratio ($(OC/EC)_{pri}$). This method is applicable when there is a constant minimum OC/EC value and the main source of OC is primary OC. The second approach is to apply a regression method for OC/EC in lower ranges. The final approach is to use the minimum R^2 method, which involves using a single OC/EC value for calculations.[54, 92]

For SOC estimation from the year-long measurements of different fractions of organic carbon (OC) with measurments taking multiple days, the second approach using regression analysis of OC/EC ratios in the lower ranges was selected. This approach provides a more robust estimation of the primary OC/EC ratio ((OC/EC)pri) compared to using a single minimum OC/EC value, as in the first and third approaches. By focusing the analysis on the lower 5-20% of OC/EC ratios, the (OC/EC)pri can be determined from conditions where primary emissions are dominant, minimizing the influence of SOC formation that increases the OC/EC ratio. The strong correlation between OC and EC in this lower range ($R \geq 0.9$) further supports that it represents primary emission conditions.[92] Compared to the third approach, which may overestimate the (OC/EC)pri due to some correlation between elemental carbon (EC) and SOC, the second approach aligns more closely with the core assumptions of the EC tracer method. Moreover, the 3-day sampling interval

provides a suitable time resolution to capture the variation in $(OC/EC)_{pri}$ over different seasons without extending too long to blend low and high OC/EC conditions, which may occur with 24-hour measurements. Therefore, using the second approach with the 3-day OC and EC measurements is expected to provide a reasonable estimate of the $(OC/EC)_{pri}$ for calculating SOC concentrations in this study.[92]

The main steps for application of Approach 2:

- Calculate the OC/EC ratio for each data point in aviliable dataset.
- Sort the data points based on their OC/EC ratios, from lowest to highest.
- Select a subset of data points with the lowest 5-20% of OC/EC ratios. The exact percentage used can be determined by examining the correlation between OC and EC within each subset (e.g., lowest 5%, 10%, 15%, 20%). Choose the subset with the strongest correlation ($R \geq 0.9$), as this indicates a dominant influence of primary emissions.
- Perform a linear regression analysis on the selected subset of data points, with OC concentrations on the y-axis and EC concentrations on the x-axis. The slope of the regression line represents the $(OC/EC)_{pri}$ ratio, while the y-intercept corresponds to non-combustion OC (OC non-comb).
- If the y-intercept is negative, it may be due to measurement uncertainties or limitations. In such cases, it is common practice to set the y-intercept to zero and re-calculate the slope, which will then represent the $(OC/EC)_{pri}$ ratio.
- Use the determined (OC/EC)pri ratio to estimate the POC concentrations for each data point in the full dataset using the following equation: $POC = (OC/EC)_{pri} \times EC$
- Calculate the SOC concentrations for each data point by subtracting the estimated POC from the total OC concentration: SOC = OC total – POC [92]

3.7 Correlation Factor

The Pearson correlation coefficient is used to calculate correlation coefficients between different parameters. It was extensively used, for example, in climate research study of the Gilgit River basin. It quantified relationships between key climate and hydrological variables, including snow cover area, temperature, precipitation, and stream flow. It revealed strong negative correlations between

snow cover area and mean temperature/stream flow (r = -0.806 for annual mean runoff), and strong positive correlations between stream flow and temperature data.[93] This coefficient is calculated by formula[94]:

$$r = \frac{\sum(x_i - \bar{x})(y_i - \bar{y})}{\sqrt{\sum(x_i - \bar{x})^2 \sum(y_i - \bar{y})^2}} \ldots\ldots\ldots (Equation\ 6)$$

Where x_i and y_i are data points, while $\bar{x}$ and $\bar{y}$ are mean of of y and x values.[94]

3.8 Meteorology at the Sampling Site

Meteorological Data were provided by Turkish State Meteorology Service directly from Bolu Merkez office. Data collection period starts from 01.02.2021 to 31.03.2022. Those data included: humidity, wind speed, wind direction, atmospheric pressure. The data recorded daily and plotted on graph where sampling periods can be tracked. The rose wind was plot also provided insights on behaviour of airmasses.

The temporal variation of meteorological parameters, during the field campaign is illustrated in Figure 3.12, while Figure 3.13 depicts the variation of wind speed with respect to wind direction. Table 4.1 provided the summary statistics of the measured parameters, revealing that between February 2021 and March 2022, the average temperature was recorded as 9.07±7.85 °C. Throughout the measurement period at the ground station, the mean relative humidity at the sampling location was determined to be 74.98±12.66 %.

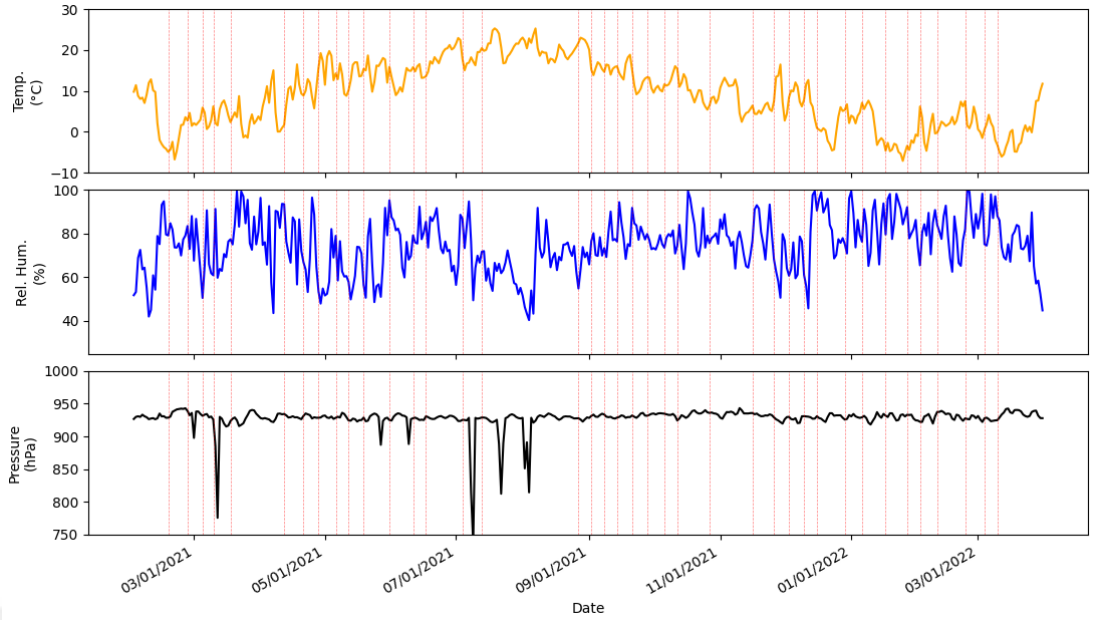


Figure 3.13. Variation of meteorological data during field campaign. Red lines represent days of sample extraction, the sampling was continuous for 4 days prior to extraction. Date format: MM.DD.YYY.

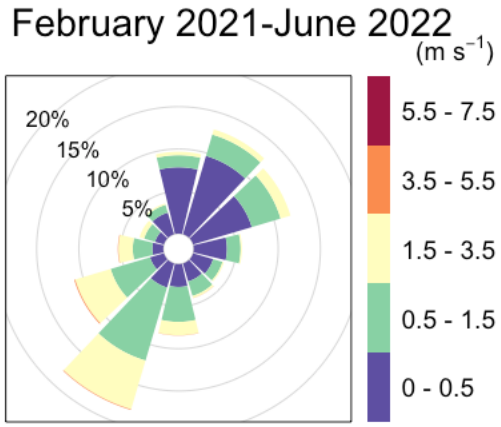


Figure 3.14. Wind speed distribution by derection through whole sampling period

According to Figure 3.13, the 66% of wind throughout the year comes from the South, West and East of the sampling site, while wind from the Northern direction blows less (33%). This pattern could be explained by the topography of the region.[95]

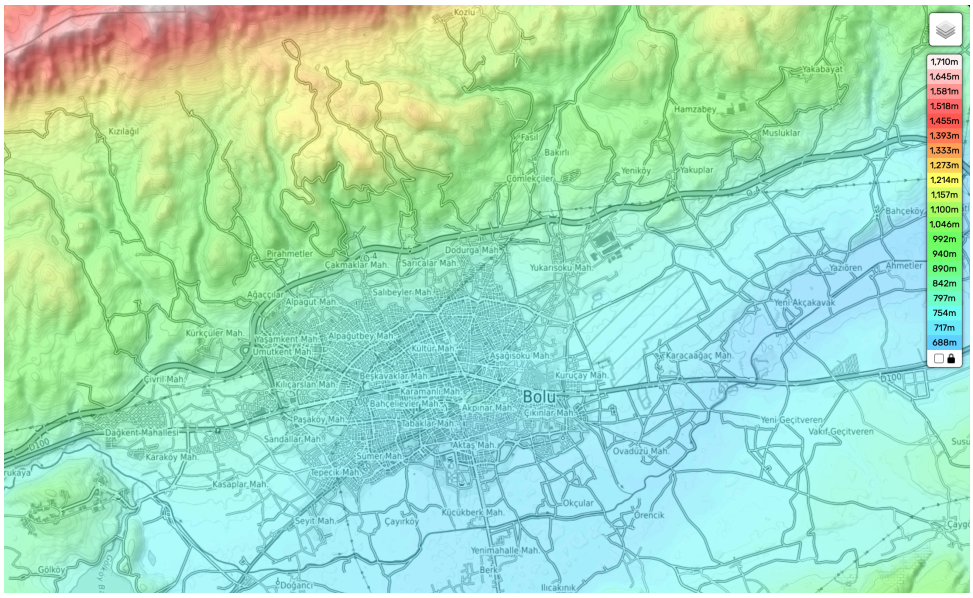


Figure 3.15. Topography of the city.[95] 1 cm on original website map is 1 km, zoom = 13

As observed in Figure 3.14, the city itself is closer to the Northern mountains. Another fact in the discussion of wind direction is that both highways are located North of the sampling site; however, both roads continue to the East until they align with the city center at almost the same latitude on the outskirts of the city. Additionally, some small-scale industries and the Bolu Cement Factory are located to the East of the city center.[82]

Wind polar graphs for the summer and winter season were depicted in Figure 3.15 and Figure 3.16, respectively. As can be seen in Figure 3.15, and 3.16 winds in summer and winter primarily blow from the South hemisphere, the impact of Northern semi-sphere is 25% for both seasons.

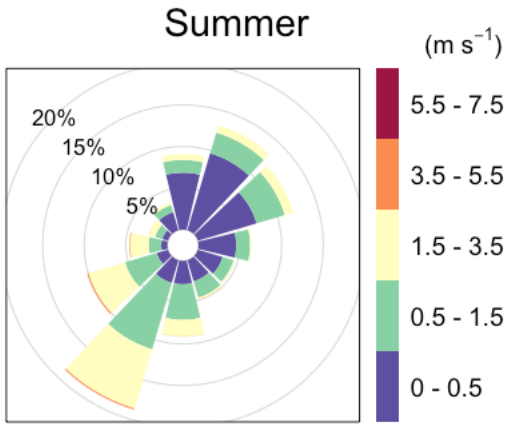


Figure 3.16. Wind speed distribution during Summer (April 2021 – October 2021)

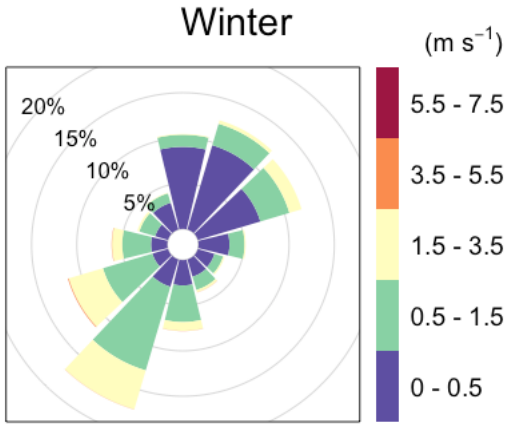


Figure 3.17. Wind speed distribution during Winter. (February 2021 – March 2021; November 2021 – March 2022)

The pressure around the sampling site showed less variation (Table 3.4), with a mean pressure of 927.72±17.30 hPa. As illustrated in Figure 3.15 and 3.16, the dominant wind direction was from 135° (which is the South-East direction), and the maximum wind speed was around 2.36 m/s, with a mean value of 0.73±0.34 m/s (Table 3.4).

Table 3.4. Summary statistics of meteorological parameters during field campaign

	Pressure (hPa)	Relative Humidity (%)	Temperature (°C)	WD (°)	WS (m/s)
Number of samples	424	424	424	424	424
Avg.	927.72	74.98	9.07	156.74	0.73
Std.Dev.	17.30	12.66	7.82	79.15	0.34
Median	929.78	75.58	9.21	144.30	0.67
Geomean	927.54	73.85		127.72	0.65
Min.	736.63	40.38	-7.10	0.77	0.02
Max.	943.20	99.46	25.28	356.94	2.36

3.9 Sattelite Images and Data.

For more robust source determination this study will utilize data from several satelites, all data are available for free and provided by NASA.

3.9.1 MODIS Aqua and Terra

In this study, MODIS (Moderate Resolution Imaging Spectroradiometer) aboard NASA's Aqua and Terra satellites was used to observe dust erupting from the African continent (Sahara), based on them NASA itself reports dust episodes[122]. The satellite data were accessed through the NASA Worldview application (worldview.earthdata.nasa.gov). This approach has been successfully employed in previous case studies, such as the investigation of the April 7, 2001 dust storm over northern China[159]. MODIS provides daily global coverage with a spatial resolution ranging from 250 m to 1 km, allowing for comprehensive monitoring of large-scale dust events. The corrected reflectance products from MODIS are particularly useful for identifying and tracking dust plumes across vast distances. While cloud cover can limit observations, satellite imagery remains a valuable tool for studying the transport and dispersion of Saharan dust. The use of both Aqua and Terra satellites enhances

temporal coverage, providing multiple observations per day and improving the chances of capturing clear views of dust events[160].

3.9.2 CALIPSO Sattelite

In this study, the Cloud-Aerosol Lidar and Infrared Pathfinder Satellite Observation (CALIPSO) satellite was utilized to obtain lidar data in the vicinity of the sampling site. CALIPSO, launched in 2006, provides continuous global measurements of aerosols and clouds in the atmosphere using its Cloud-Aerosol Lidar with Orthogonal Polarization (CALIOP) instrument. The CALIOP lidar operates at dual wavelengths of 532 nm and 1064 nm, enabling the retrieval of vertical profiles of aerosol properties with high spatial resolution. For this analysis, we focused on the 532 nm wavelength data, which is particularly useful for aerosol detection and characterization. As noted by Zhao et al. (2015)[161], the 532 nm channel provides both parallel and perpendicular polarization measurements, allowing for the calculation of the depolarization ratio, which is crucial for distinguishing between spherical and non-spherical particles such as dust. CALIPSO Level 2 aerosol layer product (version 4.10) was accessed through the NASA Langley Atmospheric Science Data Center. This dataset provides information on aerosol type classification, extinction coefficients, and aerosol optical depths.

CALIPSO data has been successfully employed in previous case studies to investigate dust transport and aerosol properties. For instance, Zhao et al. (2015)[161] used CALIPSO observations to examine the vertical distribution of dust aerosols during heavy dust storms originating from the Taklimakan and Gobi Deserts. The satellite data allowed for the identification of dust layers and their transport pathways.

One limitation of using CALIPSO data is the relatively infrequent satellite passes over a specific location, which can result in limited temporal coverage. Despite this constraint, CALIPSO observations provide valuable information on the vertical structure and optical properties of aerosols that cannot be obtained from ground-based measurements alone. The combination of CALIPSO data with in-situ sampling in this study offers a more comprehensive understanding of aerosol characteristics and transport in the region.

3.10 HYSPLIT Trajectory Modelling

To analyze the transport pathways of Saharan dust episodes (SDEs) from source regions in North Africa to Central Europe, we utilized the Hybrid Single-Particle Lagrangian Integrated Trajectory (HYSPLIT) model developed by NOAA's Air Resources Laboratory. The HYSPLIT model was configured to calculate forward trajectories originating from dust source areas in Tunisia's desert regions. Forward trajectories were computed using the Global Data Assimilation System (GDAS) meteorological dataset with a 1° spatial resolution.[162]

We selected a total runtime of 120 hours (5 days) for each trajectory simulation. This duration was chosen to adequately capture the long-range transport of dust particles, which can remain suspended in the atmosphere for several days and travel thousands of kilometers. The 5-day period allows sufficient time to track dust transport from North Africa across the Mediterranean.[162]

Trajectories were calculated at three vertical levels: 100 m, 500 m, and 1500 m above ground level (AGL). These heights were selected to represent different layers of the atmosphere where dust transport occurs[162]:

- 100 m AGL: To capture near-surface dust transport and potential deposition processes.
- 500 m AGL: To represent dust transport within the planetary boundary layer, where most of the dust is typically concentrated.
- 1500 m AGL: To account for higher-altitude transport, as dust can be lifted to several kilometers in height, especially during intense dust storm events.

This multi-level approach allows for a comprehensive analysis of dust transport patterns at different altitudes, as the behavior of dust plumes can vary significantly with height due to differences in wind patterns and atmospheric stability.

The HYSPLIT model was successfully run in published study for identified SDE events during the study period of 2005-2021. The resulting trajectories were analyzed to determine the primary transport pathways, travel times, and vertical distributions of dust plumes originating from the Tunisian desert and reaching Central Europe. This

analysis helps to elucidate the seasonal and interannual variability in dust transport patterns and the synoptic conditions conducive to long-range dust transport.[162]

By employing this HYSPLIT configuration, we aimed to provide an understanding of Saharan dust transport from source regions to deposition areas in Turkye, accounting for various atmospheric layers and transport durations relevant to dust dispersion processes.

4. RESULTS AND DISCUSSION

4.1 PM Summary Statistics

The summary statistics of size-resolved PM mass concentration are shown in Table 4.1. The highest mean PM mass concentration was measured for the backup filter, which collected particles less than 0.49 μm, at 10.0±4.9 μg/m^3. The lowest was measured for the coarse fraction (>7.2 μm) at 2.4±2.9 μg/m^3. Whole dataset is available by link in Appendix 1.

Table 4.1. Summary statistics of PM mass concentrations (Concentration Unit: μg/m^3)

	Size Fraction (μm)					
	>7.2	**3-7.2**	**1.5-3**	**0.95-1.5**	**0.49-0.95**	**<0.49**
Number of samples	37	39	39	39	39	37
Average	2.4	5.8	4.2	4.3	6.7	10.0
Std. Dev.	2.9	3.9	3.8	3.4	5.2	4.9
Geo. Mean	1.5	4.4	3.2	3.1	4.6	8.7
Median	1.5	5.4	3.4	3.4	4.9	9.2
Max	13.2	21.4	19.9	14.5	21.0	22.3
Min	0.081	0.240	0.381	0.186	0.087	1.234

In Figure 4.1, the temporal variation of size segregated PM was depicted. The total PM concentration rises quickly around the end of June 2021 and drops rapidly around the beginning of July 2021. As it was mentioned in literature revew – the Bolu City in summer is more affected by Long Term transport of particles [119]. The source of this summer peak will be discussed further in this study in Section 4.7. The peak above 40 μg/m^3 in the beginning of the sampling campaign, is explained by local heating activities since peak aligns with negative temperatures. The sudden drop in concentration in March 2021 explained by precipitation because the drop in concentration aligns with local peak in RH. The increase of PM concentration after drop in March also explained by weather, The termperature in April was around 5°C and in May there was a drop to 0. However, despite increase of temperature afterwards

the value in the beginning of the September exceeded 50 µg/m^3, this phenomenon is explained by confirmed Saharan dust incident which was described in Section 4.7. The further increase of PM concentration is also explained by decrease in temperature and usage of domestic heating. The sudden drop in PM concentration in the beginning of February 2022 is explained by heavy snowing. Percipitation is considered as unstable atmospheric condition[97, 98, 101], it prevents aging of the aerosols, while stagnant conditions preventing vertical mixing between atmospheric layers.[101] On February 3 rd it started heavy snowing and on February 11, 2022, it was recorded as the coldest city in the country, with temperatures plummeting to -19°C. The city has also seen its heaviest snowfall since 1950, with snow depth reaching 70 centimeters after three days of continuous snowfall. Such weather has severely impacted daily life, particularly in high areas and the Bolu Mountain pass. The snowfall has caused traffic accidents and disruptions, especially on critical routes like the D-100 highway and the TEM motorway.[167, 168, 169] Thus, such weather decreased PM concentration in February 2022 (Figure 4.1).

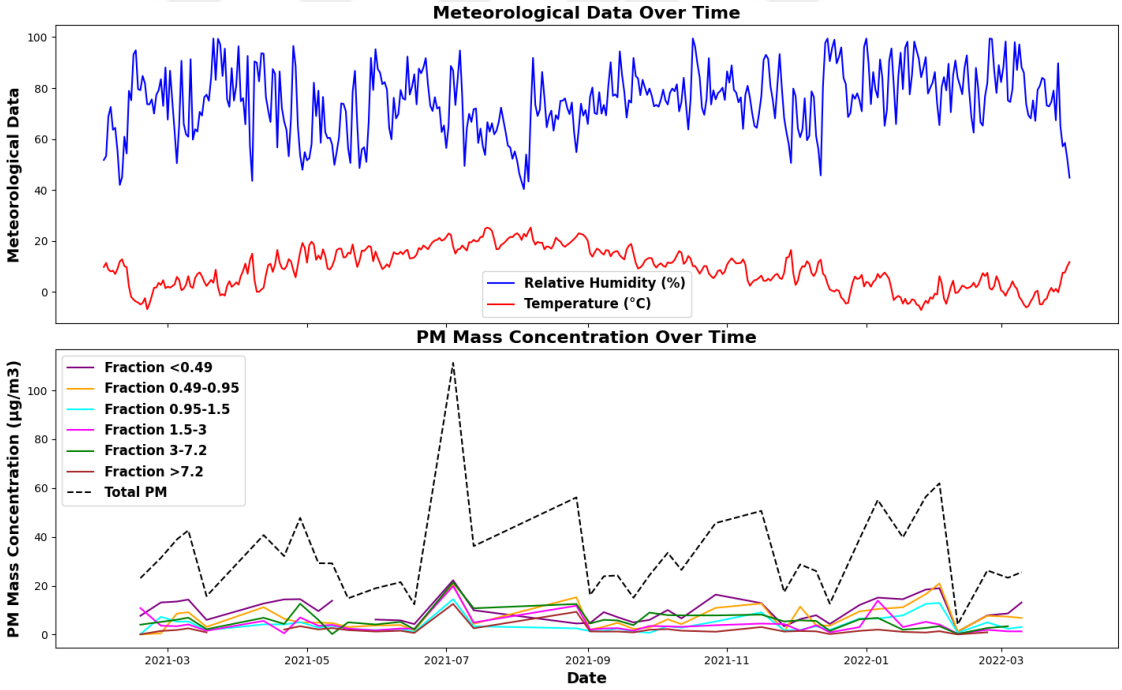


Figure 4.1. PM mass concentration over time with temperature and humidity on one timeline.

The mass of particles collected at each stage is determined gravimetrically to calculate the mass fraction for each size range. Cumulative mass fractions are then computed by progressively summing these fractions from the smallest size upwards.

A log-probability plot is constructed, the particle diameter (µm) on the logarithmic x-axis and the cumulative percentage by weight on the probability-scaled y-axis. Each cumulative mass fraction is plotted against its corresponding upper cut-off diameter. A curve is fitted to these data points, potentially resulting in an equation on Figure 4.2. The Mass Median Aerodynamic Diameter (MMAD) or dp50 is determined at the 50% point on the y-axis. The Geometric Standard Deviation (GSD) is calculated as GSD = $\sqrt{(d84.13\% / d15.87\%)}$ or GSD = d50% / d15.87%. For uni-modal and multi-modal distributions respectively.

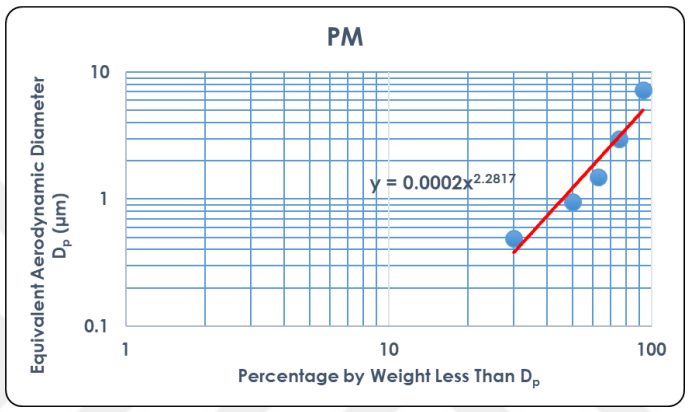


Figure 4.2. Cumulative particle size distribution

Figure 4.3 illustrates the distribution of PM mass concentrations across various size fractions in the Bolu urban atmosphere. The lower and upper line in the boxes represent 25% and 75 % of data, lower and upper whiskers represent 10 % and 90 % of data, the line in the boxes stands for the 50 % (median) and red starts in the boxes show the mean value of the data, those markings applied to all box-plots in this study.The data reveal a distinct bimodal pattern, characterized by elevated concentrations in the ultrafine (<0.49 µm) and coarse (3.0-7.2 µm) modes (Figure 4.3).

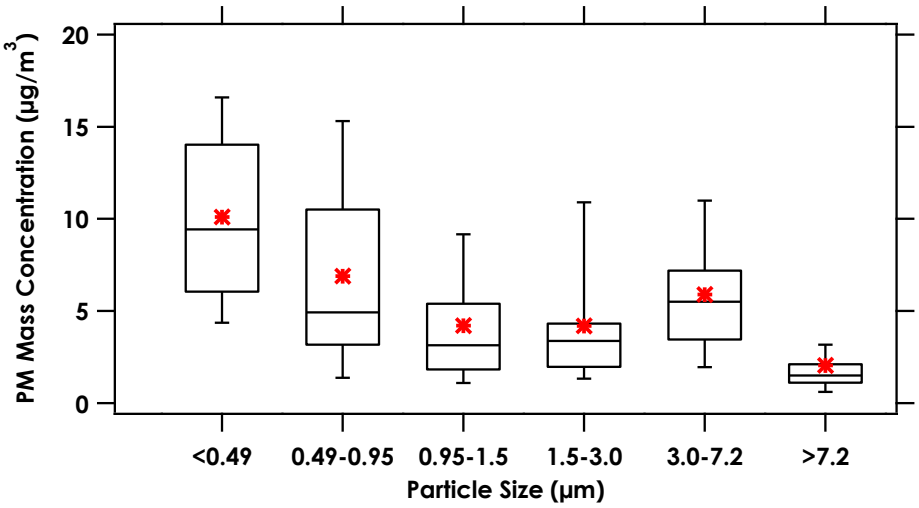


Figure 4.3. Particle size distribution of PM mass concentration

Of particular concern is the high concentration observed in the smallest size fraction (<0.49 µm), which exhibits an average PM mass concentration of approximately 10 µg/m^2. This value 2 times higher than annual WHO's $PM_{2.5}$ guideline[3].

The secondary peak observed in the coarse mode (3.0-7.2 µm) suggests the presence of diverse emission sources or formation mechanisms contributing to the overall particulate load.

4.2 Carbonatious Species

Temporal variation of TC with respect to size fractions was depicted in Figure 4.4. TC concentrations across different particle size fractions reveals significant temporal variations and concerning peak levels. Data show that TC concentrations can reach up to 40 µg/m^3, which same as the daily limit value set for PM_{10} in the Turkish Air Quality Evaluation and Monitoring Regulation[135], while carbon, in its different forms, is only one component of PM[74].

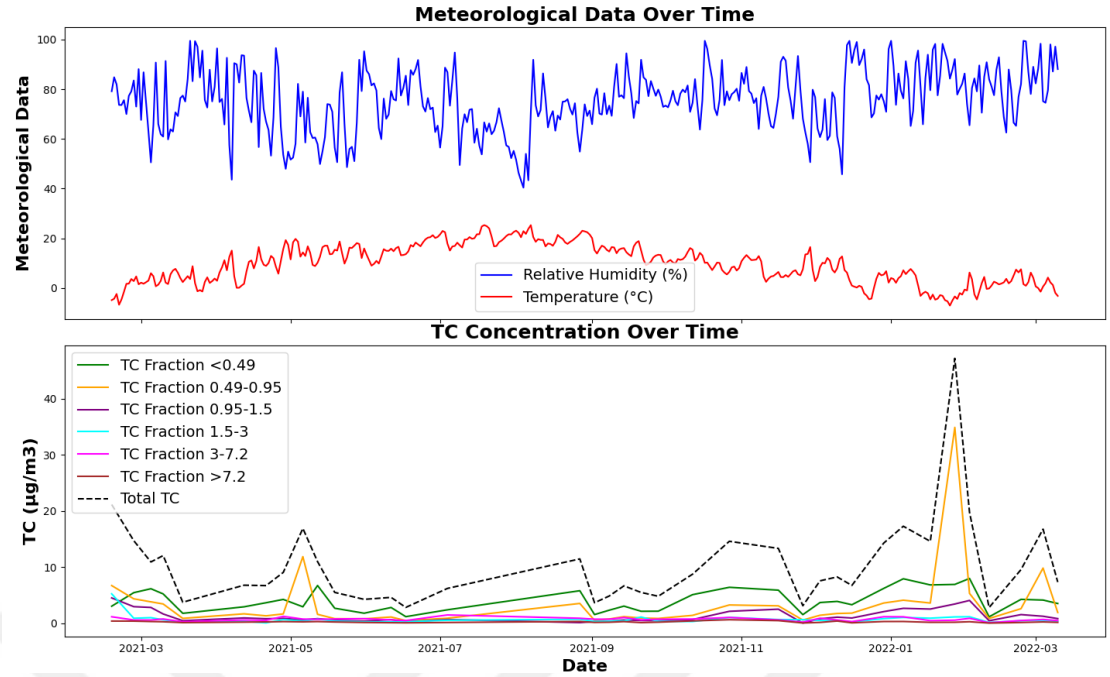


Figure 4.4. Temporal variation of TC concentration with respect to size fraction with Relative Humidity and Temperature data on one timeline.

According to the Figure 4.4, TC values are also subject of seasonal change, with higher TC values observed during winter months. This pattern is likely attributable to increased domestic heating activities, which substantially contribute to carbon emissions during colder periods.[136] The size distribution of TC shows a predominance in finer particle fractions, especially in the <0.49 µm range, indicating a significant contribution from combustion sources and secondary aerosol formation processes.[137] The peak that was observed in July 2021 on Figure 4.1 is absent on Figure 4.4. The concentration of PM is more than 12 times higher than concentration of TC. Which means that despite proved presence of smoke by signature OC/EC value and satellite LiDAR data (Section 4.7), the composition of PM in that peak is not dominated by carbon, unfortunately more detailed analysis like ion analysis in not in the scope of current study. The behaviour of TC through the year explained by outdoor temperature, lower temperature – higher TC, with peaks in the dates with low temperatures, with highest peak in the end of Januarry 2022, when the Temperature graph is at its lowest. After that it repeats same drop as PM concentration in February 2022, due to intensive precipitation.

The cumulative size distribution of TC was depicted in Figure 4.5.

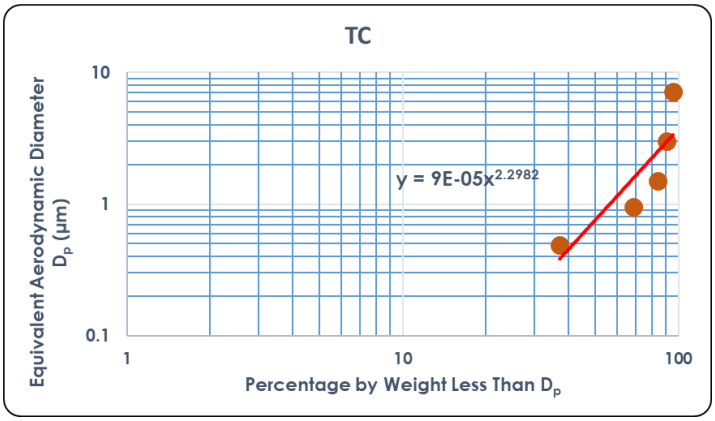


Figure 4.5. Cumulative particle size distribution of TC

The significant portion of TC – 85.81% (Figure 4.5), is concentrated within $PM_{2.5}$ fraction of PM_{10}. This accumulation in fine particles underscores predominant contribution of smaller particulates to overall TC levels.

Annual average concentration of TC in PM_{10} was determined to be 9.89 µg/m^3. $PM_{2.5}$ TC concentration is 8.49 µg/m^3 on annual average basis. Such high proportion of TC in fine particulate matter suggests substantial influence of various emission sources, including both primary emissions and secondary formation processes.

TC distribution across particle sizes reveals characteristic unimodal structure has peak in fine particle range <0.49 µm, as depicted in Figure 4.6. Annual mean TC concentration in this fraction is 3.98 ± 1.96 µg/m^3, which significantly exceeds values for larger particles.

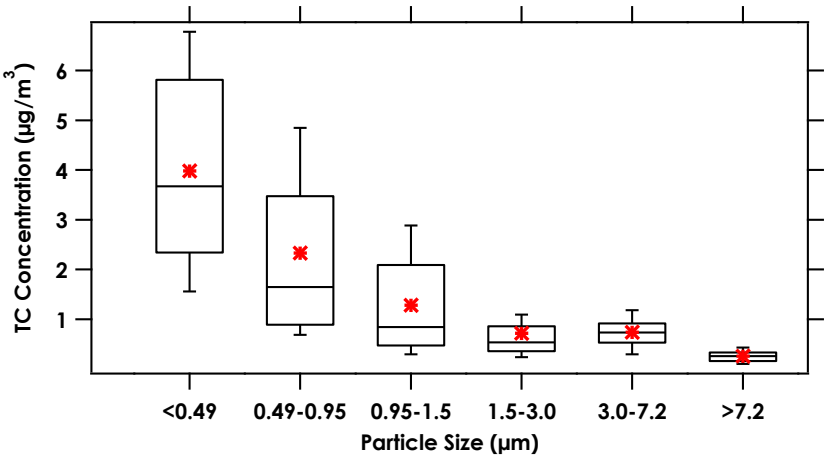


Figure 4.6. Particle size distribution of TC concentration

Fraction >7.2 μm shows minimal TC content with annual mean concentration of only 0.26 ± 0.13 μg/m^3. Such distribution suggests that main sources of TC are likely associated with combustion processes, secondary aerosol formation, and other mechanisms producing fine particles.[137]

Summary of statistics presented on Table 4.2 and Table 4.3. The annual average OC concentration in PM_{10} is reported as 8.91 μg/m³. The calculated annual average $PM_{2.5}$ OC concentration is 8.05 μg/m³ (8.91 × 90.32%). This high proportion of fine particle OC aligns with findings from previous studies in the literature.

Regarding EC, the data shows a similar trend towards fine particles. Given that 98.16% of EC is in the $PM_{2.5}$ fraction of PM_{10}, we can see that EC is predominantly found in smaller particle sizes. The highest average EC concentration is observed in the smallest size fraction (<0.49 μm) at 0.852 μg/m³, with concentrations generally decreasing as particle size increases.

For CC, data is limited, with measurements only available for larger particle sizes (>1.5 μm). This suggests that CC is primarily associated with coarser particles, unlike OC and EC.

The TC data combines the trends seen in OC and EC. The highest average TC concentration is found in the smallest size fraction (<0.49 μm) at 4.92 μg/m³, with a general trend of increasing concentration as particle size decreases. This reflects the dominant influence of OC and EC in the total carbon composition.

Table 4.2. Summary statistics of carbonaceous aerosol mass concentrations (Concentration Unit: μg/m^3)

	Size Fraction (μm)					
	>7.2	**3-7.2**	**1.5-3**	**0.95-1.5**	**0.49-0.95**	**<0.49**
				OC		
Number of samples	36	36	36	37	36	37
Average	0.19	0.58	0.67	1.25	3.06	3.28
Std. Dev.	0.08	0.27	0.81	1.06	4.47	1.63
Geo. Mean	0.17	0.52	0.49	0.86	1.87	2.83
Median	0.18	0.56	0.51	0.82	1.60	2.83
Max	0.44	1.47	5.12	4.40	26.21	6.19
Min	0.05	0.10	0.08	0.05	0.49	0.83
				EC		
Number of samples	33	35	36	36	37	29
Average	0.015	0.028	0.030	0.079	0.499	0.852
Std. Dev.	0.009	0.023	0.024	0.112	1.422	0.512
Geo. Mean	0.012	0.022	0.024	0.036	0.118	0.699
Median	0.013	0.021	0.023	0.025	0.122	0.695
Max	0.038	0.128	0.131	0.512	8.655	2.278
Min	0.003	0.007	0.006	0.001	0.007	0.168
				CC		
Number of samples	27	25	6			
Average	0.11	0.14	0.05			
Std. Dev.	0.08	0.07	0.01			
Geo. Mean	0.09	0.12	0.05			
Median	0.09	0.15	0.05			
Max	0.41	0.27	0.06			
Min	0.03	0.02	0.04			

Table 4.3. Summary statistics of carbonaceous aerosol mass concentrations (Concentration Unit: μg/m^3) (continued)

	Size Fraction (μm)					
	>7.2	**3-7.2**	**1.5-3**	**0.95-1.5**	**0.49-0.95**	**<0.49**
	TC					
Number of samples	36	36	37	36	37	15
Average	0.56	0.71	0.88	2.05	4.17	4.92
Std. Dev.	0.35	0.82	0.85	2.14	5.44	2.08
Geo. Mean	0.44	0.52	0.66	1.40	3.03	4.36
Median	0.60	0.53	0.66	1.30	2.95	4.27
Max	1.50	5.25	4.53	11.88	34.87	7.99
Min	0.05	0.08	0.14	0.05	0.59	1.17

4.2.1 OC Concentrations

Table 4.2 and Table 4.3 show the summary statistics of carbonaceous aerosol mass concentration for different particle sizes. For OC, the highest mean concentration was found at stage 5 (0.49-0.95 μm) at 6.43±9.3 μg/m^3, and the lowest mean concentration was found at the first stage at 0.40±0.20 μg/m^3. The concentration of OC through the year is depicted on Figure 4.7. The trend repeats the one for TC, with peaks aligning with temperature drops, when domestic heating intensifies. Across whole dataset the concentration of OC was higher than concentration of EC. The rise of OC in the end of August 2021 is discussed in Section 4.7 of this study.

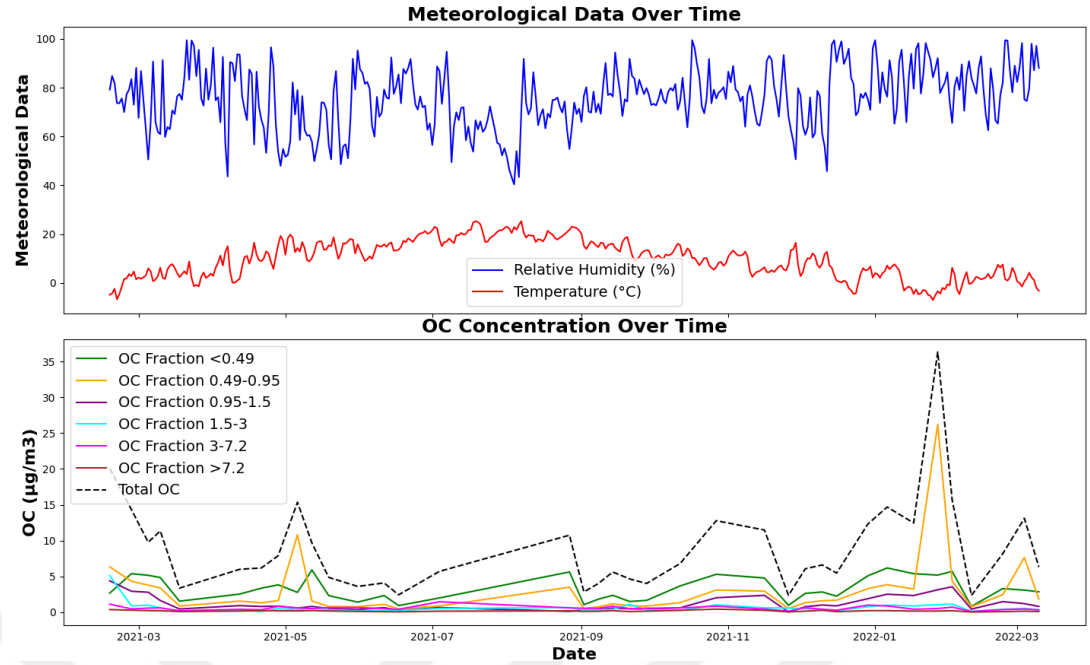


Figure 4.7. Temporal variation of OC concentration with respect to size fraction, with Relative Humidity and Temperature

The cumulative size distribution of OC was depicted in Figure 4.8. Analysis of the OC concentrations indicates that $PM_{2.5}$ OC constitutes 90.32% of the PM_{10} OC. The annual average OC concentration in PM_{10} is reported as 8.91 µg/m³. The calculated annual average $PM_{2.5}$ OC concentration is 8.05 µg/m³ (8.91 × 90.32%). This high proportion of fine particle OC aligns with findings from previous studies in the literature.

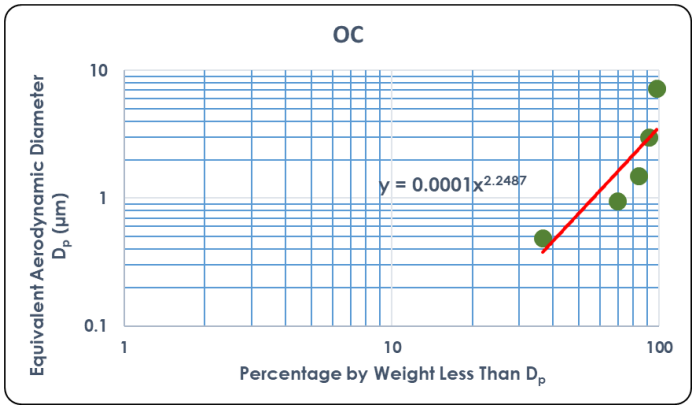


Figure 4.8. Cumulative particle size distribution of OC

Chen et al. (1997)[138] reported that 75.1% of OC mass was found in particles less than 1 µm in diameter, with 84.9% in particles less than 2.5 µm. These observations were attributed to fresh primary emissions, particularly in traffic-dominated

environments (John H. Offenberg & Joel E. Baker, 2000)[139]. More recent research by Liu et al. (2023)[140] corroborates these findings, revealing that over 90% of OC was concentrated in fine particles in samples collected in China. These reports align with observed particle size distribution of OC depicted on Figure 4.8.

The particle size distribution of OC was depicted in Figure 4.9. The smallest size fraction (<0.49 µm) consistently contributes a significant portion of the total OC, further supporting the dominance of fine particle OC in urban atmospheres.

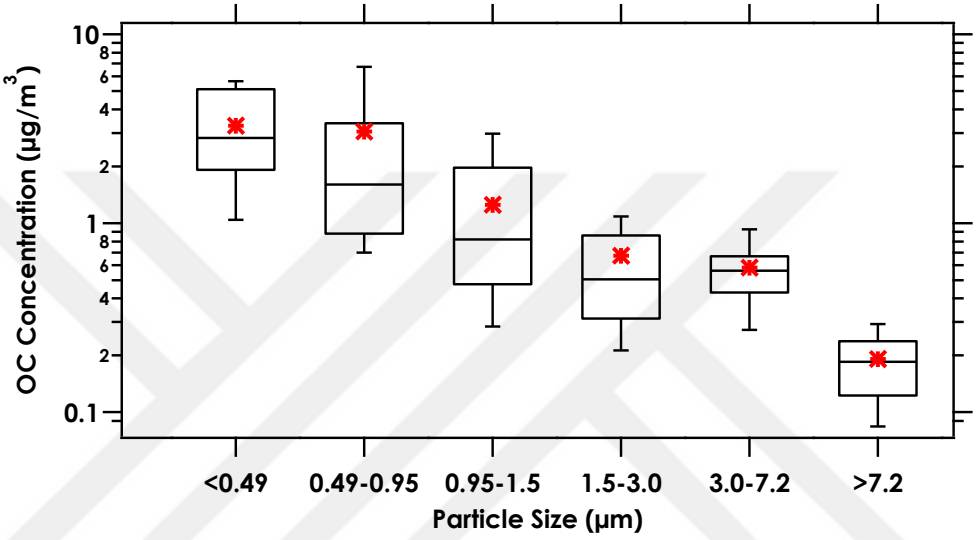


Figure 4.9. Particle size distribution of OC concentration

The observed unimodal distribution of OC presented on Figure 4.9, with a clear accumulation mode in the smallest size fraction (<0.49 µm).

Annual mean OC concentration in the <0.49 µm fraction is 3.28 ± 1.66 µg/m³. This value approaches the WHO's annual limit for $PM_{2.5}$. It is crucial to emphasize that OC represents only one component of particulate matter, and concentration of only one fraction approaches limit, indicating that the total $PM_{2.5}$ concentration in this area likely exceeds health-based guidelines substantially.

4.2.2 EC Concentrations

The temporal variation of EC concentration with respect to size fraction was shown in Figure 4.10. In comparison to OC the pattern fluctuates significantly less, with only minor peaks correlated with temperature, however, the EC behaviour completely unaffected in summer, with a peaks during heating season.

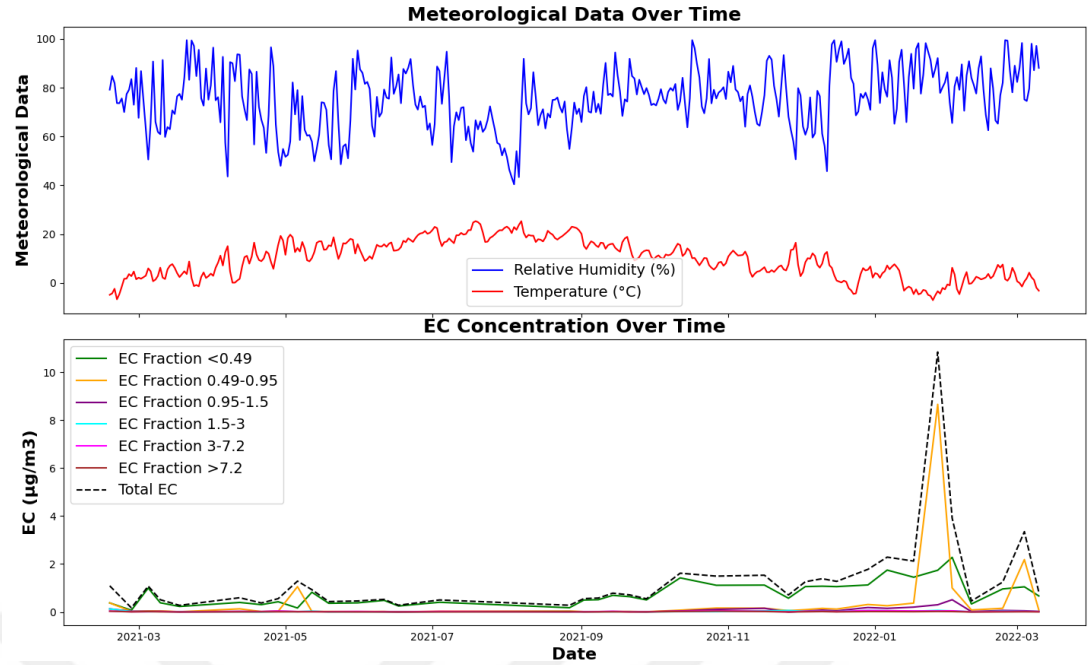


Figure 4.10. Temporal variation of EC concentration with respect to size fraction

The obtained data reveal a seasonal pattern, with significant episodic peaks occurring predominantly during the winter months, that pattern can be observed on Figure 4.10. These winter episodes are characterized by sharp increases in EC levels, particularly in the finest particle fractions (<0.49 µm and 0.49-0.95 µm). The occurrence of these high-concentration events can be attributed to a combination of stable air conditions, which limit atmospheric dispersion, and increased emissions from domestic heating necessitated by lower urban temperatures. Throughout the year, the smallest size fraction (<0.49 µm) contributes a significant portion of the total EC concentration, dominating during peak events. In contrast, coarser particle fractions (>3 µm) exhibit relatively stable and low EC concentrations through the sampling compaign.

The cumulative sparticle size distribution of EC was depicted in Figure 4.11. It indicates that 98.16% of EC $PM_{2.5}$ fraction of PM_{10}. Which is similar to OC accumulation trend. The annual average concentration of EC in PM_{10} was determined to be 1.32 µg/m^3. $PM_{2.5}$ EC concentration is 1.30 µg/m^3 on average annually.

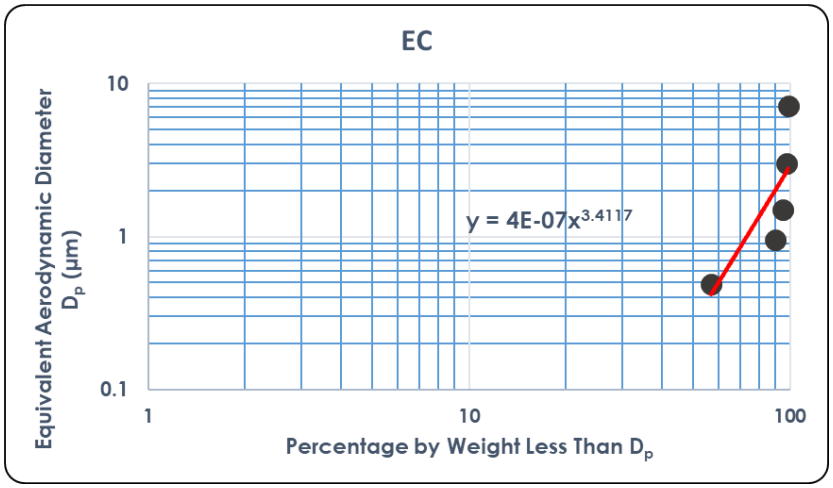


Figure 4.11. Cumulative particle size distribution of EC

EC distribution across particle sizes has unimodal structure with peak in fine particle range <0.49 µm, as presented on Figurre 4.12.

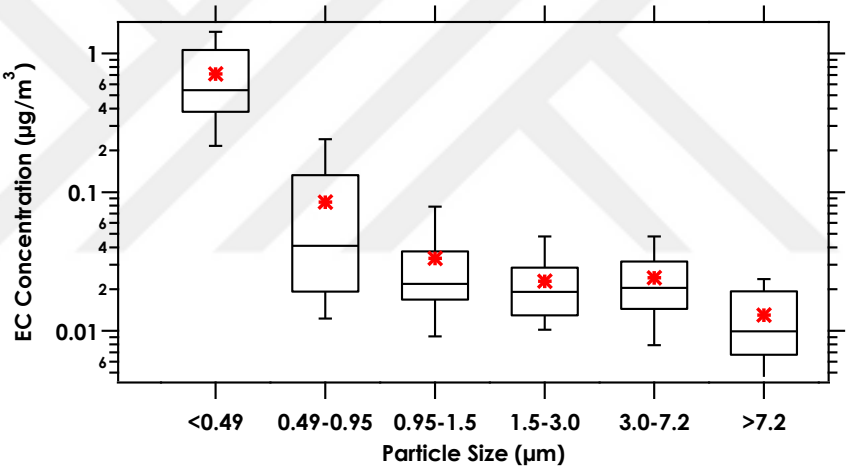


Figure 4.12. Particle size distribution of EC concentration

This indicates preferential accumulation of EC in fine aerosol fraction. Annual mean EC concentration in this fraction is 0.71±0.45 µg/m^3, which significantly exceeds values for larger particles. In contrast, fraction >7.2 µm shows minimal EC content with annual mean concentration of only 0.013±0.008 µg/m^3.

4.2.3 CC Concentrations

Temporal variation of CC concentration with respect to particle size fraction was depicted in Figure 4.13. In contract to OC and EC, the contribution of larger size particles (> 7.2 µm and 3-7.2 µm) to CC concentration is higher. CC peaks in the end

of April 2021, emd of August 2021, and in Januarry 2022 were more closely described in Section 4.7. For the rest of the data there was no evidence of long-range particle transfer from Africa. Thus, it is assumed that the rest of the CC is local dust.

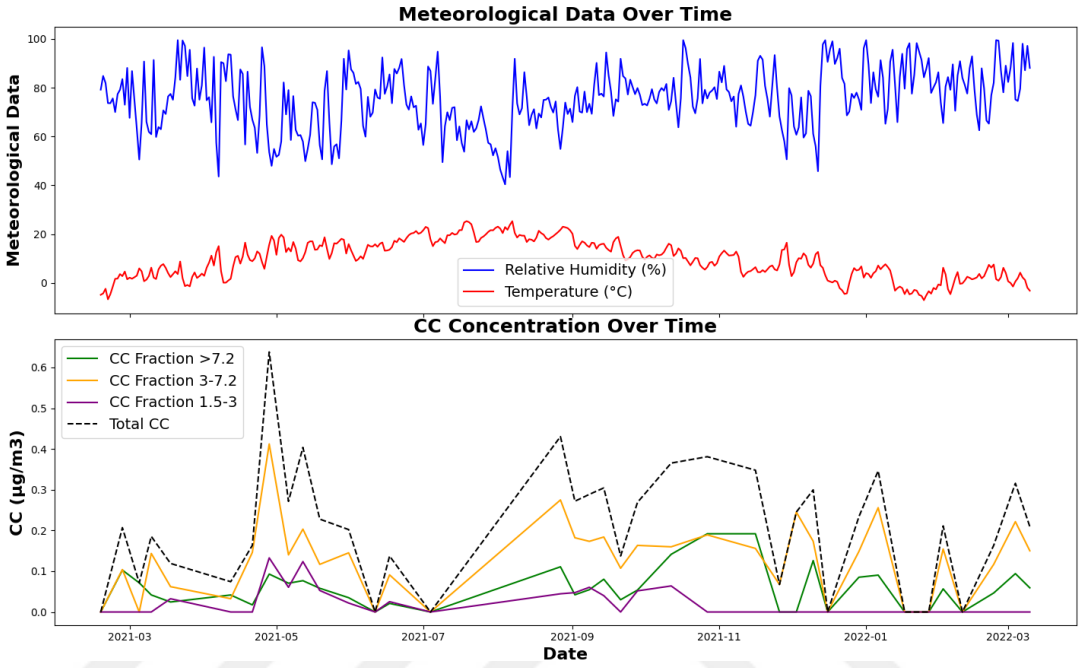


Figure 4.13. Temporal variation of CC concentration with respect to size fraction

Cumulative particle size distribution of CC was depicted in Figure 4.14. Annual average concentration of CC in PM_{10} was determined to be 0.19 µg/m^3. $PM_{3.0}$ CC concentration is 0.03 µg/m^3 on average anually. Such difference between PM_{10} and $PM_{3.0}$ underlines the dominance of CC coarse fractions.

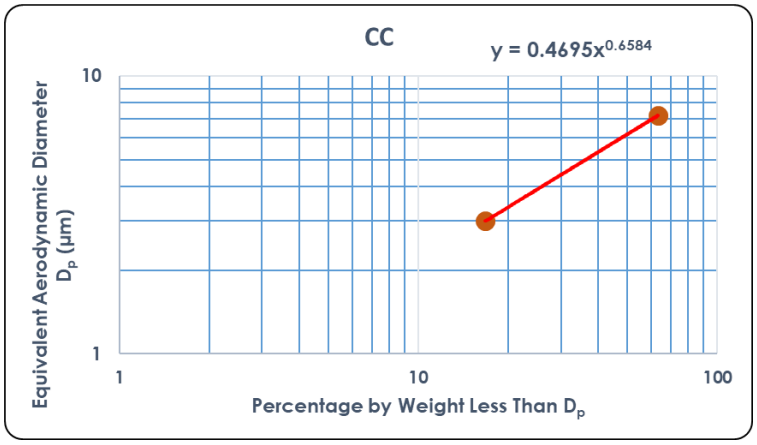


Figure 4.14. Cumulative particle size distribution of CC

According to Figures 4.13 and 4.14, 16.73% of CC, is concentrated within $PM_{3.0}$ fraction of PM_{10}. In the finer fractions presence of CC is not observed.

The particle size distribution of CC concentration was shown in Figure 4.15. The peak concentration is observed within the 3.0-7.2 µm particle size range, where CC reaches a mean value of 0.16±0.07 µg/m^3. This dominance of CC in larger particles strongly suggests its primary origin from natural sources rather than anthropogenic emissions. The observed size distribution pattern (Figure 4.15) aligns with typical characteristics of naturally released particulates, such as those derived from mechanical processes involving plant materials or soil particles.[141]

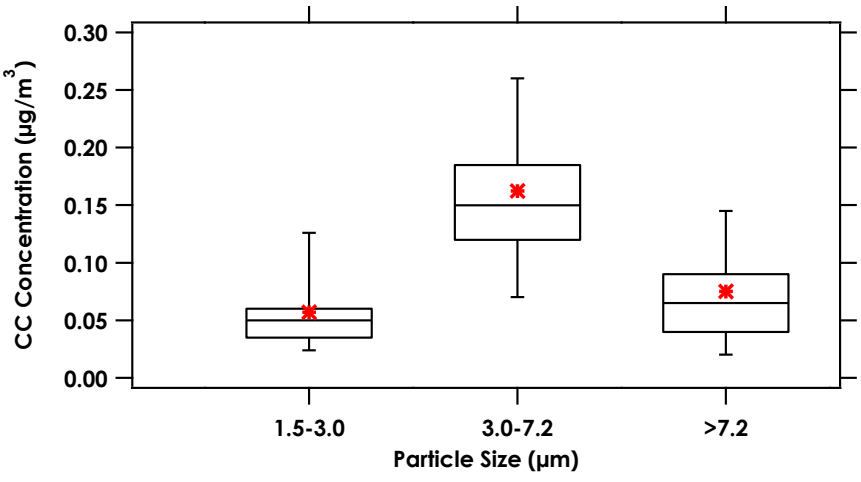


Figure 4.15. Particle size distribution of CC concentration

4.3 Literature Comparison to Other Locations

The OC and EC concentrations measured in this study are compared with other reported values in the literature as shown in Table 4.5 and location's characteristics in Table 4.4. The OC levels measured in this study in both PM_{10} and $PM_{2.5}$ fractions are in the middle values in Table 4.5. Notably, the OC/EC ratios observed in Bolu city, Türkiye (10.84 for PM_3 and 11.15 for PM_{10}) are not significantly differ than most other urban locations, suggesting a predominance of organic carbon sources (like OC_{pri} and SOC) in this area, due to observed peaks in winter, in that season main source of OC particles is domestic heating[14]. In the rural costal areas, we can observe significant OC/EC ratio for Erdemli, while Bolu is about 60 km away from Black Sea. The values for this study in Table 4.5 are averages of OC and EC, and average across all calculated values of OC/EC.

The criteria of choice of locations are based on type of the background. Since OC/EC is dimentionless parameter, the level of pollution is not the key, since it is OC/EC value that indicates source. Bolu is urban, with no heavy industry, with 2 highways piercing city and mountains around. The key factor that impacts OC/EC value is type of source, and consequently type of background. Thus, the choice of cities to compare should be around sources and background. In terms of types of location there are 4 main ones: urban, semi-urban, rural, and industrial. Some locations can be mixed like Lower Silesia, Poland. The focus of this study is Türkiye, so it is important to compare to other locations in Türkiye, like Düzce[107], which is similar and close to Bolu. Cities like Istanbul and Ankara also provide important insights as the cities with traffic emissions as main source. The comparison in tables 4.4 and 4.5 allows to understand the position of Bolu as urban location among other cities in Mediterranian region, cities in typical urban environment, how different Bolu's urban from different rural locations, and difference between Bolu and other cities in Türkiye.

Table 4.4. Characteristics of locations from literature

Reference	Location	Type	Geography	Climate	Potential Sources
[102]	Lower Silesia, Poland	Regional background, industrial, urban background	SW Poland, bordering Germany and Czech Republic	Continental (implied)	Coal combustion, transport, industrial activities
[103]	Athens, Greece	Urban background	Central Athens, small hill (110 m a.s.l.)	Mediterranean (implied)	Urban activities
[104]	Erdemli, Türkiye	Rural coastal	Eastern Mediterranean coastline, 22 m a.s.l., 10 m from sea	Mediterranean (implied)	Marine and rural sources
[105]	Elche, Spain	Urban	SE Spain, 12 km from Mediterranean coast	Dry Mediterranean	Traffic (main source), no heavy industry
[106]	Nanjing, China	Suburban	Northern Nanjing, 20 km from downtown	Subtropical monsoon (implied)	Not specified
[107]	Düzce, Türkiye	Urban and suburban	NW Türkiye, flat terrain surrounded by mountains	Not specified	Traffic, industrial zones, various plants
[108]	Pinnacle State Park, NY, USA	Urban	SW New York State, 504 m a.s.l.	Humid continental (implied)	Nearby towns and highway
[109]	Mid-Brahmaputra Valley, India	Rural institutional, remote, roadside	Assam, India, along Brahmaputra River	Four seasons: Pre-monsoon, Monsoon, Post-monsoon, Winter	Biomass burning, vehicles, some industrial activities
[110]	Lower Silesia, Poland	Urban background, industrial, regional background	SW Poland, bordering Germany and Czech Republic	Continental (implied)	Industrial activities, urban emissions

Table 4.5. Literature comparison of measured parameters

Sampling Location	Sampling Period	PM Fraction	OC	EC	OC/EC Ratio	Reference
Bolu city, Türkiye	February 2021-March 2022	PM_3	8.16	1.28	10.84	This study
Bolu city, Türkiye	February 2021-March 2022	PM_{10}	8.91	1.32	11.15	This study
Bolu city, Türkiye	December 2014-February2015	$PM_{2.5}$	59.9	5.9	10.1	Öztürk & Keleş (2016)[101]
Osieczów, Poland (indutsrial)	January2011-December 2011	PM_{10}	7.7	1.0	7.7	Górka, M., Kosztowniak (2015)[102]
Athens, Greece (urban)	December 2013-March2016	$PM_{2.5}$	4.0	1.5	2.7	Theodosi et al. (2018)[103]
Ankara, Türkiye (urban)	July 2014-September 2015)	$PM_{2.5}$	8.8	2.4	3.7	Koçak et al. (2021)[104]
Elche, Spain (urban)	February 2015-February2018	PM_{10}	7.5	1.7	4.6	Galindo et al. (2020)[105]
Nanjing, Çhina (semi-urban)	September 2018-September2019	$PM_{2.5}$	8.8	3.0	2.9	Yang et al. (2021)[106]
Düzce, Türkiye (urban)	January-March 2015	PM_{10}	28.6	2.3	12.4	Aslan Kılavuz et al. (2019)[107]
Düzce, Türkiye (semi-urban)			6.7	0.6	11.2	
Pinnacle State Park (New York), USA (urban)	December 2004-December 2008	$PM_{2.5}$	1.6	0.1	11.4	Bae et al. (2011)[108]
Brahmaputra, India (rural)	December 2010-October 2014	PM_{10}	4.1	14.7	0.3	Bhuyan et al. (2018)[109]
Zgorzelec, Polond (urban)	January-October 2011	PM_{10}	7.6	1.6	4.8	Górka et al. (2020)[110]
Działoszyn, Polond (industrial)			5.1	0.7	7.3	
İstanbul, Türkiye	January 2017- January 2018	$PM_{2.5}$	11.3	4.1	2.8	Flores et al. (2020) [89]

These high ratios could be indicator of significant secondary organic aerosol formation, biomass burning, or other organic-rich emission sources. The values are particularly high compared to urban areas like Athens, Greece (2.7)[103] or Ankara, Türkiye (3.7), which typically show lower OC/EC ratios due to higher EC emissions from traffic.[104] This observation aligns with findings from studies in China, Spain, and the Czech Republic, on those examples, for this study the observation of OC/EC dynamics in urban and rural environments can be performed. These studies reported OC/EC ratios ranging from 1.9 to 6.0[111 112 113], with higher ratios generally observed in summer and at urban sites. In the Bolu City OC/EC values are much higher (Table 4.5).

The Shanghai study, for instance, found that carbonaceous aerosols contributed significantly to $PM_{2.5}$, accounting for about 27.2% of the total mass on an annual average. Study indicated clear seasonal variations in both OC and EC concentrations, with SOC contributing between 2.4% and 66.8% of OC.[113] Similarly, the Madrid[112] study revealed seasonal variations in OC/EC ratios, with lower values in winter and higher values in spring-summer.[112] They attributed this to the fact that in summer, EC concentrations decrease more strongly than OC due to lower primary emissions and better dispersion, while complementary sources of OC (biogenic aerosol and secondary particulate formation) are present.

The formation of SOC, which is favored by higher temperatures and solar radiation, could explain the increased OC/EC ratios in Bolu city, especially if the measurements were taken during warmer months, explaining OC/EC ratio peak that was observed in Bolu city in summer. The Madrid study found that in summer, daily SOC production ranged from 80 to 92%, whereas in winter months it varied from 70 to 84%.[112]

Traffic emissions were identified as a major source of primary OC and EC in urban areas across these studies, and Bolu is not an exception. Currently in the studied period there are 4 main contributors to PM in city – automobile vehicles (for the whole year) that contribute to SOC, Saharan dust in summer, SOC in winter – due to excess of the unidentified gas emissions and in Summer due to the solar activity. In Spring and Autumn SOC shown negatie trend with the increase of temperature, for example in November 2021 temperature increased from -5 to +5 –

this increased intencity of domestic heating, while solar activity is still low in comparison to summer. And domestic heating during winter that also contributes to SOC.

4.4 Seasonal Variations of PM and Carbonaceous Species

This section will be more closely focused on comparison of obtained data between seasons, and fractionated data within particular season.

4.4.1 Seasonal variation of PM

The seasonal variation of PM mass concentration with respect to particle size was depicted in Figure 4.16.

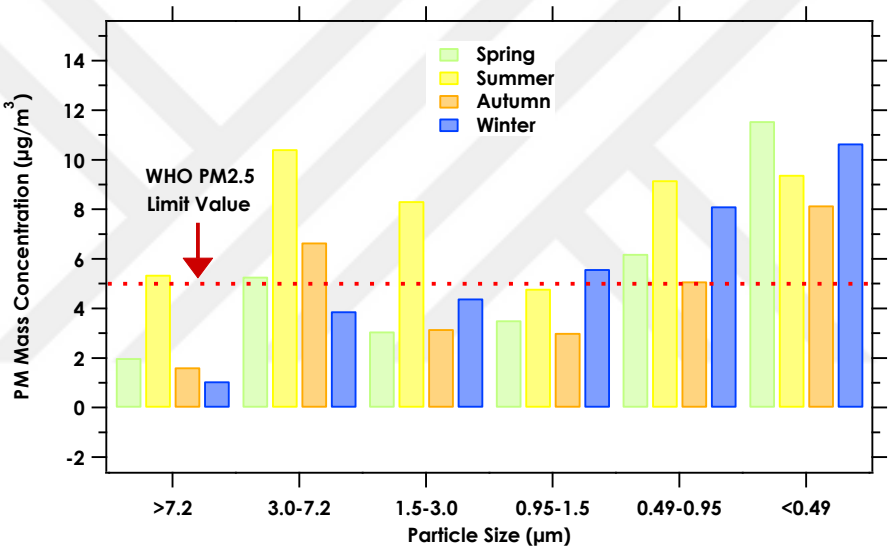


Figure 4.16. Seasonal distribution of PM mass concentration with respect to particle size fraction

The seasonal variation of different PM fraction for spring, summer, autumn, and winter are shown on Figure 4.16, covering particle sizes from >7.2 µm to <0.49 µm. A horizontal dotted line indicates the WHO $PM_{2.5}$ limit value, which is 5 µg/m^3.

PM concentrations exceed the WHO $PM_{2.5}$ limit value across all size fractions and seasons[3], pointing to a persistent air quality issue throughout the year. A significant trend emerges in the PM mass concentration, with higher levels in the two smallest size fractions (0.49-0.95 µm and <0.49 µm). The dominance of fine and ultrafine particles is particularly concerning from a health standpoint, as these

can penetrate deeper into the respiratory[24] system as was pointed out in literature review section.

Larger particles (>7.2 µm) appear more concentrated in spring and summer, possibly due to factors like dust[141] or pollen[134]. In contrast, smaller particles show elevated levels across multiple seasons, suggesting diverse and persistent sources of fine particulate pollution.

4.4.2 OC Seasonal Variations

The seasonal variation of OC concentration with respect to particle size was shown in Figure 4.17.

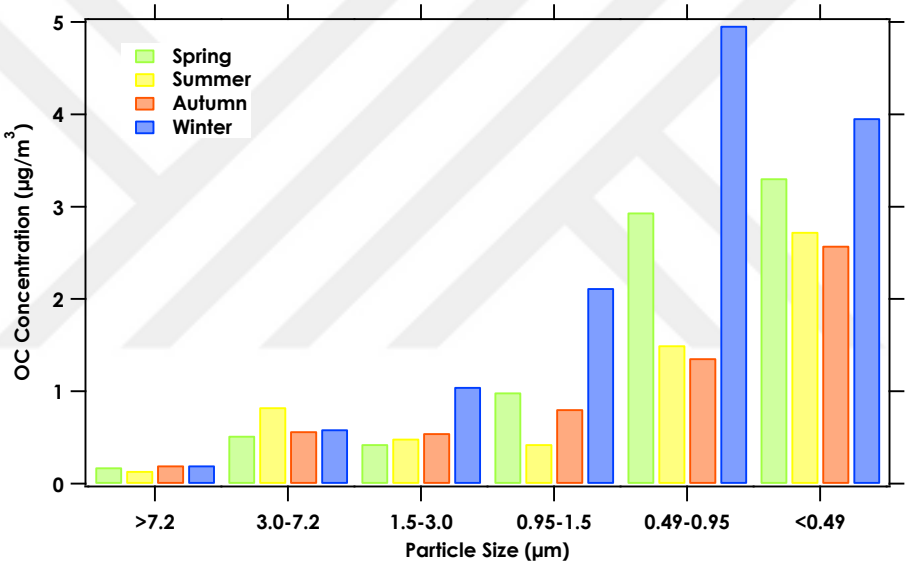


Figure 4.17. Seasonal variation of OC concentration with respect to particle size fraction

Variation of OC in the finest particle fraction (<0.49 µm) is characterized by high spread shown in the Figure 4.17. In this size range, winter and spring exhibit markedly higher average concentrations compared to summer and autumn. This seasonal disparity is likely attributed to increased combustion activities for domestic heating during colder months.

The data also demonstrate a general trend of increasing OC concentrations as particle size decreases, with the highest concentrations consistently observed in the <0.49 µm fraction across all seasons. This observation aligns with previous studies indicating the predominance of organic carbon in fine and ultrafine particles.

Seasonal variations are present across other size fractions as well, however the patterns is different. For example, in the 0.95-1.5 µm range, spring shows the highest concentration, while winter dominates in the 0.49-0.95 µm fraction.

The coarser particles (>7.2 µm) exhibit relatively low OC concentrations across all seasons, indicating that organic carbon is primarily associated with finer particle fractions in this urban environment.

4.4.3 EC Seasonal Variaton

Winter EC levels (Figure 4.18) dominate across all fractions, as shown on Figure 4.18, indicating presence of emission sources during the cold period. There is clear tendency for EC concentrations to increase as particle size decreases, reaching maximum in the finest fraction (<0.49 µm). In general, the seasonal fraction trends repeat the one for OC.

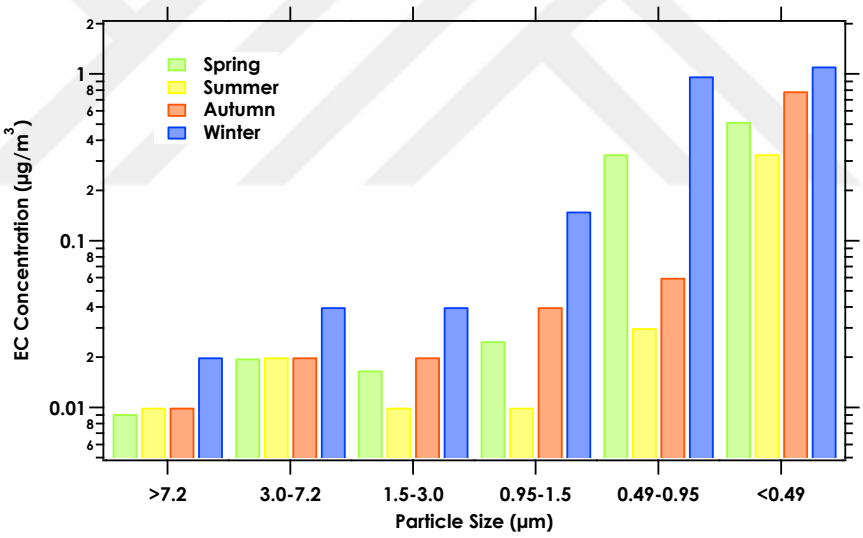


Figure 4.18. Seasonal variation of EC concentration with respect to particle size fraction

4.4.4 CC Seasonal Variations

The seasonal variation of CC with respect to particle size is depicted in Figure 4.20. According to Figure 4.19 in the coarse fraction (>7.2 µm), a relatively uniform distribution of CC is observed across seasons, with a slight predominance in autumn. This may indicate stable sources of coarse carbonate particles, such as resuspended soil dust.

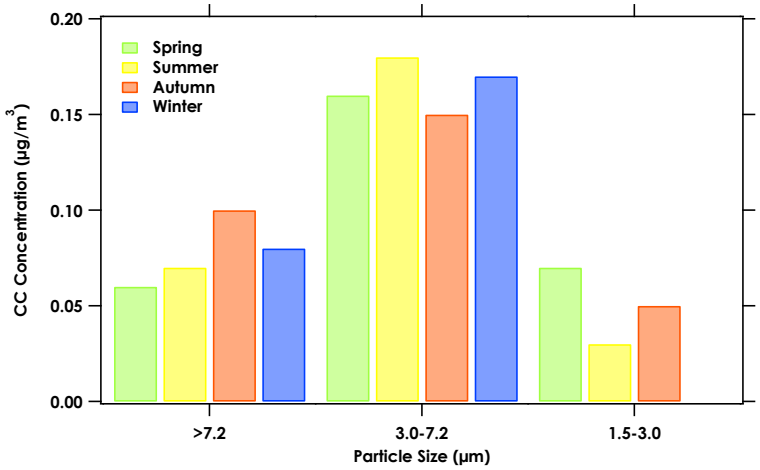


Figure 4.19. Seasonal variation of CC concentration with respect to particle size fraction

Seasonal variatiability of CC that observed in the fraction 3.0-7.2 µm is higher than that of fraction >7.2 µm, however the variation is not as evident than in OC and EC. The CC value is more likely to be impact with long-range transfer, for example Dust episodes in sahara. Urban environments tend to have higher concentration of coarser particles in summer.[29] The examples below are evidence of such impact being possible, and likely happening in Bolu, since several Saharan dust episodes were proven in section 4.7.

Varga et al. (2014)[156] analyzed Saharan dust intrusions into the Mediterranean Basin using long-term aerosol data from 1979-2012. Their study confirmed that Saharan dust is a significant component of the Mediterranean atmosphere, particularly during spring and summer. The research identified two primary synoptic patterns associated with dust events: spring events linked to eastward-moving low-pressure systems affecting the Central and Eastern Mediterranean, and summer events connected to the northward migration of the subtropical high-pressure belt impacting the Western and Central Mediterranean. The study revealed spatial variations in dust activity across the Mediterranean, with the Western region experiencing peak intrusions in summer, the Eastern region in spring, and the Central region showing peaks in both seasons.[156]

Conte et al. (2020)[157] conducted a long-term study of African dust advection in south-eastern Italy from 2013 to 2018. The research identified 56 Saharan dust (SD) events over the measurement period, covering 147 days or approximately 10%

of the total time. Analysis revealed a clear seasonal pattern in dust event frequency. During warm seasons (spring and summer), 33 events were recorded over 91 days, accounting for 12.5% of warm season measurement days. Cold seasons (autumn and winter) experienced 23 events over 56 days, representing 7.5% of cold season measurement days. This seasonality, with higher occurrence during warmer months, aligns with previous observations in the eastern Mediterranean basin and other Italian sites. The study also examined the impact of these events on particulate matter concentrations, finding significant increases in PM_{10} levels during SD events, particularly in warm seasons.[157]

Cuevas-Agulló et al. (2024)[158] examined the notable increase in Saharan dust intrusions over the western Euro-Mediterranean (WEM) region during February-March 2020-2022. Their study revealed that these dust events were closely linked to specific atmospheric circulation patterns. The researchers identified two main large-scale configurations associated with dust intrusions: European blocking with poleward-shifted jets, and Mediterranean subtropical ridges with intensified mid-latitude jets. Cut-off lows between the Canary Islands and Iberian Peninsula were found to be key synoptic drivers of dust transport.[158]

4.4.5 TC Seasonal Variations

The seasonal variation of TC concentration with respect to particle size was illustrated in Figure 4.20. TC distribution across particle sizes reveals significant seasonal variations and size-dependent trends (Figure 4.20). Winter TC levels dominate in most fractions, especially in finer particles. There is clear tendency for TC concentrations to increase as particle size decreases, reaching maximum in finest fraction (<0.49 μm).

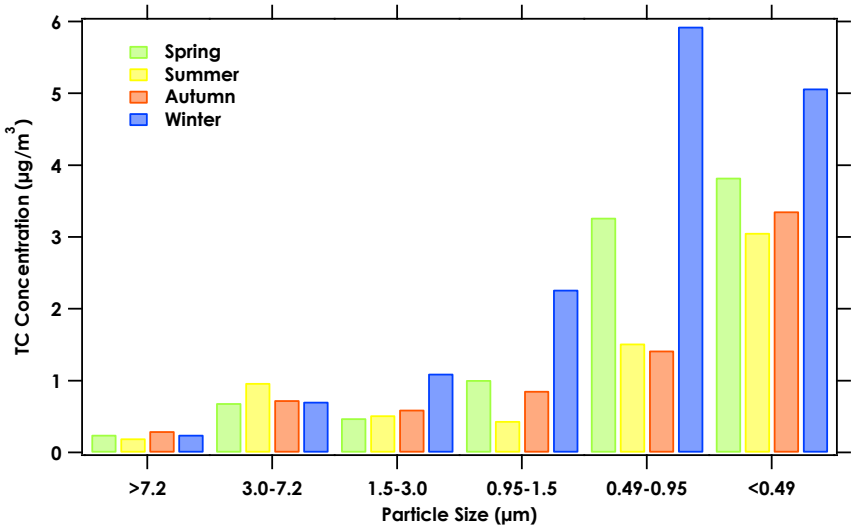


Figure 4.20. Seasonal variation of TC concentration with respect to particle size fraction

Spring shows relatively high TC levels in some mid-range particle sizes (0.49-0.95 µm). Summer generally exhibits lower TC concentrations across all size fractions.

4.5 SOC Calculation and Seasonal Variations

The percentiles with the lowest R^2 value for percentiles of lowest OC/EC for each fraction are described in Table 4.6.

Table 4.6. Summary of statistic for every fraction for best fitting percentile.

	Fraction	Chosen Percentile	OC/EC_{pri}	R-value
1	<0.49	0.05	2.641898	1.00
2	0.49-0.95	0.05	2.868462	1.00
3	0.95-1.5	0.05	5.14828	1.00
4	1.5-3	0.05	7.966807	1.00
5	3-7.2	0.10	9.717486	0.952809
6	>7.2	0.05	18.048080	1.00

The percentile was chosen by selecting the highest R^2, as presented in the Table 4.6. In Figure 4.10, SOC value is high in the $PM_{2.5}$ fraction, while in the coarse fraction, SOC does not demonstrate such a peak. Comparing it with the total

SOC graph (Figure 4.21), the level of SOC formation remains high throughout the sampling period, indicating that one of the major sources of OC in Bolu city is SOC. In source apportionment studies, SOC is usually treated as a separate source due to its separate formation processes and significant contribution to total organic carbon in particulate matter.[124, 125] To locate exact sources of SOC (released gases) special gas sencors required, those measurements are not in the scope of the current study. Thus, this study will treat SOC as separate source of OC.

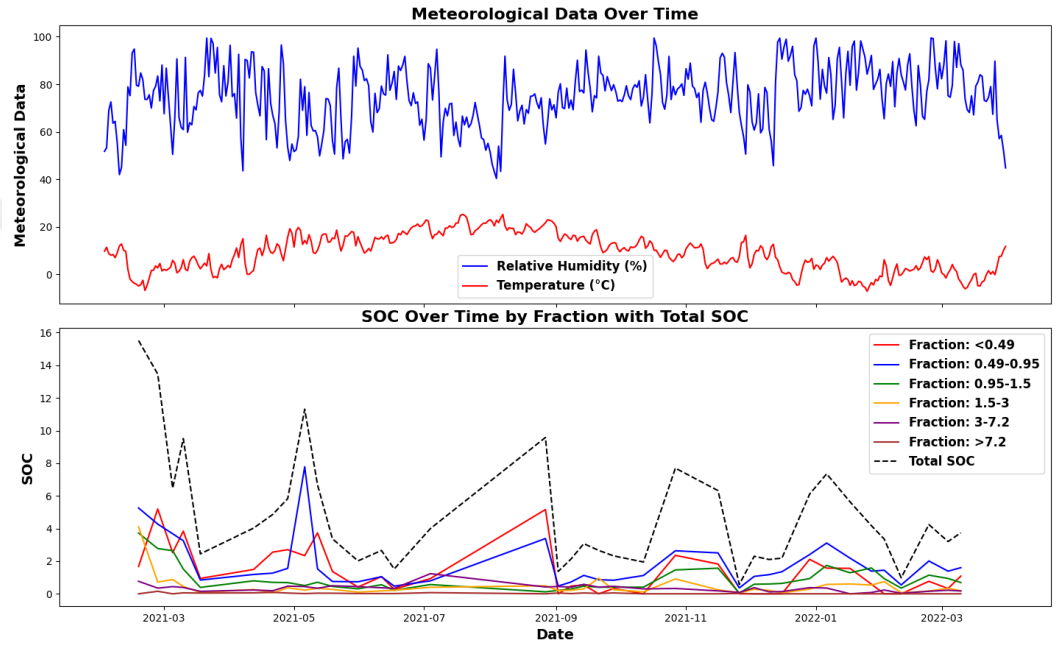


Figure 4.21. SOC values across all fractions during sampling period and meteorological data.

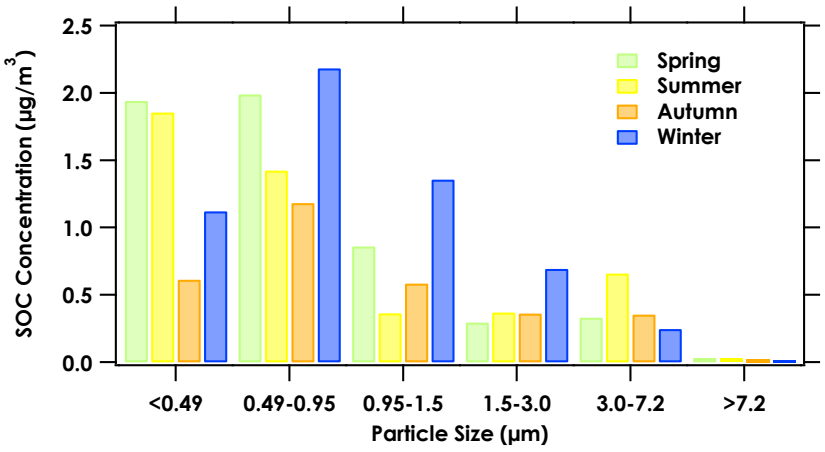


Figure 4.22. Temporal variation of SOC concentration with respect to size fraction

Winter emerges as the season with the highest SOC levels (Figure 4.22), particularly in the fine particle range. The highest mean SOC concentration is observed during winter in the 0.49-0.95 µm size fraction, reaching 2.18±1.34 µg/m^3. This peak in fine particle SOC during colder months likely results from a combination of factors, including increased emissions from residential heating, reduced atmospheric mixing, and enhanced gas-to-particle conversion processes under low temperature conditions.[142]

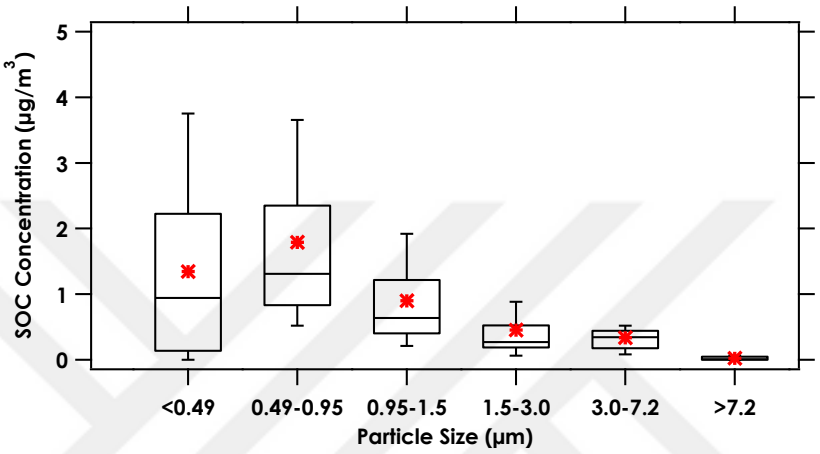


Figure 4.23. Particle size distribution of SOC concentration

The size distribution of secondary SOC (Figure 4.23) in atmospheric aerosols demonstrates unimodal pattern, with a clear accumulation mode centered in the fine particle range of 0.49-0.95 µm. This distribution profile is characteristic of SOC formation processes, which predominantly yield particles in the submicron size range. As described by Salma et al. (2022)[143], this observed unimodal SOC size distribution in the accumulation mode is consistent with the characterization of SOC as part of the fine, water-soluble fraction of OC in atmospheric aerosols.

The annual mean SOC concentration reaches its maximum of 1.79±1.51 µg/m^3 within this accumulation mode, underscoring the significance of this size fraction in overall SOC composition. In stark contrast, the coarse particle fraction (>7.2 µm) contains markedly lower SOC concentrations, with an annual mean of merely 0.024±0.034 µg/m^3.

There is proven evidence[100] that high humidity demonstrates a negative correlation with SOC, thus a correlation analysis between atmospheric conditions and total SOC is needed. The result of this calculation is displayed in Figure 4.24.

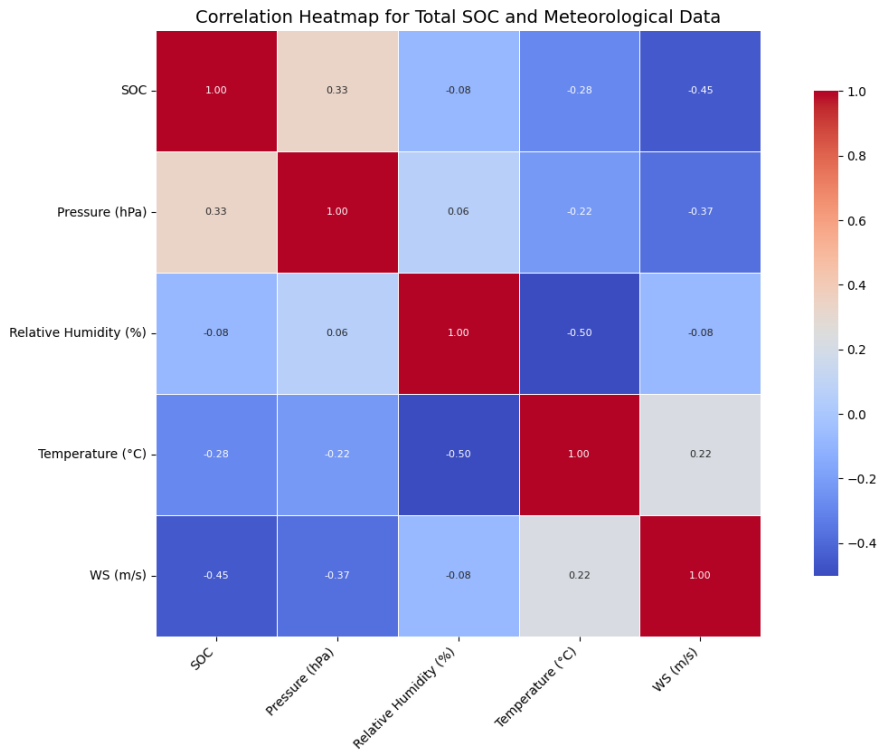


Figure 4.24. Correlation heatmap for SOC and atmospheric conditions.

The negative trend from literature is confirmed, yet it is not as significant compared to the positive trend with atmospheric pressure and negative trend with wind. This is caused by the accumulation of substances during calm weather when pressure is high, and the negative correlation with wind speed prevents substances from accumulating.[99] The negative relationship with temperature is also expected; despite heat and solar radiation being catalysts for SOC formation, when the weather is warm, there is no need for domestic heating to be turned on, and fewer SOC-forming substances enter the atmosphere.[72] SOC often displays a similar pattern to ozone concentrations, following the maximum photochemical[32] and activity and solar radiation intensity.[70, 142] This opens new areas for further investigation on SOC formation and additional scope for future study concideretion.

After calculating SOC, it is important to understand, what fraction of OC is SOC, the result of such calculation is presented on Figure 4.25:

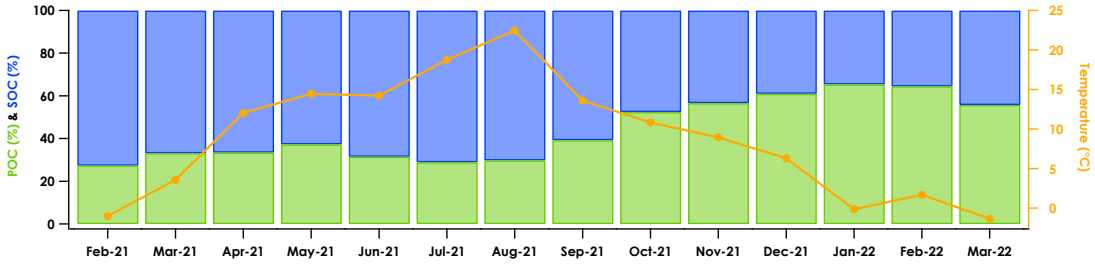


Figure 4.25. Fraction of SOC and OC_{pri} in Total OC in %

The temporal variation of SOC contribution to OC in atmospheric aerosols shows clear seasonality according to Figure 4.27, with peak values observed during the warmer months. Total SOC/OC ratios reach their zenith in June and August 2021, with mean values of 71% and 70% respectively. These months also coincide with the highest average temperatures recorded during the study period, at 18.8°C and 22.4°C respectively.

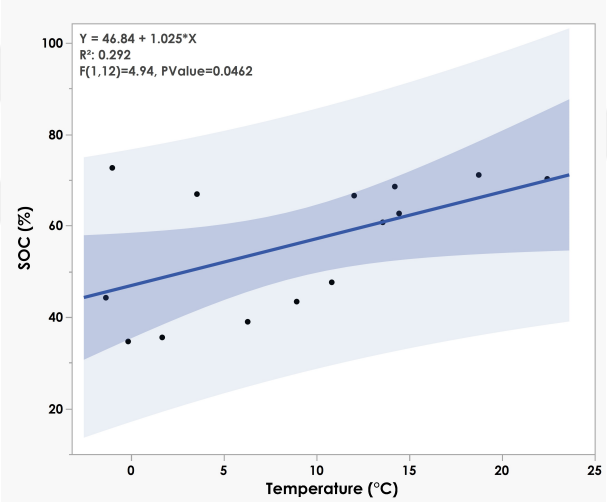


Figure 4.26. Positive correlation between temperature and SOC fraction.

This alignment between elevated SOC contributions and peak temperatures is further corroborated by a statistically significant positive correlation between SOC fraction and ambient temperature, as evidenced by a p-value below 0.05 as shown on Figure 4.26.

The observed temperature dependence of SOC formation carries profound implications for our understanding of atmospheric chemistry in the study area. It strongly suggests that photo-oxidation of volatile organic compounds (VOCs) to form SOC is enhanced under higher temperature conditions. The ncreased VOC

emissions and photochemical activity is leading to higher SOC concentrations during warmer seasons.[143]

This finding has important implications for air quality management in Bolu city, as it highlights the need for strategies that not only target primary emissions but also focus on controlling the precursor gases that lead to SOC formation.

4.6 OC/EC Ratios, Correlations and Seasonal Variations

For PM_3 (particles up to 3 μm in diameter), OC/EC ratios were calculated for four size ranges: 1.5-3 μm, 0.95-1.5 μm, 0.49-0.95 μm, and <0.49 μm. The ratios varied from 3.85 ± 4.23 for the smallest particles to 22.33 ± 44.87 for the largest PM_3 particles. We combined these using a weighted average, resulting in an overall PM_3 OC/EC ratio of 12.00 ± 31.61.

For PM_{10}, all size ranges up to 7.2 μm were included. The OC/EC ratios ranged from 3.85 ± 4.23 for the smallest particles to 20.71 ± 26.66 for the 3-7.2 μm range. The overall PM_{10} OC/EC ratio was 13.89 ± 29.07. The high standard deviations (31.61 for PM_3 and 29.07 for PM_{10}) show that these ratios vary a lot, reflecting the complex nature of air particles and their sources.

The mid-range particle sizes (1.5-3 μm and 0.95-1.5 μm) showed the most variation, which is also seen in Figure 4.27.

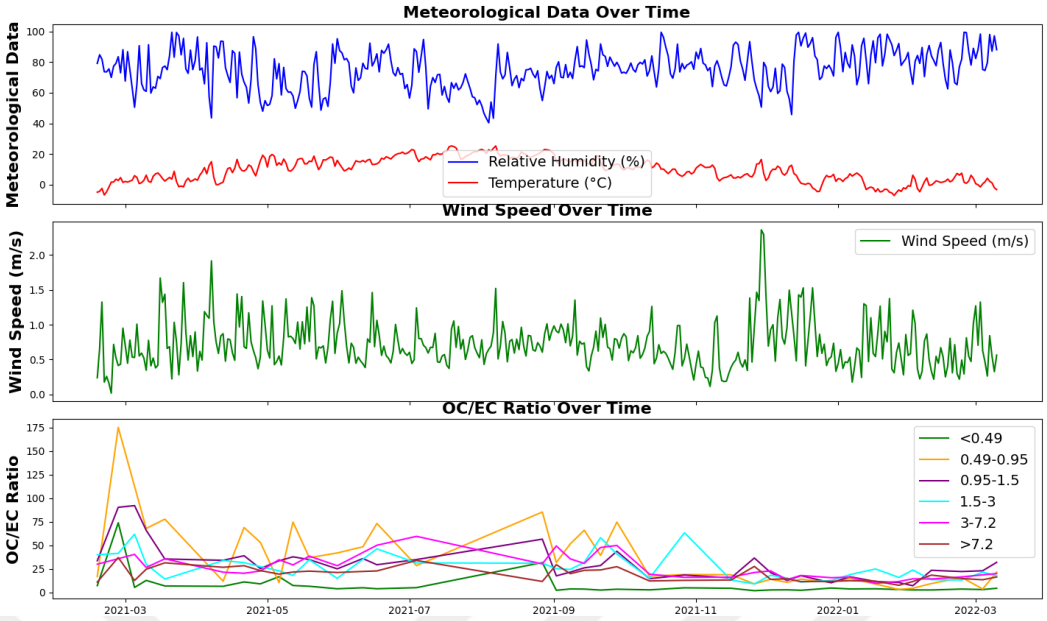


Figure 4.27. OC/EC values for each individual fraction with meteorology data of RH and Temperature and Wind speed on one timeline.

Such peak in the beginning of the sampling period, could be explained by cold weather conditions in the beginning of 2021, the highest peak corresponds to drop of temperature in February, for instance in 2021 in one day Bolu city became coldest city in Türkiye with almost 30 degrees below zero[96], which lead to excesive use of domestic heating. That lowest peak was reported in February 20[96] while peak value observed in February 26, since without wind and precipitation air is charachterised as stagnant, it leads to retension of PM in atmosphere and chemical aging, which increase SOC values[101] and consequently increases OC/EC value. In general OC/EC values in finer fractions, due to the more intensive SOC formation in them[72,101,142,143] follows temperature pattern and aligns with OC (Figure 4.7) and SOC (Figure 4.21). However, during end of Fall 2021 – Winter 2022. Despite below 0 temperatures, the windspeed was higher in the beginning of December 2021, and wind, as it was mentioned previously in this study (Section 4.1), prevents accumulation and aerosol aging, significant drop in SOC value and OC/EC values in the end of November 2021 alligns with increase of windspeed those days. The absence of peak in January despite low temperature and low windspeed explained by peak in EC values, that was low in February 2021 in comparison to January 2022. OC/EC values does not increase further due to heavy snowing in the beginning of February 2022, that decreased concentration of PM (Section 4.1).

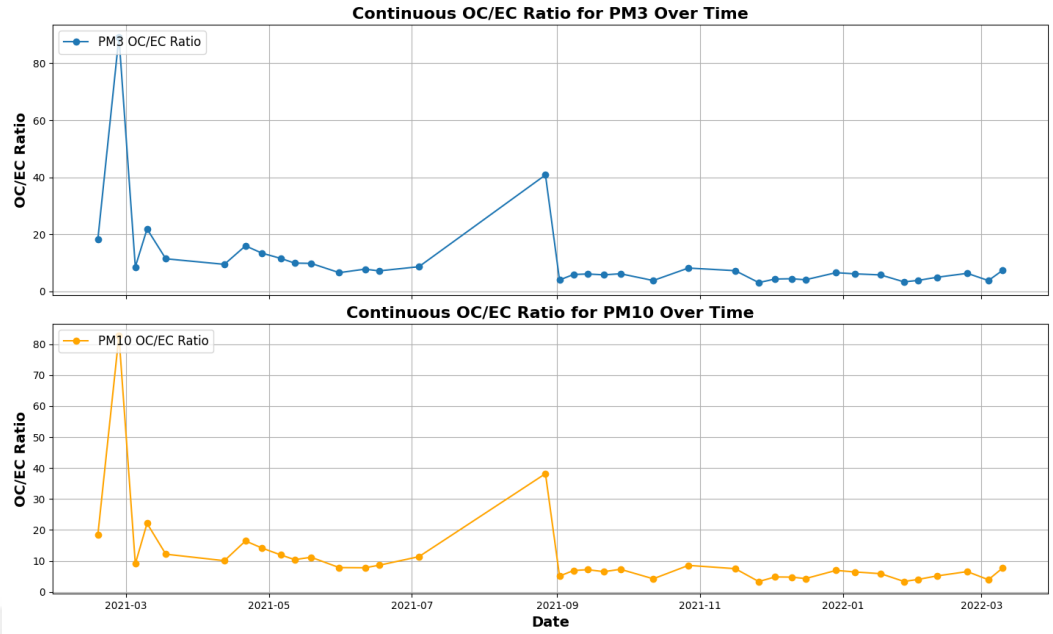


Figure 4.28. OC/EC for PM_3 and PM_{10} fractions with standart deviations.

This peak is more clearly observed in Figure 4.28 – on a high peak of OC/EC graph in February 2021, where standard deviations are high in that period for both PM_3 and PM_{10} ranges. A similarity in coarse and fine fraction behavior can also be observed in the correlation factors between OC/EC and meteorological data, with the coefficients presented in the heatmap in Figure 4.29.

Both fractions demonstrate almost identical positive correlation with atmospheric pressure and negative correlation with wind speed. This can be explained by stable atmospheric conditions (no precipitation, no vertical temperature gradient, leading to the absence of wind[98]). Atmospheric pressure higher during calm weather[97], thus trapping in a mountain environment, for instance, products of combustion from domestic heaters, where the OC/EC value is high.[99] The opposite observed in February 2022, when heavy snowing agitated atmosphere.

When relative humidity (RH) increases, the behavior of OC in the atmosphere becomes more complex, potentially leading to a decrease in the OC/EC ratio. This happens because of increased water uptake by OC compounds, weakened photochemistry, and reduced concentrations of gaseous oxidants like ozone, all of which can limit the formation of SOA. Additionally, high RH can alter aerosol acidity and viscosity, further affecting SOA formation processes and ultimately

contributing to a relative decrease in OC concentrations compared to the more stable EC.[100]

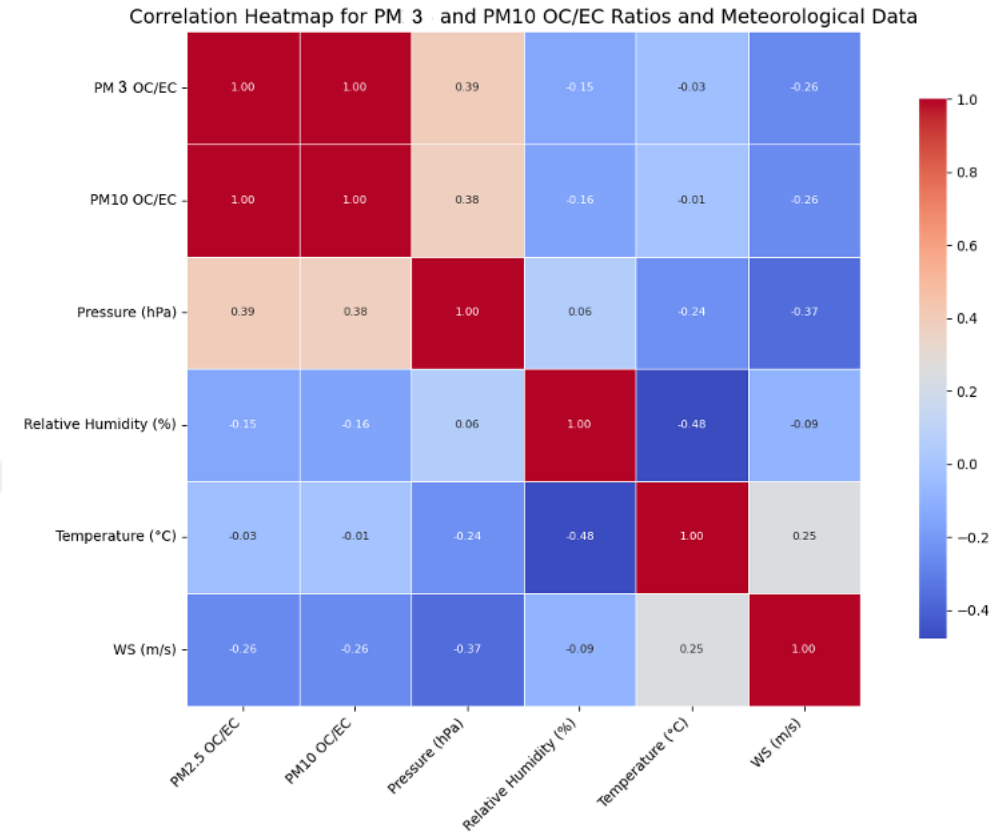


Figure 4.29. Correlation heatmap between atmospheric conditions and OC/EC ratio

4.7 Case Studies of high PM, CC and OC/EC

This section will describe separate peaks and episodes that are important to observe separately and more closely.

4.7.1 Case Study of high PM in July 2021.

On the Figure 4.1, there is a clear peak on total PM concentration observed on sample collected at July 4th 2021. The peak in summer that exceeds 110 mg/m^3 is charachterised as the product of organic combustion (like wildfire).

This is further supported by the characteristic OC/EC ratio for forest fires, which is reported as 15.67 in Table 4.8. The elevated OC/EC ratios (around 40), observed during this period in Bolu, indicates a significant contribution from

wildfire emissions. It is explained by long-range transport of aged biomass burning aerosols, which undergo chemical transformations during transport, and enhanced photochemical activity in the summer months, promoting secondary aerosol formation.[142, 143]

The influence of biomass burning is significant during the peak of PM concentration observed in July. Characteristic OC/EC ratios for biomass burning sources include: the summer peak in Bolu's OC/EC ratio, while the forest fire ratio of 15.67 and higher. This suggests that during such events, wildfire emissions can become a dominant source of carbonaceous aerosols in Bolu. The CALIPSO satellite data from NASA on Figure 4.30 indicates different types of aerosols in atmosphere.[144]

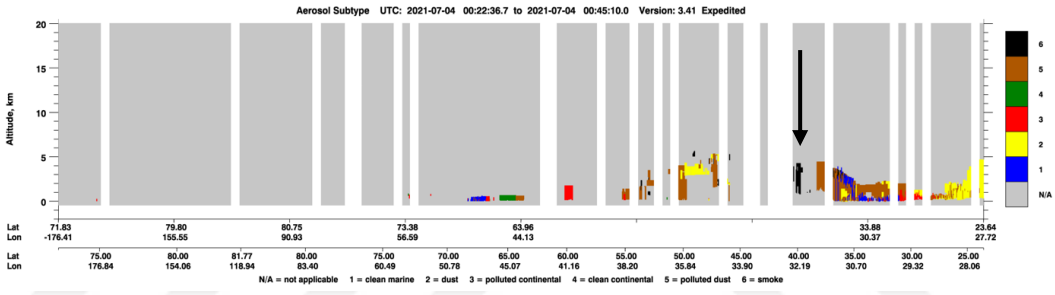


Figure 4.30. CALIPSO satellite LIDAR data on Aerosol Subtypes in different locations on 4th July 2021[144], arrow indicates coordinates of interest.

The wildfires in 2021 burned significant territory of woods globally[60, 61, 62], here initial assumption for PM peak was wildfires in Limassol, Cyprus, that started July 3 and finished July 7, 2021[133], however, further trajectory analysis proved this assumption to be wrong. The trajectories obtained the days of this episode, covering 4 days of sampling (Figure 4.31) shows that movement of airmasses mostly originated from northerly direction, satellite data did not indicate any remote source for this day, since the presence of smoke were detectable 2 days later[145]. For this reason, the episode observed on 4th of July seems to be associated with the local sources. Since observed OC/EC>40 for fine fractions, and confirmed presence of smoke from satellite, it can be concluded that biomass burning was responsible for this particular episode, since it is one of the main sources of $PM_{2.5}$ itself.[30]

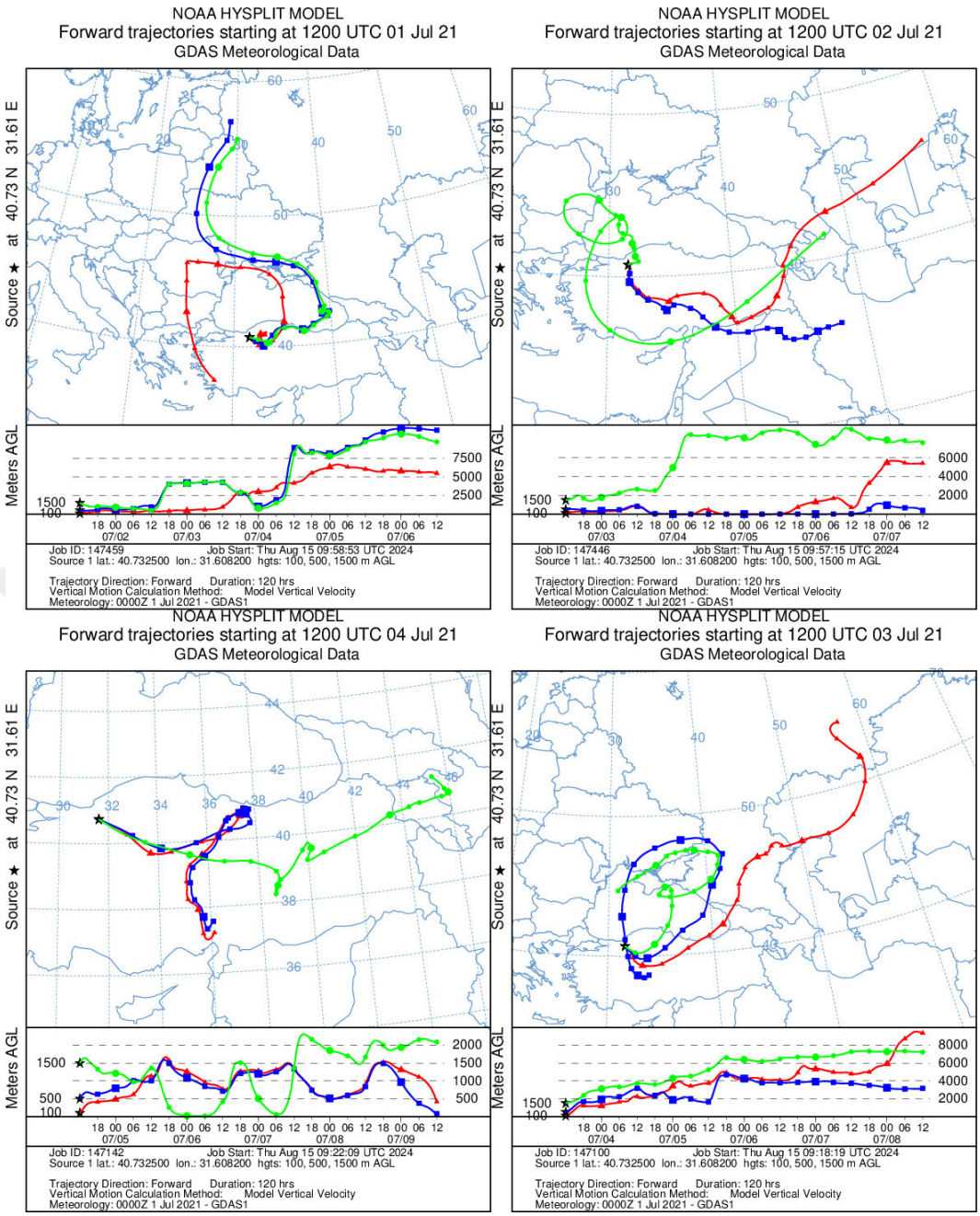


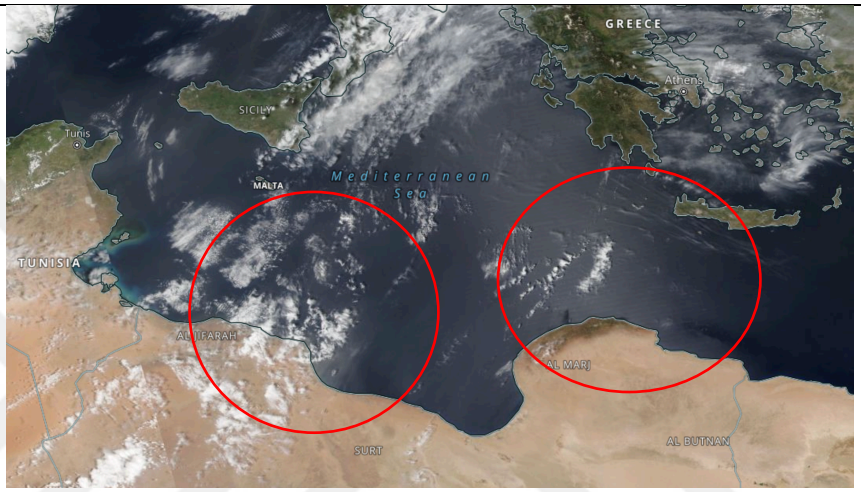
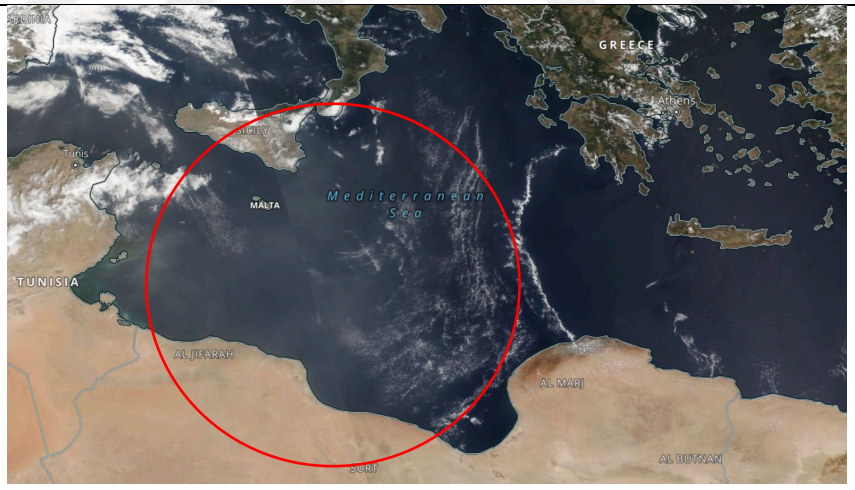
Figure 4.31. HYSPLIT trajectory of air mases, dates 01.07.2021 – 04.07.2021

4.7.2 Case Studies of high CC peaks, Possible Dust Episodes

On the other hand, as it was mentioned during the analysis of CC, the possible source of carbonate carbon is dust, that can be of local origin, and long-range transport origin. Here there are several cases of peaks of CC values that can be confirmed of long-range transfer. For all possible CC values where CC fraction is non-zero, and the CALIPSO LIDAR images available (Figure 4.31-Figure 4.34), as

well as images from MODIS Aqua and VIIRS Suomi NPP satellites (Table 4.7), those images were obtained from NASA website. Unfortunately for Aqua and Suomi NPP it was not possible to obtain clear image, due to hugh density of clouds above Mediterranian sea and Türkiye itself.

Table 4.7. Aqua and NPP images from NASA[146]

CC peak Date/Image Date	Image, red circle – area with observed dust eruptions to atmosphere
28.04.2021/ 27.04.2021	
08.09.2021/ 03.09.2021	

As it was mentioned in literature revew – the Bolu City in Summer is more affected by Long Term transport of particles[119], while the ability of Sharan dust reach Eastern[121] and Northwestern regions is proved.[123] For CALIPSO image observed on 09.04.2021 the presence of dust was confirmed on altitude of 2.5 kilometers – which is the evidence of long-range transport of PM. For 27.04.2021 both True Color and CALIPSO images available, True Color images from Aqua

and VIIRS confirm the eruption of dust towards Turkye from Africa, the CALIPSO image confirms presence of dust above 5 km around Bolu region. On 03.09.2021 we can observe dust eruption from same direction, as well as presence of dust around Bolu region on 05.09.2021. On 06.01.2022 despite high CC CALIPSO detected mix of dust and smoke, that aligns with peak of OC and EC concentrations around this date on Figures 4.7 and 4.10 respectively. The types of pollution were categorized by CALIPSO and present on Figures 4.31, 4.32, 4.33 and 4.34.

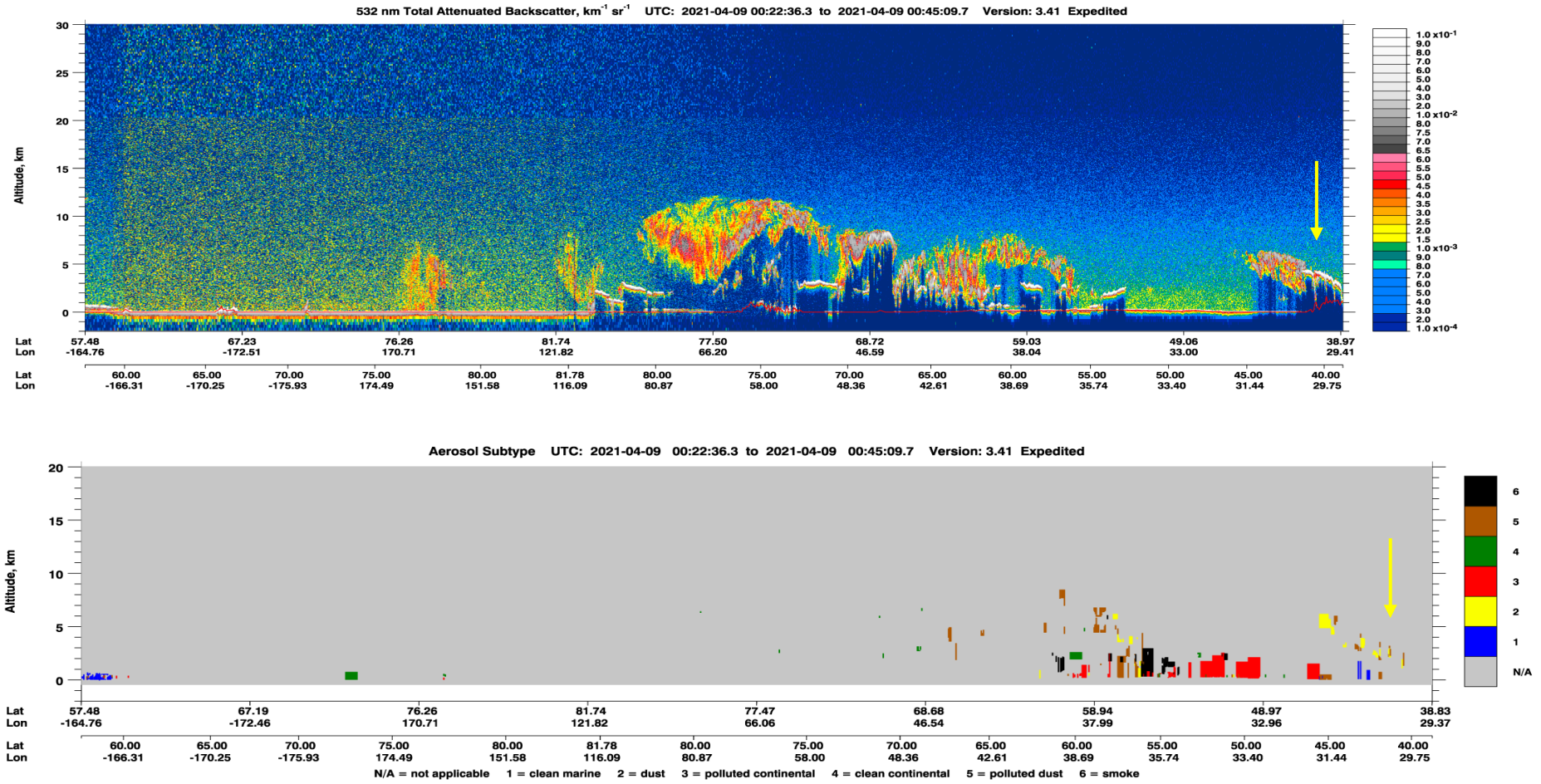


Figure 4.31. 12.04.2021/09.04.2021 (CC peak Date/ Image Date) CALIPSO images from NASA[147], arrows indicate coordinates of interest (Türkiye). Backscatter image (upper panel), Aerosol Subtype image (lower panel).

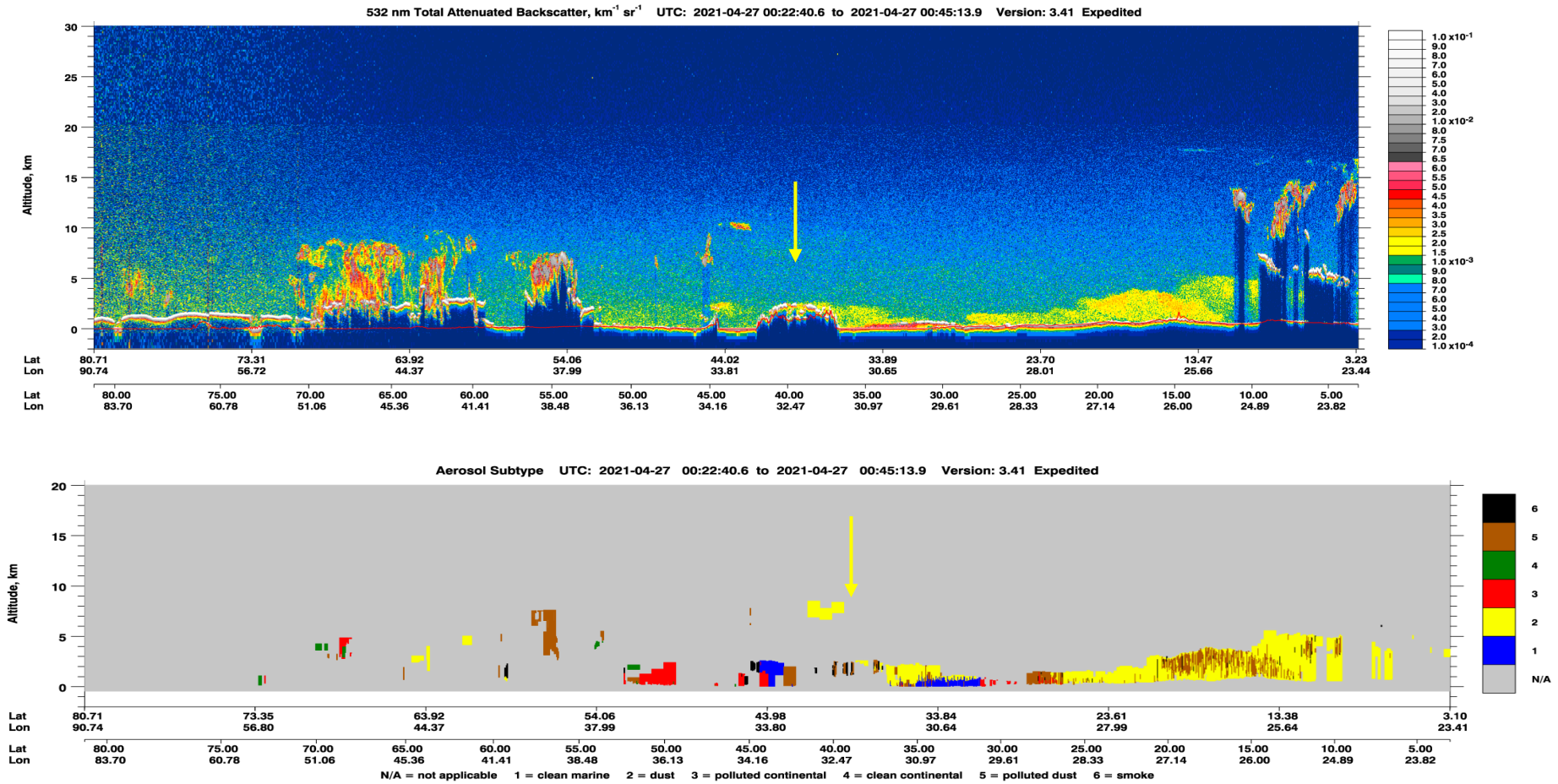


Figure 4.32. 28.04.2021/ 27.04.2021 (CC peak Date/ Image Date) CALIPSO images from NASA[147], arrows indicate coordinates of interest (Türkiye). Backscatter image (upper panel), Aerosol Subtype image (lower panel).

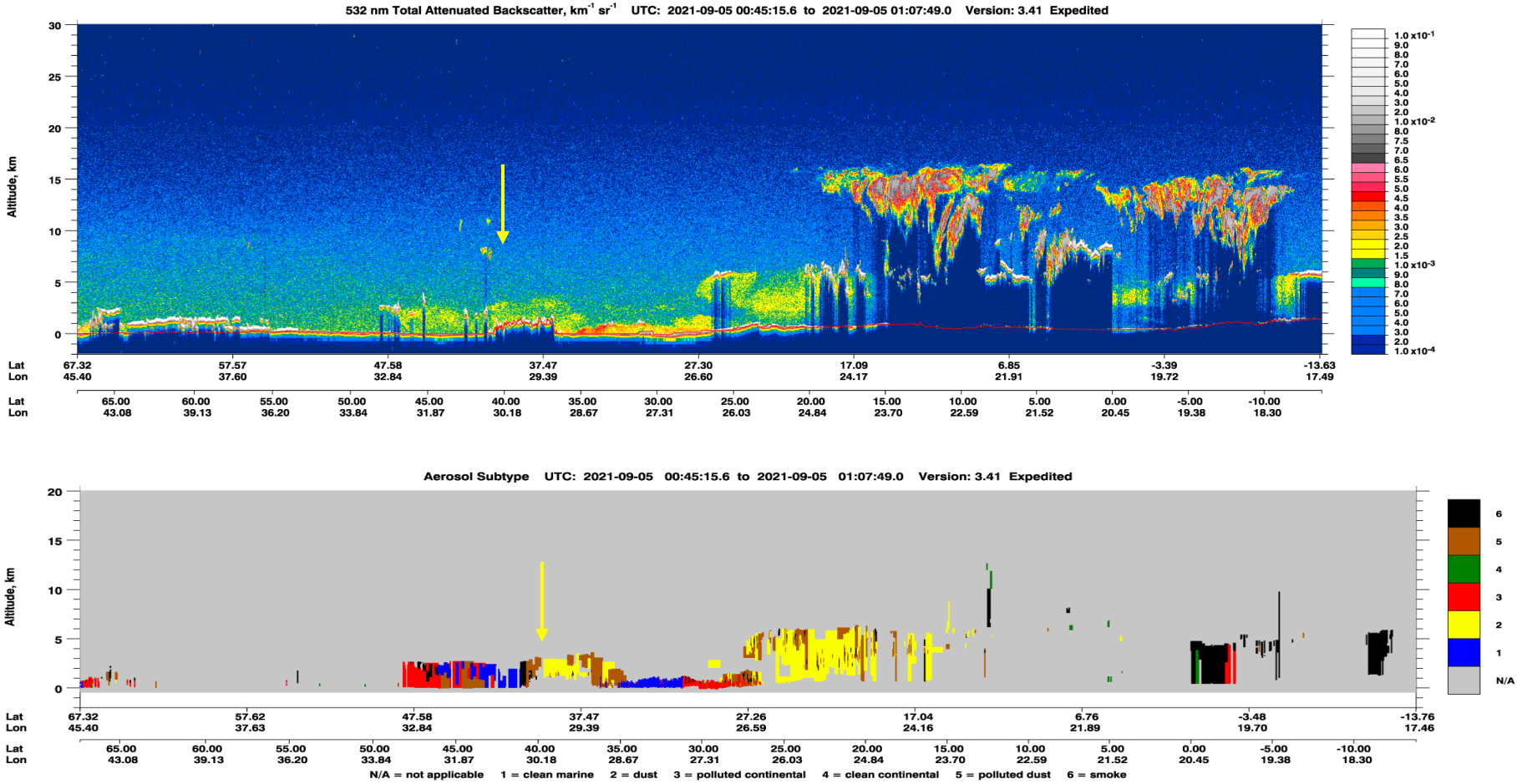


Figure 4.33. 08.09.2021/ 05.09.2021 (CC peak Date/ Image Date) CALIPSO images from NASA[147], arrows indicate coordinates of interest (Türkiye). Backscatter image (upper panel), Aerosol Subtype image (lower panel).

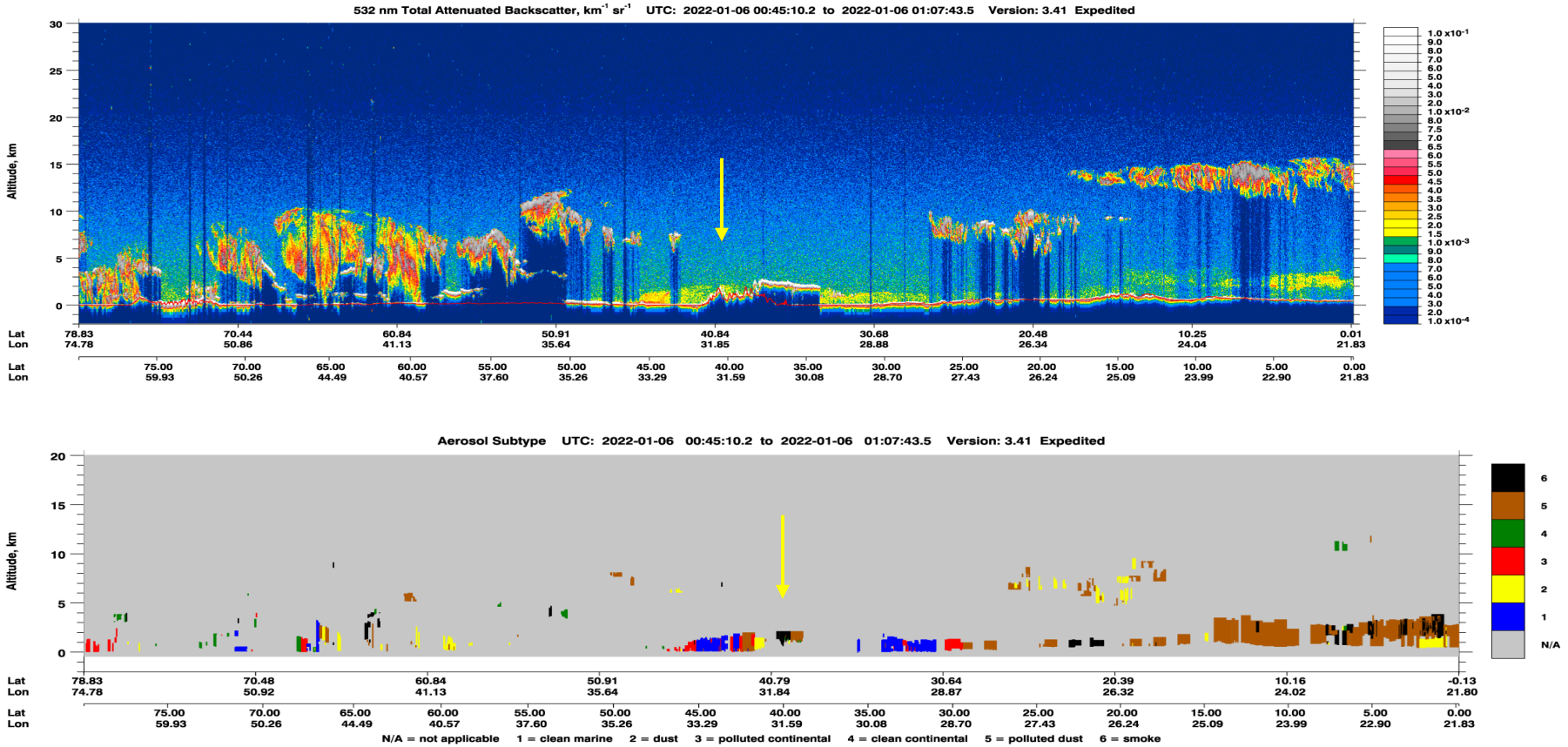


Figure 4.34. 06.01.2022/ 06.01.2022 (CC peak Date/ Image Date) CALIPSO images from NASA[147], arrows indicate coordinates of interest (Türkiye). Backscatter image (upper panel), Aerosol Subtype image (lower panel).

According to Figure 4.35 for CC peak at 12.04.2021 for 4 days prior to sampling the wind is directed from above Mediterranian sea and from Middle east, as well as from the North on 12.04.2021. It is Porssible for the winds to carry dust that was brought to Mediterranian sea. On Figure 4.31 there is a detected presence of dust in upper levels of the atmosphere.

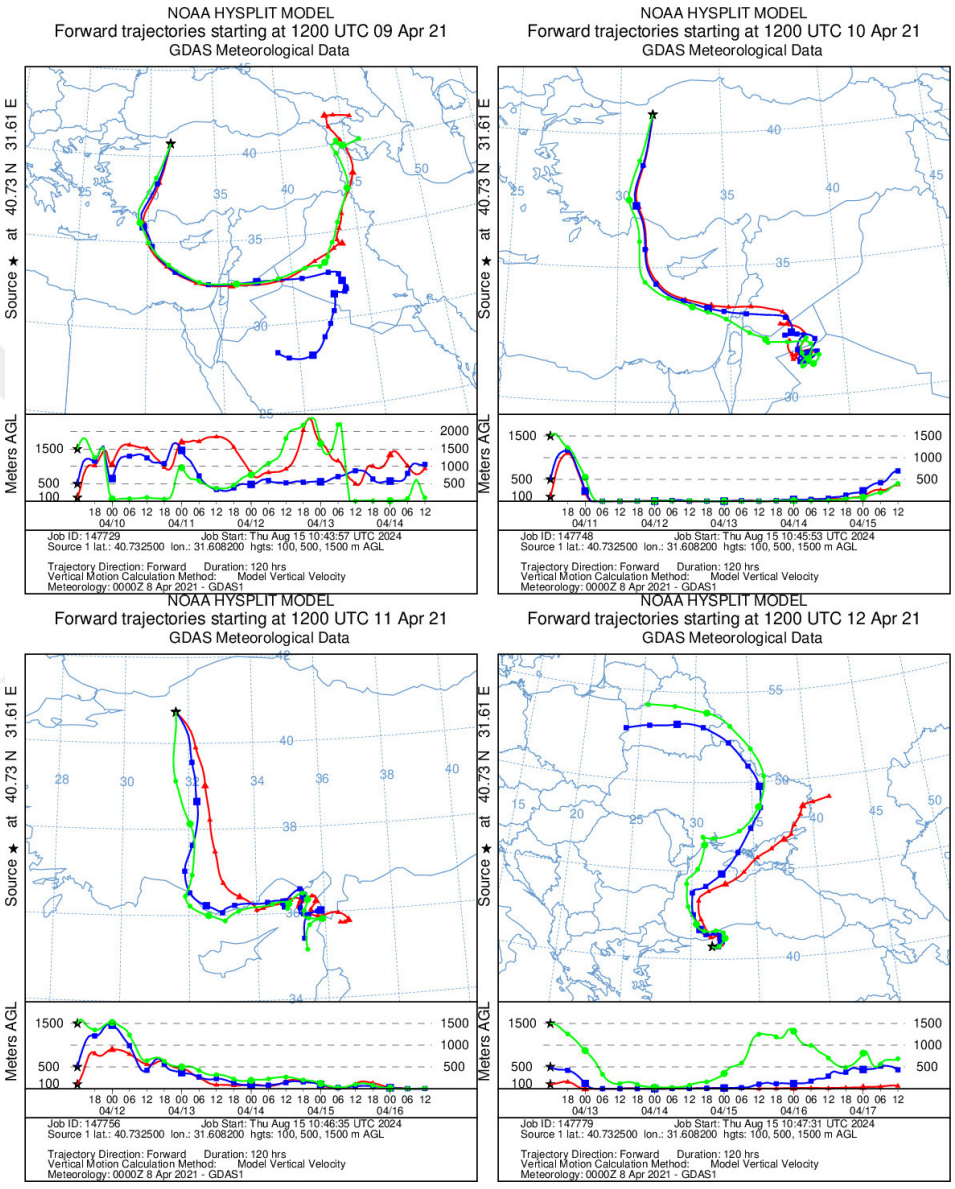


Figure 4.35. HYSPLIT trajectory model from 09.04.2021 – 12.04.2021, for CC peak on 12.04.2021

Episode on 28.04.2021 repeats that trend, According to Figure 4.36 the airmasses moves from Middle East, which is also characterized by deserted areas. It is also supported by CALIPSO images, detecting dust in the 4km altitude (Figure 4.32).

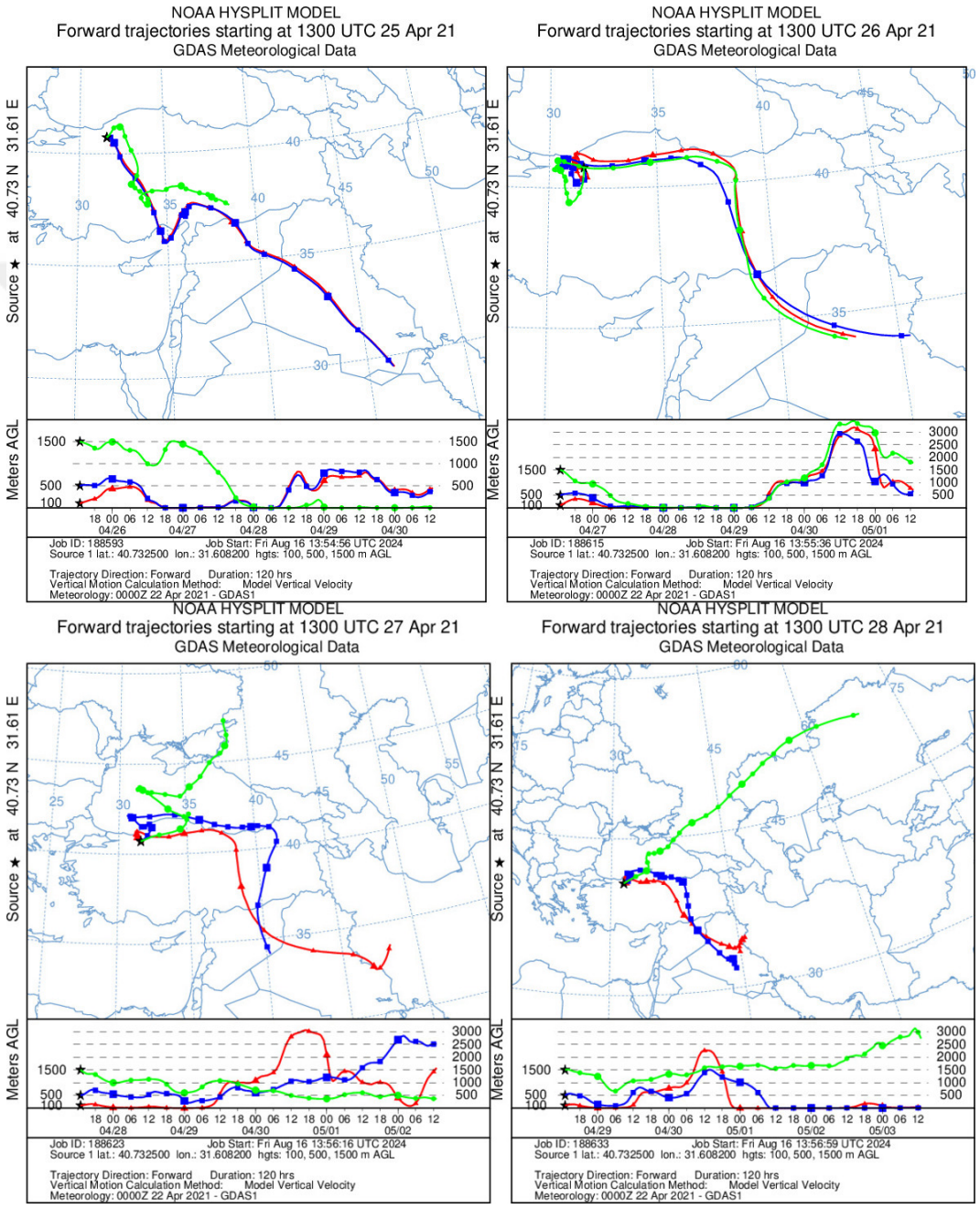


Figure 4.36. HYSPLIT trajectory model from 25.04.2021 – 28.04.2021, for CC peak on 28.04.2021

Figure 4.37 demonstrates trajectories of air masses that comes from African region for three days during sampling period, thus it might be evidence of Saharan dust episode in September 2021. According to CALIPSO (Figure 4.33) the high level of dust presented in 2 km layer in the atmosphere.

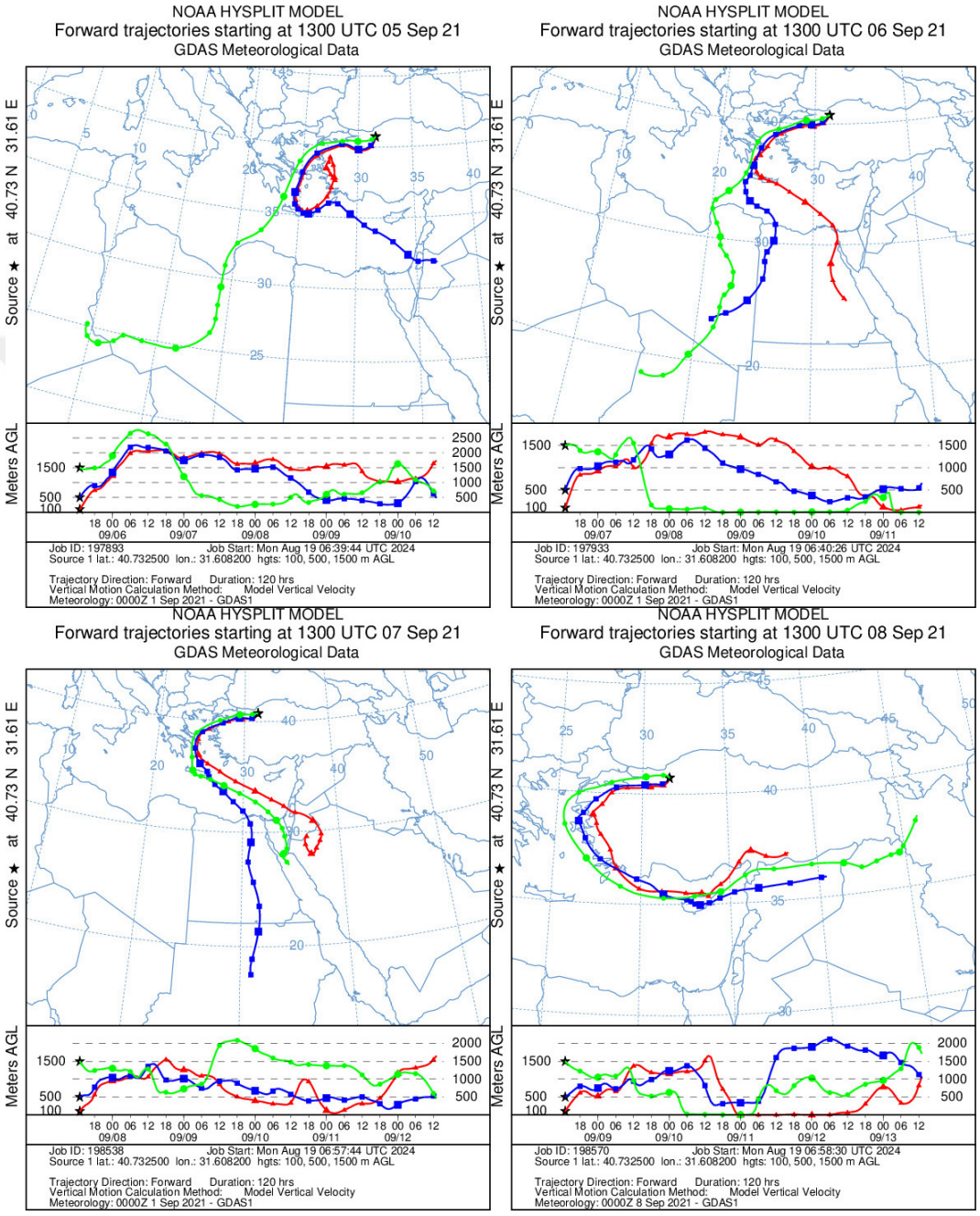


Figure 4.37. HYSPLIT trajectory model from 05.09.2021 – 08.09.2021, for CC peak on 08.09.2021

According to Figure 4.38, trajectories soncentrated on Eastern and Northern direction, due to absence of deserts in those regions, CALIPSO detecting smoke pollution, but no dust present (Figure 4.34), thus the CC peak is assumed to be of local origin.

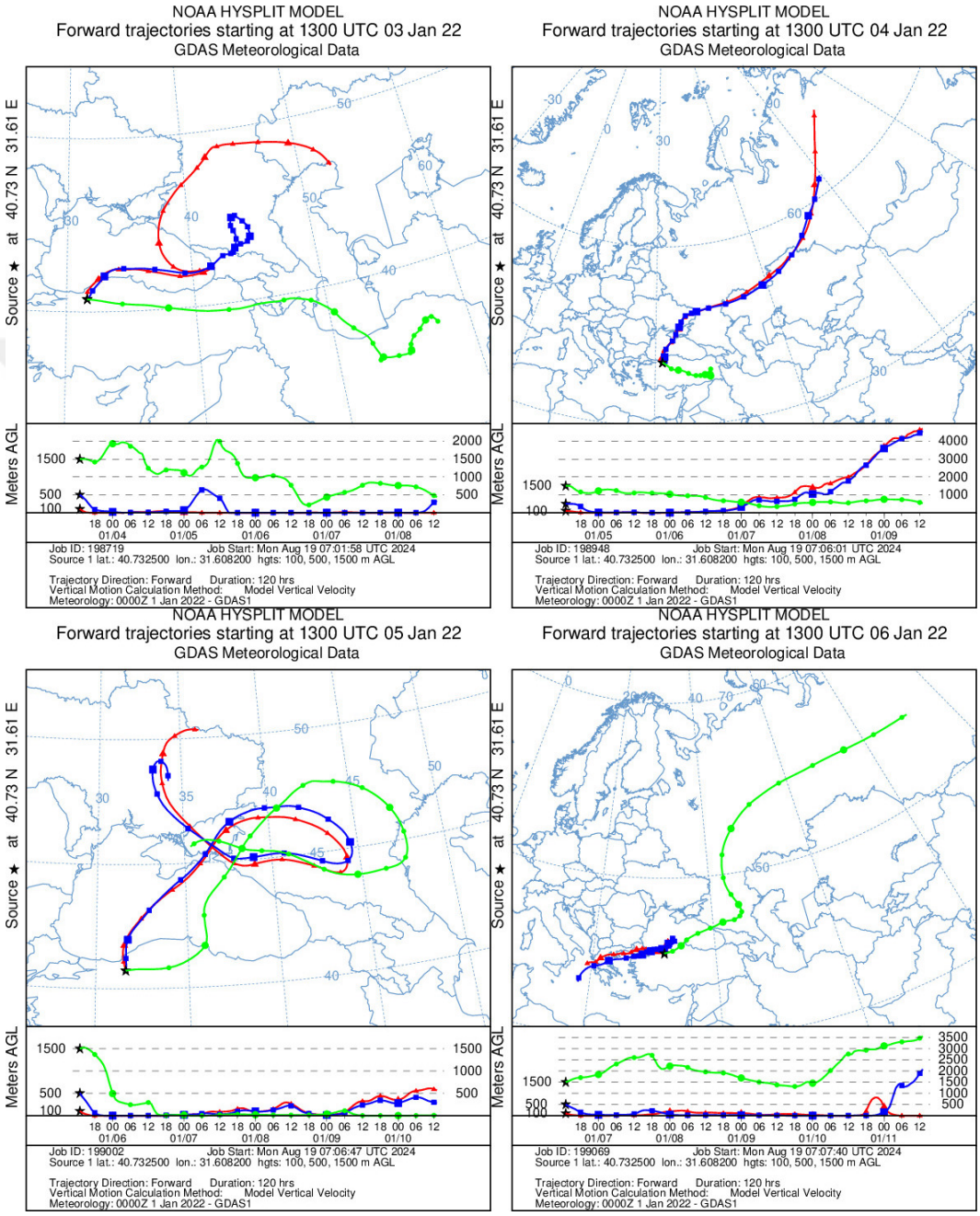


Figure 4.38. HYSPLIT trajectory model from 03.01.2022 – 06.01.2022, for CC peak on 06.01.2022

4.7.3 Case Study of Increasing OC in the end of August 2021.

There is a small peak in the end of Summer 2021, which cannot be explained by domestic heating or other heating activities. Thus, the availiable CALIPSO Images were obtained around sampling date. On a Figure 4.39 yellow arrow represents the coordinates of interest around Bolu. According to satellite data, the air contained mixture of polluted dust and smoke. Since no news on local fires were observed, it indicates that increase of OC in the end of Summer 2021 is due to the transported smoke particles from other locations.

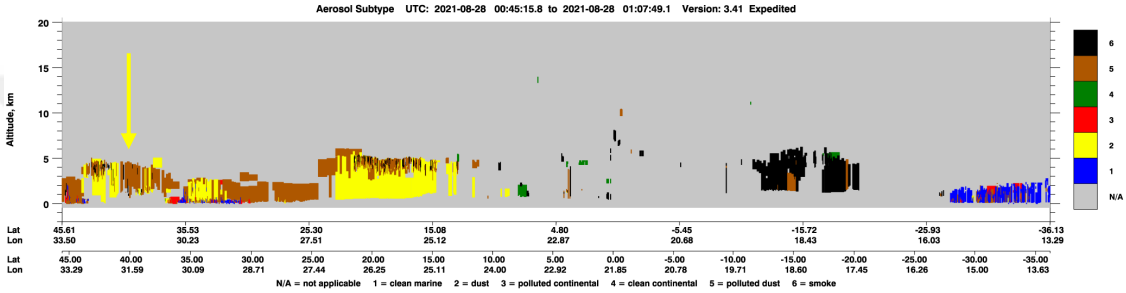


Figure 4.39. 28.08.2021 CALIPSO images from NASA[147], arrows indicate coordinates of interest (Türkiye). Aerosol Subtype image.

Trajectories were also analysed for that particular episode (Figure 4.40). The sampling date is 27.08.2021, for continues sampling all 4 days prior is checked. For the three days the airmasses moved from the direction of Black Sea with only one day (sample extraction day) air mostly circulated around Türkiye. The google search on news between 24.08.2021 and 27.08.2021 did not reveal any local fire episode. Meaning that smoke and dust in the altitude above 2 km came from long range particle transfer.

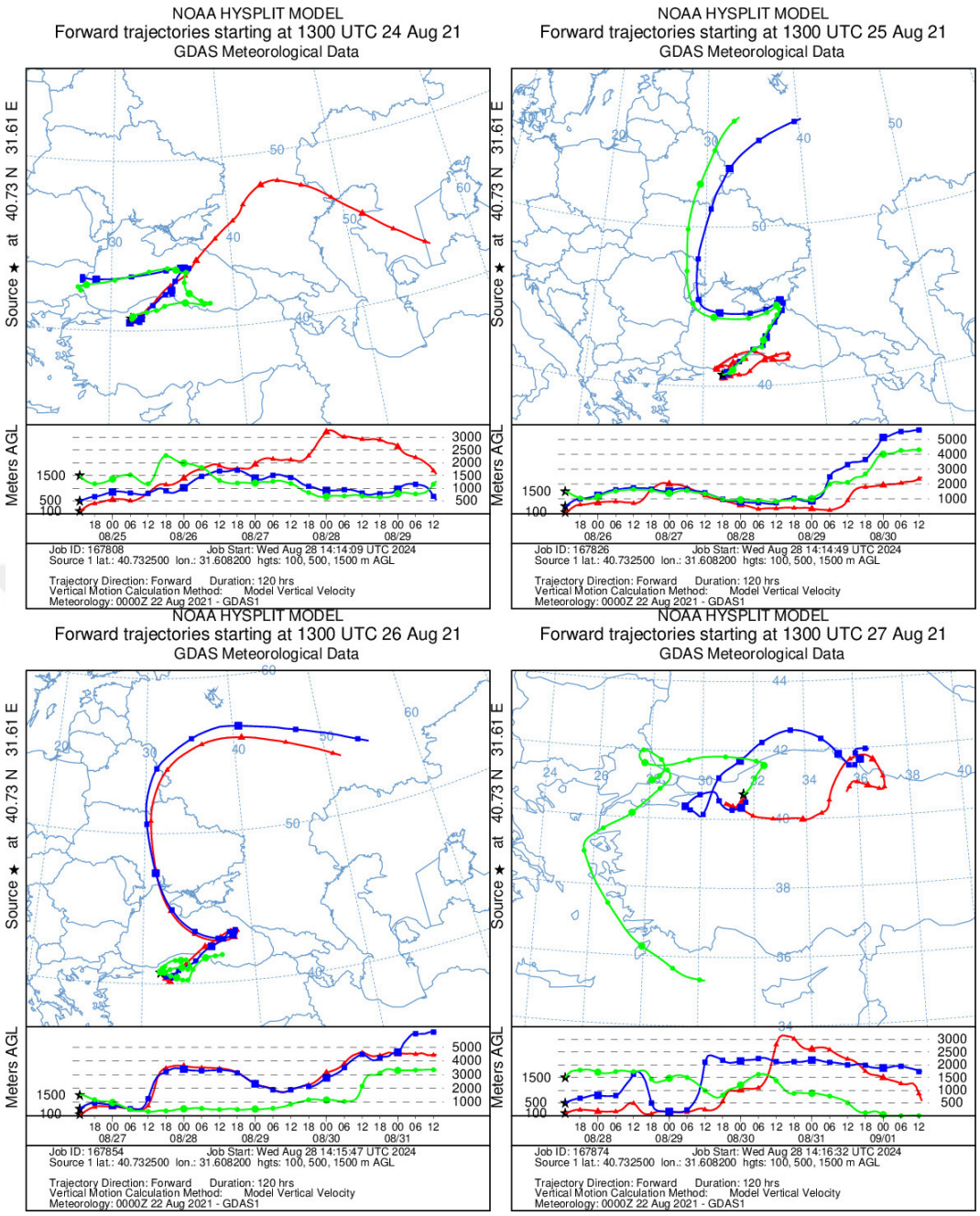


Figure 4.40. HYSPLIT trajectory model from 24.08.2021 – 27.08.2021, for OC peak on 27.08.2021

4.7.4 Case Studies of OC/EC Ratios for Different Sources

Table 4.8 shows the results of the research in different urban locations, with primary source in those locations. To ease the comparison the studies that

investigated the charachteristic OC/EC values for different sources also were added to the table.

Table 4.8. Sources and OC/EC values for different locations

Study		Location	Source	Charachteristic source	Source OC/EC	Ref. of Source
Plaza et al. (2011)[148]						
Season:	OC/EC ratio	Madrid, Sub-Urban	Traffic, 50/50 – Diesel and gasoline	Vehicle emissions	0.6±0.2	Cheng et al. (2010)[126] Cao et al. (2006)[127]
Winter	2.12 ± 0.32					
Spring	3.38 ± .91					
Summer	4.40 ± 0.95					
Fall	2.18 ± 0.34					
Raparthi et al. (2023)[149]						
Summer Morning	1.19	Mumbai, India, JVLR	Incomplete combustion of vehicle's fuel	Vehicle emissions	<2	Same study
Summer Afternoon	1.14	Mumbai, India, JVLR				
Summer Morning	5.9	IIT Bombay campus	Secondary reactions			
Summer Afternoon	4.5	IIT Bombay campus				
Křůmal et al. (2015)[150]						
Winter 2009	3.10	Brno, Czech Republic	Main source in winter – wood and	Residential wood burning	4.26	Watson et al. (2001)[151]
Winter 2010	5.32	Brno				
					2.70	

Winter 2009	4.13	Šlapanice, Czech Republic	coal combustion	Residential Coal burning		
Winter 2010	4.05	Šlapanice				
Summer 2009	3.65	Brno	Main source in summer – Vihicle combustion (mainly diesel) with minor impact of residential wood and coal burning.	Forest fires	15.67	
Summer 2010	3.67	Brno		Roadside	0.92 – 2	
Summer 2009	2.59	Šlapanice				
Summer 2010	2.85	Šlapanice				
Sharma et al. (2014)[152]			Sources			
Winter (November to February)	3.74	Delhi, India, Urban	Annual average impact of sources to PM_{10} concnentration: Soil dust: 20.7%; Secondary aerosols: 21.7%; Vehicle emissions: 17.0%; Fossil fuel combustion: 17.4%; Biomass burning: 14.3%; Industrial emissions: 4.5%; Sea salt: 4.4%			
Summer (March to June)	5.38					
Monsoon (July to October)	4.39					
Annual average	4.38					
Srinivas & Sarin (2014)[153]						
Overall study period November 9 – March 10	7.0 ± 2.2	Kharagpur (KGP)	Biomass burning sources	Biofuel burning	6.7	Same study
	7.7 ± 2.2	Indo-Gangetic Plain		Savannah fires in Brazil	8.3	

Early winter November 9 – January 10		Latitude: 22.3°N Longitude: 87.3°E		Biomass burning in Tanzania	7.8 for dry season 6.0 for wet season	
Late winter/spring February– March 10	5.7 ± 1.4					
Summer Afternoon	4.5					
Hou et al. (2011)[154]						
Spring	2.5 ± 1.3	Shanghai, China, Urban	In spring and winter – dust mixed with coal-mining and coal burning areas. In summer and autumn, the prevailing southeasterly monsoon wind brings clean air masses from the East China Sea to Shanghai			
Summer	3.5 ± 0.9					
Autumn	3.2 ± 0.8					
Winter	2.2 ± 0.2					
Górka et al. (2020)[155]						
January 6 – March 19 November 9 – December 24	April 4 – October 26					
4.74	5.14	Zgorzelec Urban	Heating season: Mainly coal burning from heating and power plants, and to a lesser extent household heating Vegetative season: Primarily combustion of liquid fuels (road and cargo traffic) Nowa Ruda (specific): All year shows higher influence of coal burning due to proximity to an old coal tailing and its location in a valley subject to thermal inversion layers			
8.44	6.79	Nowa Ruda Urban				
8.48	6.17	Polkowice Urban				
5.31	3.78	Legnica Urban				
5.05	5.41	Świdnica Urban				
7.42	7.70	Osieczów Regional background	Main source appears to be transportation (liquid fuel combustion)			

7.26	7.48	Czerniawa Regional background	
8.28	7.14	Działoszyn (industrial)	Combustion of liquid fuels (transportation)

The average OC/EC ratios observed in Bolu city (10.84 for PM_3 and 11.15 for PM_{10}) fall within the mid-range of values reported in various urban and semi-urban locations worldwide, as shown in Table 4.4.

Bolu's ratios are notably higher than those found in some major urban centers like Athens (2.7), Istanbul (2.8), or Shanghai (2.2-3.5), but insignificantly different from other Turkish cities like Düzce (12.4 for urban and 11.2 for semi-urban areas). The ratios are different to those observed in Madrid (2.12-4.40) and Delhi (3.74-5.38), indicating a difference urban and semi-urban characteristic, by literature observation data in Table 4.8.

Seasonal variations in OC/EC ratios are evident across multiple studies and in Bolu. The trend of higher summer ratios, observed in Madrid, Delhi, and Bolu, is often attributed to increased SOA formation due to higher temperatures and solar radiation. The extreme SOC/OC ratio (98%) found in Bolu's $PM_{2.5}$ fraction in Winter (February 2021) is far exceeding typical values and suggesting intense photochemical activity or unique local conditions. This high SOC fraction aligns with observations in other locations like Kharagpur, India, where SOC contributed up to 66.8% of OC, however, still lower than Bolu's high levels.

Traffic emissions emerge as a consistent major source of primary OC and EC across various urban studies.[129] Characteristic OC/EC ratios for vehicle emissions typically range from 0.5 to 4.2, depending on the fuel type and vehicle class:

- Diesel vehicles: 0.8-1.0
- Gasoline vehicles: 2.5-3.0
- Mixed urban traffic (Madrid study): 0.59 ± 0.25

Bolu's ratios (>10) suggest that while traffic is likely a significant contributor, it's not the sole major source of carbonaceous aerosols. The higher ratios indicate

substantial contributions from other sources or significant secondary aerosol formation.

Biomass burning, including residential wood burning, appears as another important contributor in many locations. Characteristic OC/EC ratios for biomass burning sources (Table 4.8) include:

- Residential wood burning: 4.26
- Forest fires: 15.67
- Savannah fires in Brazil: 8.3
- Biomass burning in Tanzania: 6.0-7.8

Bolu's ratios, especially the winter peak, align with these values, suggesting a significant contribution from domestic heating using biomass. This is consistent with patterns seen in other cities like Brno, Czech Republic, there residential heating significantly impacted OC/EC ratios.

Coal combustion, particularly for domestic heating and power generation, can significantly impact OC/EC ratios. Characteristic values include:

- Residential coal burning: 2.7-9.0
- Coal-fired power plants: 2.2-5.0

These sources are likely contributed to its OC/EC profile, especially during colder months, it highlights the need in investigation on types of fuel used in the City.[128, 130]

While Bolu doesn't have heavy industry, it's worth noting the impact of industrial activities on OC/EC ratios in other areas:

- Industrial sites (e.g., Działoszyn, Poland): 7.14-8.28
- Regional background (e.g., Osieczów, Poland): 7.42-7.70

The ratios observed in Bolu suggest a mix of sources:

- Significant secondary organic aerosol formation, indicated by the exceptionally high SOC fraction.

- Substantial contribution from biomass burning, particularly during winter months, likely due to domestic heating.
- Contribution from traffic emissions, though not as dominant as in some major urban centers.
- Influence of long-range transport, given Bolu's geographical location, as was proved in other studies and in this study with CALIPSO images and charachteristic OC/EC ratio in summer.
- Influence of long-range transport of dust from other locations proved by Sattelite images and CC values peak.

The city's proximity to the Black Sea (about 60 km) and its surrounding mountains likely have impact on its air quality dynamics, potentially influencing the formation and accumulation of secondary organic aerosols.

5. CONCLUSIONS AND RECOMMENDATIONS

This one-year study has provided valuable insights into the PM dynamics and SOA formation in Bolu city, revealing complex patterns that challenges in our understanding of urban air quality. The key findings and their implications are as follows:

- **Unique OC/EC Ratios:** Bolu's average OC/EC ratios are higher than those in many major urban centers but not significantly lower than some other Turkish cities. These ratios suggest a mix of urban and semi-urban characteristics, indicating diverse sources of carbonaceous aerosols, such as traffic, SOC formation, domestic heating.
- **Exceptional SOC Formation:** an extraordinarily high maximum SOC/OC ratio (98%) in Bolu's $PM_{2.5}$ fraction during winter, far exceeding typical values. This suggests intense photochemical activity or unique local conditions promoting year-round SOC formation, contrasting with the summer peaks observed in other regions.
- **Multiple Emission Sources:** While traffic emissions are significant, Bolu's high OC/EC ratios indicate substantial contributions from other sources:
    1) Biomass burning, particularly for domestic heating in winter
    2) Potential influence from coal combustion for heating and power generation
    3) Long-range transport of pollutants, including dust and wildfire emissions
- **Seasonal Variations:** The study observed distinct seasonal patterns, with higher OC/EC ratios in summer, likely due to increased SOA formation. However, the persistent high ratios throughout the year suggest continuous SOA formation processes unique to Bolu.
- **Long-Range Transport:** CALIPSO, Aqua and NPP satellite data and characteristic OC/EC ratios provide evidence of long-range transport of particles, including dust from Saharan regions and smoke from distant wildfires or local biomass fires.

- **Geographical Influences:** Bolu's proximity to the Black Sea and its surrounding mountains likely impact its air quality dynamics, potentially influencing the formation and accumulation of secondary organic aerosols.

These findings highlight the complexity of air quality issues in Bolu and allows to derrive following recommendations for further research:

- Establishing a network of sampling sites across Bolu to better understand the spatial distribution and movement of PM.
- Investigating specific mechanisms driving year-round SOA formation in Bolu, considering local PM emission sources, gas emission sources (as one of precursors for SOA formation), atmospheric chemistry, and meteorological factors.
- Study used types of fuel by local citizens, buisness and industry, for better understanding of the possible emissions source and future risk assesment.
- Extending the study to include analysis of specific organic compounds and collaborating with health experts to assess potential health impacts.
- Improving meteorological data monitoring across different city locations better consideration of Bolu's complex topography and its effects on pollutant dispersion.

For polycymakers and authorities the following recomendations can be derrived:

- Implement a training program for apartment building staff on optimizing burner efficiency to reduce emissions from domestic heating, which is a significant contributor to PM and SOA formation.
- Although traffic is not the dominant source, it remains significant. Consider relocating main roads or implementing traffic reduction measures in areas with high PM concentrations.
- Encourage the transition from biomass and coal to cleaner heating alternatives, such as natural gas or electric heating systems, to reduce emissions from domestic and industrial sources.
- Develop and implement public education campaigns on the impacts of various activities (e.g., biomass burning, vehicle use) on air quality, and promote practices that reduce individual contributions to PM emissions.

In conclusion, while Bolu shares some similarities with other urban and semi-urban areas, its exceptionally high SOC fraction and year-round SOA formation set it apart. This unique profile emphasizes the necessity for further investigation into the specific local conditions promoting such intense secondary aerosol formation.

6. REFERENCES

1.Xing YF, Xu YH, Shi MH, Lian YX. The Impact of PM2.5 on the Human Respiratory System. Journal of Thoracic Disease. 2016 Jan;8(1):E69-74.

2.Gokul T, Kumar KR, Prema P, Arun A, Balaji P, Faggio C. Particulate Pollution and Its Toxicity to fish: an Overview. Comparative Biochemistry and Physiology Part C: Toxicology & Pharmacology [Internet]. 2023 Aug 1;270:109646. Available from: https://www.sciencedirect.com/science/article/abs/pii/S1532045623001011#:~:text=Particle%20pollution%20can%20transport%20contaminants

3.Sweileh WM, Al-Jabi SW, Zyoud SH, Sawalha AF. Outdoor Air Pollution and Respiratory health: a Bibliometric Analysis of Publications in peer-reviewed Journals (1900 – 2017). Multidisciplinary Respiratory Medicine. 2018 Jun 1;13(1).

4.Gaulding CL. Definition of Air Quality Control Regions:approach and Experience to Date. Journal of the Air Pollution Control Association. 1968 Sep;18(9):591–5.

5.Manisalidis I, Stavropoulou E, Stavropoulos A, Bezirtzoglou E. Environmental and Health Impacts of Air pollution: a Review. Frontiers in Public Health [Internet]. 2020;8(14):1–13. Available from: https://www.ncbi.nlm.nih.gov/pmc/articles/PMC7044178/

6.Braggion A, Dugerdil A, Wilson O, Hovagemyan F, Flahault A. Indoor Air Quality and COVID-19: a Scoping Review. Public Health Reviews (2107-6952). 2024 Jan 24;44:1–8.

7.Elsaid AM, Ahmed MS. Indoor Air Quality Strategies for Air-Conditioning and Ventilation Systems with the Spread of the Global Coronavirus (COVID-19) Epidemic: Improvements and Recommendations. Environmental Research. 2021 Aug;199:111314.

8.Tran VV, Park D, Lee YC. Indoor Air Pollution, Related Human Diseases, and Recent Trends in the Control and Improvement of Indoor Air Quality. International Journal of Environmental Research and Public Health. 2020 Apr 23;17(8):2927.

9.WHO. WHO Global Air Quality Guidelines. Geneva Who; 2021.

10.Intergovernmental Panel on Climate Change. Climate Change 2022: Impacts, Adaptation and Vulnerability [Internet]. IPCC Sixth Assessment Report. IPCC; 2022. Available from: https://www.ipcc.ch/report/ar6/wg2/

11.Semczuk-Kaczmarek K, Rys-Czaporowska A, Sierdzinski J, Kaczmarek LD, Szymanski FM, Platek AE. Association between Air Pollution and COVID-19 Mortality and Morbidity. Internal and Emergency Medicine. 2021 Oct 12;17(2):467–73.

12.Sokhi R, Moussiopoulos N, Baklanov A, Bartzis J, Coll I, Finardi S, et al. at-mospheric chemist, Awarded the Nobel Prize in Chemistry 1995; Mario Molina (1943-2020), Atmospheric chemist, Awarded the No-bel Prize in. Atmos Chem Phys [Internet]. 2022;22(7):4615–703. Available from: https://acp.copernicus.org/articles/22/4615/2022/acp-22-4615-2022.pdf

13.US EPA O. Managing Air Quality - Air Pollutant Types [Internet]. US EPA. 2015. Available from: https://www.epa.gov/air-quality-management-process/managing-air-quality-air-pollutant-types#:~:text=Common%20Air%20Pollutants

14.Obaidullah M, Bram S, Verma VK, De Ruyck J. A Review on Particle Emissions from Small Scale Biomass Combustion. International Journal of Renewable Energy Research-IJRER [Internet]. 2012;2(1):147–59. Available from: https://www.ijrer.org/ijrer/index.php/ijrer/article/view/147/pdf

15.Miller MR, Newby DE. Air Pollution and Cardiovascular disease: Car Sick. Cardiovascular Research. 2019 Oct 4;116(2).

16.Schraufnagel DE. The Health Effects of Ultrafine Particles. Experimental & Molecular Medicine

[Internet]. 2020 Mar 1;52(3):311–7. Available from: https://www.nature.com/articles/s12276-020-0403-3

17.Turner MC, Andersen ZJ, Baccarelli A, Diver WR, Gapstur SM, Pope CA, et al. Outdoor Air Pollution and cancer: an Overview of the Current Evidence and Public Health Recommendations. CA: a Cancer Journal for Clinicians [Internet]. 2020 Aug 25;70(6). Available from: https://acsjournals.onlinelibrary.wiley.com/doi/full/10.3322/caac.21632

18.Kim KH, Kabir E, Jahan SA. Airborne Bioaerosols and Their Impact on Human Health. Journal of Environmental Sciences. 2018 May;67:23–35.

19.Wilson WE, Chow JC, Claiborn C, Fusheng W, Engelbrecht J, Watson JG. Monitoring of Particulate Matter Outdoors. Chemosphere. 2002 Dec;49(9):1009–43.

20.Park M, Joo HS, Lee K, Jang M, Kim SD, Kim I, et al. Differential Toxicities of Fine Particulate Matters from Various Sources. Scientific Reports. 2018 Nov 19;8(1).

21.Bessagnet B, Allemand N, Putaud JP, Couvidat F, André JM, Simpson D, et al. Emissions of Carbonaceous Particulate Matter and Ultrafine Particles from Vehicles—A Scientific Review in a Cross-Cutting Context of Air Pollution and Climate Change. Applied Sciences. 2022 Apr 2;12(7):3623.

22.Reid JS, Koppmann R, Eck TF, Eleuterio DP. A Review of Biomass Burning Emissions Part II: Intensive Physical Properties of Biomass Burning Particles. Atmospheric Chemistry and Physics. 2005 Mar 14;5(3):799–825.

23.Philip S, Martin RV, van Donkelaar A, Lo JWH, Wang Y, Chen D, et al. Global Chemical Composition of Ambient Fine Particulate Matter for Exposure Assessment. Environmental Science & Technology [Internet]. 2014 Nov 6;48(22):13060–8. Available from: https://www.ncbi.nlm.nih.gov/pmc/articles/PMC4238642/

24.Alves C, Evtyugina M, Vicente E, Vicente A, Rienda IC, de la Campa AS, et al. PM2.5 Chemical Composition and Health Risks by Inhalation near a Chemical Complex. Journal of Environmental Sciences [Internet]. 2023 Feb 1;124:860–74. Available from: https://www.sciencedirect.com/science/article/pii/S1001074222000778

25.Tchounwou PB, Yedjou CG, Patlolla AK, Sutton DJ. Heavy Metal Toxicity and the Environment. Experientia Supplementum. 2014 Aug 26;101(1):133–64.

26.Taiwo AM, Beddows DCS, Shi Z, Harrison RM. Mass and Number Size Distributions of Particulate Matter components: Comparison of an Industrial Site and an Urban Background Site. Science of the Total Environment [Internet]. 2014 Mar 15;475:29–38. Available from: https://www.sciencedirect.com/science/article/pii/S004896971301557X

27.Correa M, Bedoya R, María L, Aguiar D, Alberto C, Colorado HA. A Review on the Characterization and Measurement of the Carbonaceous Fraction of Particulate Matter. Sustainability. 2023 May 28;15(11):8717–7.

28.Rigler M, Drinovec L, Lavrič G, Vlachou A, Prévôt A, Luc Jaffrezo J, et al. The New Instrument Using a TC–BC (total Carbon–black carbon) Method for the Online Measurement of Carbonaceous Aerosols. Atmospheric Measurement Techniques. 2020 Aug 17;13(8):4333–51.

29.Held A, Zerrath A, McKeon U, Fehrenbach T, Niessner R, Plass-Dülmer C, et al. Aerosol Size Distributions Measured in urban, Rural and high-alpine Air with an Electrical Low Pressure Impactor (ELPI). Atmospheric Environment. 2008 Nov 1;42(36):8502–12.

30.Sirignano C, Riccio A, Chianese E, Ni H, Zenker K, D'Onofrio A, et al. High Contribution of Biomass Combustion to PM2.5 in the City Centre of Naples (Italy). Atmosphere. 2019 Aug 6;10(8):451.

31.Dabek-Zlotorzynska E, Celo V, Ding L, Herod D, Jeong CH, Evans G, et al. Characteristics and

Sources of PM2.5 and Reactive Gases near Roadways in Two Metropolitan Areas in Canada. Atmospheric Environment. 2019 Dec;218:116980.

32.Vörösmarty M, Uzu G, Jaffrezo JL, Dominutti P, Kertész Z, Papp E, et al. Oxidative Potential in rural, Suburban and City Centre Atmospheric Environments in Central Europe. Atmospheric Chemistry and Physics. 2023 Nov 16;23(22):14255–69.

33.Long CM, Nascarella MA, Valberg PA. Carbon Black vs. Black Carbon and Other Airborne Materials Containing Elemental carbon: Physical and Chemical Distinctions. Environmental Pollution. 2013 Oct;181:271–86.

34.Khodeir M, Shamy M, Alghamdi M, Zhong M, Sun H, Costa M, et al. Source Apportionment and Elemental Composition of PM2.5 and PM10 in Jeddah City, Saudi Arabia. Atmospheric Pollution Research. 2012 Jul;3(3):331–40.

35.Thangavel P, Park D, Lee YC. Recent Insights into Particulate Matter (PM2.5)-Mediated Toxicity in Humans: an Overview. International Journal of Environmental Research and Public Health. 2022 Jun 19;19(12):7511.

36.Xue H, Liu G, Zhang H, Hu R, Wang X. Similarities and Differences in PM10 and PM2.5 concentrations, Chemical Compositions and Sources in Hefei City, China. Chemosphere. 2019 Apr;220:760–5.

37.Jahedi F, Dehdari Rad H, Goudarzi G, Tahmasebi Birgani Y, Babaei AA, Ahmadi Angali K. Polycyclic Aromatic Hydrocarbons in PM1, PM2.5 and PM10 Atmospheric particles: identification, sources, Temporal and Spatial Variations. Journal of Environmental Health Science and Engineering. 2021 Apr 2;19(1):851–66.

38.Benedict KB, Lee T, Collett JL. Cloud Water Composition over the Southeastern Pacific Ocean during the VOCALS Regional Experiment. Atmospheric Environment. 2012 Jan;46:104–14.

39.American Lung Association. Particle Pollution. American Lung Association [Internet]. 2020 Mar 24; Available from: https://www.lung.org/clean-air/outdoors/what-makes-air-unhealthy/particle-pollution

40.Li T, Hu R, Chen Z, Li Q, Huang S, Zhu Z, et al. Fine Particulate Matter (PM2.5): the Culprit for Chronic Lung Diseases in China. Chronic Diseases and Translational Medicine [Internet]. 2018 Sep;4(3):176–86. Available from: https://www.ncbi.nlm.nih.gov/pmc/articles/PMC6160608/

41.Li B, Ma Y, Zhou Y, Chai E. Research Progress of Different Components of PM2.5 and Ischemic Stroke. Scientific Reports. 2023 Sep 25;13(1).

42.Bukowska B, Mokra K, Michałowicz J. Benzo[a]pyrene-Environmental Occurrence, Human Exposure, and Mechanisms of Toxicity. International Journal of Molecular Sciences [Internet]. 2022 Jun 6;23(11):6348. Available from: https://pubmed.ncbi.nlm.nih.gov/35683027/

43.Wang C, Meng Z, Yao P, Zhang L, Wang Z, Lv Y, et al. Sources-specific Carcinogenicity and Mutagenicity of PM2.5-bound PAHs in Beijing, China: Variations of Contributions under Diverse Anthropogenic Activities. Ecotoxicology and Environmental Safety [Internet]. 2019 Nov 15;183:109552. Available from: https://pubmed.ncbi.nlm.nih.gov/31442804/

44.Jung KH, Yan B, Chillrud SN, Perera FP, Whyatt R, Camann D, et al. Assessment of Benzo(a)pyrene-equivalent Carcinogenicity and Mutagenicity of Residential Indoor versus Outdoor Polycyclic Aromatic Hydrocarbons Exposing Young Children in New York City. International Journal of Environmental Research and Public Health. 2010 Apr 27;7(5):1889–900.

45.Klein C. The Great Smog of 1952 [Internet]. History. 2012. Available from: https://www.history.com/news/the-killer-fog-that-blanketed-london-60-years-ago

46.Biswaranjan Paital, Pawan Kumar Agrawal. Role of Environmental Factors in Transmission of COVID-19. Elsevier eBooks. 2022 Jan 1;35–72.

47.European Commission. EU Air Quality Standards [Internet]. environment.ec.europa.eu. 2010. Available from: https://environment.ec.europa.eu/topics/air/air-quality/eu-air-quality-standards_en

48.THE EUROPEAN PARLIAMENT AND THE COUNCIL OF THE EUROPEAN UNION. EUR-Lex - 32008L0050 - EN - EUR-Lex [Internet]. eur-lex.europa.eu. 2008. Available from: http://data.europa.eu/eli/dir/2008/50/oj

49.McDuffie EE, Martin RV, Spadaro JV, Burnett R, Smith SJ, O'Rourke P, et al. Source Sector and Fuel Contributions to Ambient PM2.5 and Attributable Mortality across Multiple Spatial Scales. Nature Communications [Internet]. 2021 Jun 14;12(1):3594. Available from: https://www.nature.com/articles/s41467-021-23853-y#Sec2

50.European Environment Agency. Europe's Air Quality Status 2021- Update — European Environment Agency [Internet]. www.eea.europa.eu. 2021. Available from: https://www.eea.europa.eu/publications/air-quality-in-europe-2021/air-quality-status-briefing-2021

51.Barwise Y, Kumar P. Designing Vegetation Barriers for Urban Air Pollution abatement: a Practical Review for Appropriate Plant Species Selection. npj Climate and Atmospheric Science. 2020 Mar 26;3(1).

52.Chen SL, Chang SW, Chen YJ, Chen HL. Possible Warming Effect of Fine Particulate Matter in the Atmosphere. Communications Earth & Environment [Internet]. 2021 Oct 1;2(1):1–9. Available from: https://www.nature.com/articles/s43247-021-00278-5

53.Gupta T, Rajeev P, Rajput R. Emerging Major Role of Organic Aerosols in Explaining the Occurrence, Frequency, and Magnitude of Haze and Fog Episodes during Wintertime in the Indo Gangetic Plain. ACS Omega. 2022 Jan 5;7(2):1575–84.

54.Chu SH. Stable Estimate of Primary OC/EC Ratios in the EC Tracer Method. Atmospheric Environment. 2005 Mar;39(8):1383–92.

55.Chakraborty A, B. Ervens, Gupta T, Sachchida Nand Tripathi. Characterization of Organic Residues of Size‐resolved Fog Droplets and Their Atmospheric Implications. Journal of Geophysical Research: Atmospheres. 2016 Apr 27;121(8):4317–32.

56.Kundu S, Stone ElizabethA. Composition and Sources of Fine Particulate Matter across Urban and Rural Sites in the Midwestern United States. Environmental science Processes & Impacts [Internet]. 2014 May 1;16(6):1360–70. Available from: https://www.ncbi.nlm.nih.gov/pmc/articles/PMC4191923/

57.Salma I, Vasanits-Zsigrai A, Machon A, Varga T, Major I, Gergely V, et al. Fossil Fuel combustion, Biomass Burning and Biogenic Sources of Fine Carbonaceous Aerosol in the Carpathian Basin. Atmospheric Chemistry and Physics. 2020 Apr 9;20(7):4295–312.

58.Moreno-Ríos AL, Tejeda-Benítez LP, Bustillo-Lecompte CF. Sources, characteristics, toxicity, and Control of Ultrafine particles: an Overview. Geoscience Frontiers. 2022 Jan;13(1):101147.

59.Voiland A. Aerosols: Tiny Particles, Big Impact [Internet]. Nasa.gov. NASA Earth Observatory; 2010. Available from: https://earthobservatory.nasa.gov/features/Aerosols

60.State of California. Statistics | CAL FIRE [Internet]. www.fire.ca.gov. 2024. Available from: https://www.fire.ca.gov/our-impact/statistics

61.Jaffe DA, O'Neill SM, Larkin NK, Holder AL, Peterson DL, Halofsky JE, et al. Wildfire and Prescribed Burning Impacts on Air Quality in the United States. Journal of the Air & Waste Management Association. 2020 Apr 2;70(6).

62.Kramer AL, Liu J, Li L, Connolly R, Barbato M, Zhu Y. Environmental Justice Analysis of wildfire-related PM2.5 Exposure Using low-cost Sensors in California. Science of the Total Environment [Internet]. 2023 Jan 15;856:159218. Available from: https://www.sciencedirect.com/science/article/pii/S0048969722063173

63.Li C, Managi S. Contribution of on-road Transportation to PM2.5. Scientific Reports [Internet]. 2021 Oct 29;11(1):21320. Available from: https://www.nature.com/articles/s41598-021-00862-x

64.Perera F. Pollution from Fossil-Fuel Combustion Is the Leading Environmental Threat to Global Pediatric Health and Equity: Solutions Exist. International Journal of Environmental Research and Public Health [Internet]. 2018 Dec 23;15(1):16. Available from: https://www.ncbi.nlm.nih.gov/pmc/articles/PMC5800116/

65.Maffia J, Dinuccio E, Amon B, Balsari P. PM Emissions from Open Field Crop management: Emission factors, Assessment Methods and Mitigation Measures – a Review. Atmospheric Environment. 2020 Apr;226:117381.

66.Kong L, Feng M, Liu Y, Zhang Y, Zhang C, Li C, et al. Elucidating the Pollution Characteristics of nitrate, Sulfate and Ammonium in PM2.5 in Chengdu, Southwest China, Based on 3-year Measurements. Atmospheric Chemistry and Physics [Internet]. 2020 Sep 30;20(19):11181–99. Available from: https://acp.copernicus.org/articles/20/11181/2020/

67.Wu G, Wan X, Gao S, Fu P, Yin Y, Li G, et al. Humic-Like Substances (HULIS) in Aerosols of Central Tibetan Plateau (Nam Co, 4730 M asl): Abundance, Light Absorption Properties, and Sources. Environmental Science & Technology. 2018 Jun 6;52(13):7203–11.

68.Hannigan MP, Busby WF, Cass GR. Source Contributions to the Mutagenicity of Urban Particulate Air Pollution. Journal of the Air & Waste Management Association. 2005 Apr;55(4):399–410.

69.Sun J, Chen H, Mao J, Zhao J, Zhang Y, Lin W, et al. Secondary Inorganic Ions Characteristics in PM 2.5 along Offshore and Coastal Areas of the Megacity Shanghai. Journal of Geophysical Research: Atmospheres. 2021 Oct 22;126(20).

70.Guo S, Hu M, Peng J, Wu Z, Zamora ML, Shang D, et al. Remarkable Nucleation and Growth of Ultrafine Particles from Vehicular Exhaust. Proceedings of the National Academy of Sciences [Internet]. 2020 Feb 18;117(7):3427–32. Available from: https://www.pnas.org/content/117/7/3427

71.Pierce JR. Cosmic rays, aerosols, clouds, and climate: Recent Findings from the CLOUD Experiment. Journal of Geophysical Research: Atmospheres. 2017 Aug 14;122(15):8051–5.

72.Zhang R, Wang G, Guo S, Zamora ML, Ying Q, Lin Y, et al. Formation of Urban Fine Particulate Matter. Chemical Reviews. 2015 May 5;115(10):3803–55.

73.Hussein T, Li X, Bakri Z, Alastuey A, Arar S, Al-Hunaiti A, et al. Organic and Elemental Carbon in the Urban Background in an Eastern Mediterranean City. Atmosphere [Internet]. 2022 Feb 1;13(2):197. Available from: https://www.mdpi.com/2073-4433/13/2/197

74.Bimenyimana E, Pikridas M, Oikonomou K, Iakovides M, Christodoulou A, Sciare J, et al. Fine Aerosol Sources at an Urban Background Site in the Eastern Mediterranean (Nicosia; Cyprus): Insights from Offline versus Online Source Apportionment Comparison for Carbonaceous Aerosols. Science of the Total Environment. 2023 Oct 1;893:164741–1.

75.Chrit M, Sartelet K, Sciare J, Pey J, Nicolas JB, Marchand N, et al. Aerosol Sources in the Western Mediterranean during summertime: a model-based Approach. Atmospheric Chemistry and Physics. 2018 Jul 9;18(13):9631–59.

76.White WH, Roberts PT. On the Nature and Origins of visibility-reducing Aerosols in the Los Angeles Air Basin. Atmospheric Environment (1967). 1977 Jan;11(9):803–12.

77.Urdiales-Flores D, Zittis G, Hadjinicolaou P, Osipov S, Klingmüller K, Mihalopoulos N, et al. Drivers of Accelerated Warming in Mediterranean climate-type Regions. npj Climate and Atmospheric Science [Internet]. 2023 Jul 20;6(1):1–9. Available from: https://www.nature.com/articles/s41612-023-00423-1

78.Neira M, Erguler K, Ahmady-Birgani H, DaifAllah AL-Hmoud N, Fears R, Gogos C, et al. Climate Change and Human Health in the Eastern Mediterranean and Middle east: Literature review, Research Priorities and Policy Suggestions. Environmental Research [Internet]. 2022 Oct 21;114537. Available from: https://www.sciencedirect.com/science/article/pii/S0013935122018643

79.Islam M. Evaluation of Cookstove Technologies in a Field Intervention Trial in Rural India: Quantifying Indoor Air Quality and Emissions Performance [Internet] [Dissertation]. [North Carolina State University]; 2021. Available from: https://repository.lib.ncsu.edu/server/api/core/bitstreams/e6431fa2-6c8a-439f-b08f-af48a82b3e22/content

80.Öztürk F, Özgül M. Assessing Long Term Trends of Air Pollutants and Associated Health Risks Imposed on Residents in Bolu (Türkiye) during Winter. Türkiye Halk Sağlığı Dergisi. 2019 Aug 31;17(2):102–22.

81.Chan YC, Vowles PD, McTainsh GH, Simpson RW, Cohen DD, Bailey GM, et al. Characterisation and Source Identification of PM10 Aerosol Samples Collected with a High Volume Cascade Impactor in Brisbane (Australia). Science of the Total Environment. 2000 Oct 30;262(1-2):5–19.

82.Dörter M, Odabasi M, Yenisoy-Karakaş S. Source apportionment of Biogenic and anthropogenic vocs in Bolu Plateau. Science of The Total Environment. 2020 Aug;731:139201. doi:10.1016/j.scitotenv.2020.139201

83.Sillanpää M, Hillamo R, Mäkelä T, Pennanen AS, Salonen RO. Field and laboratory tests of a high volume Cascade Impactor. Journal of Aerosol Science. 2003 Apr;34(4):485–500. doi:10.1016/s0021-8502(02)00214-8

84.Ammerlaan, B.A.J., Jedynska, A.D., Henzing, J.S., Holzinger, R., 2015. On a possible bias in elemental carbon measurements with the Sunset thermal/optical carbon analyser caused by unstable laser signal. Atmos. Environ. 122, 571–576. https://doi.org/10.1016/j.atmosenv.2015.09.076

85.PM10 particulate samplers [Internet]. 2024 [cited 2024 Apr 1]. Available from: https://tisch-env.com/high-volume-air-sampler/pm10

86. Karanasiou A, Minguillón MC, Viana M, Alastuey A, Putaud J-P, Maenhaut W, et al. Thermal-optical analysis for the measurement of Elemental Carbon (EC) and organic carbon (OC) in ambient air a literature review. 2015 Sept 16; doi:10.5194/amtd-8-9649-2015

87.Cavalli F, Viana M, Yttri KE, Genberg J, Putaud J-P. Toward a standardised thermal-optical protocol for measuring atmospheric organic and Elemental Carbon: The eusaar protocol. Atmospheric Measurement Techniques. 2010 Jan 26;3(1):79–89. doi:10.5194/amt-3-79-2010

88.Bautista AT, Pabroa PC, Santos FL, Quirit LL, Asis JL, Dy MA, et al. Intercomparison between NIOSH, IMPROVE_A, and eusaar_2 protocols: Finding an optimal thermal–optical protocol for Philippines OC/EC SAMPLES. Atmospheric Pollution Research. 2015 Mar;6(2):334–42. doi:10.5094/apr.2015.037

89.Flores RM, Mertoğlu E, Özdemir H, Akkoyunlu BO, Demir G, Ünal A, et al. A high-time resolution study of PM2.5, Organic Carbon, and elemental carbon at an urban traffic site in Istanbul. Atmospheric Environment. 2020 Feb;223:117241. doi:10.1016/j.atmosenv.2019.117241

90.Lee J, Kim D, Lee J. Elemental carbon and its fractions during evolved gas analysis with respect

to pyrolytic carbon and split time. Applied Sciences. 2021 Aug 17;11(16):7544. doi:10.3390/app11167544

91.Bocchicchio S, Commodo M, Sgro LA, Chiari M, D'Anna A, Minutolo P. Thermo-optical-transmission OC/EC and Raman spectroscopy analyses of flame-generated carbonaceous nanoparticles. Fuel. 2022 Feb;310:122308. doi:10.1016/j.fuel.2021.122308

92.Yoo HY, Kim KA, Kim YP, Jung CH, Shin HJ, Moon KJ, et al. Validation of SOC estimation using OC and EC concentration in PM2.5 measured at Seoul. Aerosol and Air Quality Research. 2022;22(4):210388. doi:10.4209/aaqr.210388

93.Hussain D, Kuo C-Y, Hameed A, Tseng K-H, Jan B, Abbas N, et al. Spaceborne satellite for snow cover and hydrological characteristic of the Gilgit River basin, hindukush–karakoram mountains, Pakistan. Sensors. 2019 Jan 27;19(3):531. doi:10.3390/s19030531

94.Strength of Correlation [Internet]. Newcastle University; [cited 2024 Apr 4]. Available from: https://www.ncl.ac.uk/webtemplate/ask-assets/external/maths-resources/statistics/regression-and-correlation/strength-of-correlation.html

95 Bolu Merkez Topographic map, elevation, terrain [Internet]. [cited 2024 Apr 4]. Available from: https://en-ca.topographic-map.com/map-sf3tf3/Bolu-merkez/?center=40.80749%2C31.6047&base=2&zoom=11

96.Bolu Sıfırın altında 29,7 dereceyle türkiye'nin gece en soğuk Ili Oldu [Internet]. [cited 2024 Apr 5]. Available from: https://www.aa.com.tr/tr/turkiye/bolu-sifirin-altinda-29-7-dereceyle-turkiyenin-gece-en-soguk-ili-oldu/2151250

97.Why is the weather different in high and low-pressure areas? [Internet]. 2016 [cited 2024 Apr 17]. Available from: https://www.americangeosciences.org/education/k5geosource/content/weather/why-is-the-weather-different-in-high-and-low-pressure-areas#:~:text=As%20air%20leaves%20the%20high,areas%20of%20fair%2C%20settled%20weather.

98.Atmospheric stability [Internet]. 2014 [cited 2024 Apr 17]. Available from: https://www.aiche.org/ccps/resources/glossary/process-safety-glossary/atmospheric-stability

99.Yao T, Fung JCH, Ma H, Lau AKH, Chan PW, Yu JZ, et al. Enhancement in secondary particulate matter production due to mountain trapping. Atmospheric Research. 2014 Oct;147–148:227–36. doi:10.1016/j.atmosres.2014.05.007

100.Liang L, Engling G, Cheng Y, Zhang X, Sun J, Xu W, et al. Influence of high relative humidity on secondary organic carbon: Observations at a background site in East China. Journal of Meteorological Research. 2019 Oct;33(5):905–13. doi:10.1007/s13351-019-8202-2

101. Öztürk, F., & Keleş, M. (2016). Wintertime chemical compositions of coarse and fine fractions of particulate matter in Bolu, Türkiye. Environmental Science and Pollution Research, 23(14). https://doi.org/10.1007/s11356-016-6584-6

102.Górka, M., Kosztowniak, E. (2015). Assessing environmental anthropogenic pressure in Lower Silesia based on atmospheric PM10: carbon isotopic and OC/EC ratio approach. XXIInd Meeting of the Petrology Group of the Mineralogical Society of Poland At: Sandomierz.

103.Theodosi, C., Tsagkaraki, M., Zarmpas, P., Grivas, G., Liakakou, E., Paraskevopoulou, D., Lianou, M., Gerasopoulos, E., & Mihalopoulos, N. (2018). Multi-year chemical composition of the fine-aerosol fraction in Athens, Greece, with emphasis on the contribution of residential heating in wintertime. Atmospheric Chemistry and Physics, 18(19), 14371–14391. https://doi.org/10.5194/acp-18-14371-2018

104. Koçak, M., Mihalopoulos, N., & Kubilay, N. (2009). Origin and source regions of PM10 in the Eastern Mediterranean atmosphere. Atmospheric Research, 92(4), 464–474.

https://doi.org/10.1016/j.atmosres.2009.01.005

105.Galindo, N., Yubero, E., Clemente, Á., Nicolás, J. F., Varea, M., & Crespo, J. (2020). PM events and changes in the chemical composition of urban aerosols: A case study in the western Mediterranean. Chemosphere, 244, 125520. https://doi.org/10.1016/j.chemosphere.2019.125520

106.Yang, L., Shang, Y., Hannigan, M. P., Zhu, R., Wang, Q., Qin, C., & Xie, M. (2021). Collocated speciation of PM2.5 using tandem quartz filters in northern nanjing, China: Sampling artifacts and measurement uncertainty. Atmospheric Environment, 246, 118066. https://doi.org/10.1016/j.atmosenv.2020.118066

107.Aslan Kılavuz, S., Bozkurt, Z., & Öztürk, F. (2019). Characterization and source estimates of primary and secondary carbonaceous aerosols at urban and suburban atmospheres of Düzce, Türkiye. Environmental Science and Pollution Research, 26(7). https://doi.org/10.1007/s11356-018-3998-3

108.Bae, M.-S., Schwab, J. J., Chen, W.-N., Lin, C.-Y., Rattigan, O. V., & Demerjian, K. L. (2011). Identifying pollutant source directions using multiple analysis methods at a rural location in New York. Atmospheric Environment, 45(15), 2531–2540. https://doi.org/10.1016/j.atmosenv.2011.02.020

109.Bhuyan, P., Deka, P., Prakash, A., Balachandran, S., & Hoque, R. R. (2018). Chemical characterization and source apportionment of aerosol over mid Brahmaputra Valley, India. Environmental Pollution, 234, 997–1010. https://doi.org/10.1016/j.envpol.2017.12.009

110.Górka, M., Kosztowniak, E., Lewandowska, A. U., & Widory, D. (2020). Carbon isotope compositions and TC/OC/EC levels in atmospheric PM10 from Lower Silesia (SW Poland): Spatial variations, seasonality, sources and implications. Atmospheric Pollution Research, 11(7), 1099–1114. https://doi.org/10.1016/j.apr.2020.04.003

111.Vodička P, Schwarz J, Cusack M, Ždímal V. Detailed comparison of OC/EC aerosol at an urban and a rural Czech background site during summer and Winter. Science of The Total Environment. 2015 Jun;518–519:424–33. doi:10.1016/j.scitotenv.2015.03.029

112.Plaza J, Artíñano B, Salvador P, Gómez-Moreno FJ, Pujadas M, Pio CA. Short-term secondary organic carbon estimations with a modified OC/EC primary ratio method at a suburban site in Madrid (Spain). Atmospheric Environment. 2011 May;45(15):2496–506. doi:10.1016/j.atmosenv.2011.02.037

113.Hou B, Zhuang G, Zhang R, Liu T, Guo Z, Chen Y. The implication of carbonaceous aerosol to the formation of haze: Revealed from the characteristics and sources of OC/EC over a mega-city in China. Journal of Hazardous Materials. 2011 Jun;190(1–3):529–36. doi:10.1016/j.jhazmat.2011.03.

114.Sokhi RS, Moussiopoulos N, Baklanov A, Bartzis J, Coll I, Finardi S, et al. Advances in air quality research – current and emerging challenges. Atmospheric Chemistry and Physics. 2022 Apr 11;22(7):4615–703. doi:10.5194/acp-22-4615-2022

115.Aslan A, Altinoz B, Ozsolak B. The link between urbanization and air pollution in Türkiye: Evidence from dynamic autoregressive distributed lag simulations. Environmental Science and Pollution Research. 2021 May 19;28(37):52370–80. doi:10.1007/s11356-021-14408-1

116.IPCC. Global warming of 15°C. 2022 May 24; doi:10.1017/9781009157940

117.Fan J, Rosenfeld D, Zhang Y, Giangrande SE, Li Z, Machado LA, et al. Substantial convection and precipitation enhancements by ultrafineaerosol particles. Science. 2018 Jan 26;359(6374):411–8. doi:10.1126/science.aan8461

118.Pope CA, Dockery DW. Health effects of fine particulate air pollution: Lines that connect. Journal of the Air & Waste Management Association. 2006 Jun;56(6):709–42. doi:10.1080/10473289.2006.10464485

119.Lang-Yona N, Öztürk F, Gat D, Aktürk M, Dikmen E, Zarmpas P, et al. Links between airborne microbiome, meteorology, and chemical composition in northwestern Türkiye. Science of The Total Environment. 2020 Jul;725:138227. doi:10.1016/j.scitotenv.2020.138227

120.Flores RM, Özdemir H, Akkoyunlu BO, Ünal A, Tayanç M. Seasonal variation of carbonaceous PM2.5 in an Istanbul Traffic Site. Atmospheric Pollution Research. 2020 Dec;11(12):2110–8. doi:10.1016/j.apr.2020.06.022

121.Rodríguez S, Alastuey A, Alonso-Pérez S, Querol X, Cuevas E, Abreu-Afonso J, et al. Transport of desert dust mixed with North African industrial pollutants in the subtropical saharan air layer. Atmospheric Chemistry and Physics. 2011 Jul 13;11(13):6663–85. doi:10.5194/acp-11-6663-2011

122.A burst of Saharan dust [Internet]. NASA; [cited 2024 Jul 22]. Available from: https://earthobservatory.nasa.gov/images/149918/a-burst-of-saharan-dust

123.Baltaci H. Meteorological characteristics of dust storm events in Türkiye. Aeolian Research. 2021 Mar;50:100673. doi:10.1016/j.aeolia.2021.100673

124.Power AL, Tennant RK, Jones RT, Tang Y, Du J, Worsley AT, et al. Monitoring impacts of urbanisation and industrialisation on air quality in the Anthropocene Using Urban Pond Sediments. Frontiers in Earth Science. 2018 Sept 7;6. doi:10.3389/feart.2018.00131

125.Srivastava D, Favez O, Perraudin E, Villenave E, Albinet A. Comparison of measurement-based methodologies to apportion secondary organic carbon (SOC) in PM2.5: A review of recent studies. Atmosphere. 2018 Nov 16;9(11):452. doi:10.3390/atmos911045

126.Cheng Y, Lee SC, Ho KF, Chow JC, Watson JG, Louie PKK, et al. Chemically-speciated on-road PM2.5 motor vehicle emission factors in Hong Kong. Science of The Total Environment. 2010 Mar;408(7):1621–7. doi:10.1016/j.scitotenv.2009.11.061

127.Cao JJ, Lee SC, Ho KF, Fung K, Chow JC, Watson JG. Characterization of roadside fine particulate carbon and its eight fractions in Hong Kong. Aerosol and Air Quality Research. 2006;6(2):106–22. doi:10.4209/aaqr.2006.06.0001

128.Zhang Y, Schauer JJ, Zhang Y, Zeng L, Wei Y, Liu Y, et al. Characteristics of particulate carbon emissions from real-world chinese coal combustion. Environmental Science & Technology. 2008 Jun 7;42(14):5068–73. doi:10.1021/es7022576

129.Hao Y, Gao C, Deng S, Yuan M, Song W, Lu Z, et al. Chemical characterisation of PM2.5 emitted from motor vehicles powered by diesel, gasoline, natural gas and methanol fuel. Science of The Total Environment. 2019 Jul;674:128–39. doi:10.1016/j.scitotenv.2019.03.410

130.Published by Zeynep Dierks, 29 J. Türkiye: Share of registered cars by Fuel Type 2023 [Internet]. 2024 [cited 2024 Jul 22]. Available from: https://www.statista.com/statistics/1323803/Türkiye-share-of-registered-cars-by-fuel-type/

131.Yenisoy-Karakaş S, Gaga EO, Cankur O, Karakaş D. Uncertainty of high resolution inductively coupled plasma mass spectrometry based aerosol measurements. Talanta. 2009 Oct 15;79(5):1298–305. doi:10.1016/j.talanta.2009.05.044

132.Singh N, Ojha V, Kayal N, Ahuja T, Gupta PK. Quantifying uncertainty in the measurement of arsenic in suspended particulate matter by atomic absorption spectrometry with hydride generator. Chemistry Central Journal. 2011 Apr 5;5(1). doi:10.1186/1752-153x-5-17

133.E. Lekkas, C. Cadis, A. Gregoriou, S. Mavroulis, M. Diakakis, M. Mavrouli, M. Gogou, E. Stamati (2021). The early July 2021 Arakapas (Cyprus) forest fire. Newsletter of Environmental, Disaster and Crises Management Strategies, 24, ISSN 2653-9454.

134.Ribeiro H, Guimarães F, Duque L, Noronha F, Abreu I. Characterisation of particulate matter on airborne pollen grains. Environmental Pollution. 2015 Nov;206:7–16. doi:10.1016/j.envpol.2015.06.015

135.Ministry of Justice. Regulation on the Working Procedures and Principles of Institution and Organization [Internet]. Ankara: Ministry of Justice; 2021 [cited 2024 Aug 4]. Available from: https://www.mevzuat.gov.tr/File/GeneratePdf?mevzuatNo=12188&mevzuatTur=KurumVeKurulusYonetmeligi&mevzuatTertip=5

136.Tian S, Wang L, Liu Q, Luo L, Qian C, Wang B, et al. Associations between indoor and outdoor size-resolved particulate matter in Urban beijing: Chemical Compositions, sources, and Health Risks. Atmosphere. 2024 Jun 16;15(6):721. doi:10.3390/atmos15060721

137.Du Z, Hu M, Peng J, Zhang W, Zheng J, Gu F, et al. Comparison of primary aerosol emission and secondary aerosol formation from gasoline direct injection and port fuel injection vehicles. Atmospheric Chemistry and Physics. 2018 Jun 28;18(12):9011–23. doi:10.5194/acp-18-9011-2018

138.Chen S-J, Liao S-H, Jian W-J, Lin C-C. Particle size distribution of aerosol carbons in ambient air. Environment International. 1997 Jan;23(4):475–88. doi:10.1016/s0160-4120(97)00029-9

139.Offenberg JH, Baker JE. Aerosol size distributions of elemental and organic carbon in urban and over-water atmospheres. Atmospheric Environment. 2000 Jan;34(10):1509–17. doi:10.1016/s1352-2310(99)00412-4

140.Liu F, Peng L, Dai S, Bi X, Shi M. Size-segregated characteristics of organic carbon (OC) and Elemental Carbon (EC) in marine aerosol in the northeastern South China Sea. Atmosphere. 2023 Mar 31;14(4):661. doi:10.3390/atmos14040661

141.Napolitano DC, Hartnett HE, Herckes P. A novel method for carbonate quantification in atmospheric particulate matter. Atmosphere. 2020 Jun 20;11(6):661. doi:10.3390/atmos11060661

142.Hama S, Ouchen I, Wyche KP, Cordell RL, Monks PS. Carbonaceous aerosols in five European cities: Insights into primary emissions and Secondary Particle Formation. Atmospheric Research. 2022 Aug;274:106180. doi:10.1016/j.atmosres.2022.106180

143.Salma I, Varga PT, Vasanits A, Machon A. Secondary organic carbon in different atmospheric environments of a continental region and seasons. Atmospheric Research. 2022 Nov;278:106360. doi:10.1016/j.atmosres.2022.106360

144.NASA. CALIPSO satellite aerosol subtype images for July 4, 2021 [Internet]. Washington, D.C.: NASA; 2021 [cited 2024 Aug 8]. Available from: https://www-calipso.larc.nasa.gov/products/lidar/browse_images/exp_showdate.php?browse_date=2021-07-04

145.NASA. CALIPSO satellite aerosol subtype images for July 6, 2021 [Internet]. Washington, D.C.: NASA; 2021 [cited 2024 Aug 8]. Available from: https://www-calipso.larc.nasa.gov/products/lidar/browse_images/exp_showdate.php?browse_date=2021-07-06

146.Worldview: Explore your dynamic planet [Internet]. NASA; [cited 2024 Aug 2]. Available from: https://worldview.earthdata.nasa.gov/

147.Winker D. Cloud-Aerosol Lidar and Infrared Pathfinder Satellite Observations [Internet]. NASA; [cited 2024 Aug 8]. Available from: https://www-calipso.larc.nasa.gov/products/lidar/browse_images/exp_index.php

148.Plaza J, Artíñano B, Salvador P, Gómez-Moreno FJ, Pujadas M, Pio CA. Short-term secondary organic carbon estimations with a modified OC/EC primary ratio method at a suburban site

in Madrid (Spain). Atmospheric Environment. 2011 May;45(15):2496–506. doi:10.1016/j.atmosenv.2011.02.037

149.Raparthi N, Yadav S, Khare A, Dubey S, Phuleria HC. Chemical and oxidative properties of fine particulate matter from near-road traffic sources. Environmental Pollution. 2023 Nov;337:122514. doi:10.1016/j.envpol.2023.122514

150.Křůmal K, Mikuška P, Večeřa Z. Monosaccharide anhydrides, monocarboxylic acids and OC/EC in PM1 aerosols in urban areas in the Czech Republic. Atmospheric Pollution Research. 2015 Nov;6(6):917–27. doi:10.1016/j.apr.2015.04.001

151.Watson JG, Chow JC, Houck JE. PM2.5 chemical source profiles for vehicle exhaust, vegetative burning, geological material, and coal burning in northwestern Colorado during 1995. Chemosphere. 2001 Jun;43(8):1141–51. doi:10.1016/s0045-6535(00)00171-5

152.Sharma SK, Mandal TK, Saxena M, Rashmi, Sharma A, Datta A, et al. Variation of OC, EC, WSIC and trace metals of PM10 in Delhi, India. Journal of Atmospheric and Solar-Terrestrial Physics. 2014 Jun;113:10–22. doi:10.1016/j.jastp.2014.02.008

153.Srinivas B, Sarin MM. PM2.5, EC and OC in atmospheric outflow from the indo-gangetic plain: Temporal variability and aerosol organic carbon-to-organic mass conversion factor. Science of The Total Environment. 2014 Jul;487:196–205. doi:10.1016/j.scitotenv.2014.04.002

154.Hou B, Zhuang G, Zhang R, Liu T, Guo Z, Chen Y. The implication of carbonaceous aerosol to the formation of haze: Revealed from the characteristics and sources of OC/EC over a mega-city in China. Journal of Hazardous Materials. 2011 Jun;190(1–3):529–36. doi:10.1016/j.jhazmat.2011.03.072

155.Górka M, Kosztowniak E, Lewandowska AU, Widory D. Carbon isotope compositions and TC/OC/EC levels in atmospheric PM10 from Lower Silesia (SW Poland): Spatial variations, seasonality, sources and implications. Atmospheric Pollution Research. 2020 Jul;11(7):1099–114. doi:10.1016/j.apr.2020.04.003

156.Varga G, Újvári G, Kovács J. Spatiotemporal patterns of Saharan dust outbreaks in the Mediterranean Basin. Aeolian Research. 2014 Dec;15:151–60. doi:10.1016/j.aeolia.2014.06.005

157.Conte M, Merico E, Cesari D, Dinoi A, Grasso FM, Donateo A, et al. Long-term characterisation of African dust advection in south-eastern Italy: Influence on fine and coarse particle concentrations, size distributions, and carbon content. Atmospheric Research. 2020 Mar;233:104690. doi:10.1016/j.atmosres.2019.104690

158.Cuevas-Agulló E, Barriopedro D, García RD, Alonso-Pérez S, González-Alemán JJ, Werner E, et al. Sharp increase in Saharan dust intrusions over the western Euro-Mediterranean in February–March 2020–2022 and associated atmospheric circulation. Atmospheric Chemistry and Physics. 2024 Apr 8;24(7):4083–104. doi:10.5194/acp-24-4083-2024

159.Zhang P, Lu N, Hu X, Dong C. Identification and physical retrieval of dust storm using three Modis thermal IR channels. Global and Planetary Change. 2006 Jul;52(1–4):197–206. doi:10.1016/j.gloplacha.2006.02.014

160.Schumacher V, Setzer A. Assessment and characteristics of S-NPP viirs deep blue and dark target aerosol properties under clean, polluted and fire scenarios over the Amazon. Atmospheric Environment. 2024 Apr;323:120398. doi:10.1016/j.atmosenv.2024.120398

161.Zhao S, Yin D, Qu J. Identifying sources of dust based on Calipso, Modis satellite data and backward trajectory model. Atmospheric Pollution Research. 2015 Jan;6(1):36–44. doi:10.5094/apr.2015.005

162.Gammoudi N, Kovács J, Gresina F, Varga G. Combined use of HYSPLIT model and Modis aerosols optical depth to study the spatiotemporal circulation patterns of Saharan dust events over Central Europe. Aeolian Research. 2024 Sept;67–69:100899.

doi:10.1016/j.aeolia.2024.100899

163.Tuna Tuygun G, Elbir T. Long-term temporal analysis of the columnar and surface aerosol relationship with planetary boundary layer height at a southern coastal site of Türkiye. Atmospheric Pollution Research. 2020 Dec;11(12):2259–69. doi:10.1016/j.apr.2020.09.008

164.Ara Aksoy S, Kiziltan A, Kiziltan M, Aydınalp Köksal M, Öztürk F, Tekeli E, et al. Mortality and morbidity costs of road traffic-based air pollution in Türkiye. Journal of Transport & Health. 2021 Sept;22:101142. doi:10.1016/j.jth.2021.101142

165.Bayramoğlu Karşı MB, Berberler E, Berberler T, Aslan Ö, Yenisoy-Karakaş S, Karakaş D. Correction and source apportionment of Vehicle Emission Factors obtained from Bolu Mountain Highway Tunnel, Türkiye. Atmospheric Pollution Research. 2020 Dec;11(12):2133–41. doi:10.1016/j.apr.2020.06.021

166.Kayalar Ö, Arı A, Babuççu G, Konyalılar N, Doğan Ö, Can F, et al. Existence of SARS-COV-2 RNA on ambient particulate matter samples: A nationwide study in Turkey. Science of The Total Environment. 2021 Oct;789:147976. doi:10.1016/j.scitotenv.2021.147976

167.Sputnik Türkiye. Bolu, türkiye'nin en soğuk Ili Oldu [Internet]. Sputnik Türkiye feedback.tr@sputniknews.com+74956456601MIA „Rossiya Segodnya" 25260; 2022 [cited 2024 Aug 25]. Available from: https://anlatilaninotesi.com.tr/20220211/bolu-turkiyenin-en-soguk-ili-oldu-1053750283.html

168.Son Dakika... Kar Kalınlığı 7 metreyi Buldu! Böylesi Görülmedi... meteoroloji'den çok önemli Uyarı [Internet]. [cited 2024 Aug 25]. Available from: https://www.hurriyet.com.tr/gundem/son-dakika-kar-kalinligi-7-metreyi-buldu-boylesi-gorulmedi-meteorolojiden-cok-onemli-uyari-42001623

169.Iha. Meteoroloji Uyarmıştı! Bolu'da Kar Yağışı Başladı - Sondakika Haberler [Internet]. Künye; [cited 2024 Aug 25]. Available from: https://www.cnnturk.com/turkiye/meteoroloji-uyarmisti-boluda-kar-yagisi-basladi-1755795

170.[Internet]. [cited 2024 Aug 25]. Available from: https://www.eurachem.org/images/stories/Guides/pdf/QUAM2012_P1.pdf

7. APPENDICES

APPENDIX 1 EXCEL File With Raw Data

The file available by following link is raw data of fractionated PM, OC, EC, CC, TC concentrations.

ANNEX 1 PM Data.xlsx

Same data from the excel spreadsheet in the link above is available in following set of tables:

Table 1.1 PM fractionated concentrations data

Date	Size Fraction (µm)	PM Mass Conc. (µg/m^3)	Date	Size Fraction (µm)	PM Mass Conc. (µg/m^3)
17.02.2021	<0.49	7,716828449	**17.02.2021**	0.95-1.5	0,185655915
26.02.2021	<0.49	13,17953416	**26.02.2021**	0.95-1.5	7,295872199
05.03.2021	<0.49	13,55766016	**05.03.2021**	0.95-1.5	5,331306653
10.03.2021	<0.49	14,35929942	**10.03.2021**	0.95-1.5	5,388532024
18.03.2021	<0.49	6,044003366	**18.03.2021**	0.95-1.5	1,805698109
12.04.2021	<0.49	12,75316663	**12.04.2021**	0.95-1.5	4,215369873
21.04.2021	<0.49	14,4287194	**21.04.2021**	0.95-1.5	4,198259684
28.04.2021	<0.49	14,5251703	**28.04.2021**	0.95-1.5	5,120600099
06.05.2021	<0.49	9,633039985	**06.05.2021**	0.95-1.5	2,901178709
12.05.2021	<0.49	13,90121469	**12.05.2021**	0.95-1.5	3,60033967
19.05.2021	<0.49		**19.05.2021**	0.95-1.5	2,423900673
31.05.2021	<0.49	6,18297493	**31.05.2021**	0.95-1.5	1,824688291
11.06.2021	<0.49	5,83713326	**11.06.2021**	0.95-1.5	2,380190261
17.06.2021	<0.49	4,312929208	**17.06.2021**	0.95-1.5	1,086115398
04.07.2021	<0.49	22,28326657	**04.07.2021**	0.95-1.5	14,53365356
13.07.2021	<0.49	9,993656627	**13.07.2021**	0.95-1.5	3,438464951
27.08.2021	<0.49	4,56958991	**27.08.2021**	0.95-1.5	2,583047461
02.09.2021	<0.49	4,782016407	**02.09.2021**	0.95-1.5	1,42051996
08.09.2021	<0.49	9,211394839	**08.09.2021**	0.95-1.5	1,578851892
14.09.2021	<0.49	7,17349522	**14.09.2021**	0.95-1.5	2,447590351
21.09.2021	<0.49	5,005830834	**21.09.2021**	0.95-1.5	1,315788982
28.09.2021	<0.49	6,040915558	**28.09.2021**	0.95-1.5	0,75904961
06.10.2021	<0.49	10,07863687	**06.10.2021**	0.95-1.5	3,497014871
12.10.2021	<0.49	6,64932363	**12.10.2021**	0.95-1.5	2,84401912
27.10.2021	<0.49	16,39284127	**27.10.2021**	0.95-1.5	5,391219458
16.11.2021	<0.49	12,90920157	**16.11.2021**	0.95-1.5	9,151973438
26.11.2021	<0.49	3,420819103	**26.11.2021**	0.95-1.5	1,815929796

03.12.2021	<0.49	6,343629157	**03.12.2021**	0.95-1.5	1,923753103
10.12.2021	<0.49	7,944338803	**10.12.2021**	0.95-1.5	3,441620329
16.12.2021	<0.49	4,374630988	**16.12.2021**	0.95-1.5	1,95208515
29.12.2021	<0.49	12,1316713	**29.12.2021**	0.95-1.5	6,559915825
06.01.2022	<0.49	15,15649068	**06.01.2022**	0.95-1.5	6,592688595
17.01.2022	<0.49	14,51286185	**17.01.2022**	0.95-1.5	7,868862183
27.01.2022	<0.49	18,44500203	**27.01.2022**	0.95-1.5	12,57679383
02.02.2022	<0.49	19,01784762	**02.02.2022**	0.95-1.5	12,97710171
10.02.2022	<0.49	1,234095813	**10.02.2022**	0.95-1.5	0,796347168
23.02.2022	<0.49	7,880435101	**23.02.2022**	0.95-1.5	5,028707894
04.03.2022	<0.49	8,681096872	**04.03.2022**	0.95-1.5	2,420690474
10.03.2022	<0.49	13,18820156	**10.03.2022**	0.95-1.5	3,138941365
17.02.2021	>7.2	0,146910332	**17.02.2021**	1.5-3	10,89880939
26.02.2021	>7.2	1,514020744	**26.02.2021**	1.5-3	3,671746621
05.03.2021	>7.2	1,903798889	**05.03.2021**	1.5-3	3,457647059
10.03.2021	>7.2	2,598975853	**10.03.2021**	1.5-3	4,182647706
18.03.2021	>7.2	0,925357757	**18.03.2021**	1.5-3	1,5972842
12.04.2021	>7.2		**12.04.2021**	1.5-3	5,647257417
21.04.2021	>7.2	2,075021706	**21.04.2021**	1.5-3	0,54415507
28.04.2021	>7.2	3,463259065	**28.04.2021**	1.5-3	7,034413331
06.05.2021	>7.2	2,1441964	**06.05.2021**	1.5-3	3,61943169
12.05.2021	>7.2	2,709839393	**12.05.2021**	1.5-3	3,992438617
19.05.2021	>7.2	1,856792717	**19.05.2021**	1.5-3	2,443334279
31.05.2021	>7.2	1,281012909	**31.05.2021**	1.5-3	1,748289463
11.06.2021	>7.2	1,604503256	**11.06.2021**	1.5-3	2,532494102
17.06.2021	>7.2	0,711230406	**17.06.2021**	1.5-3	2,442007846
04.07.2021	>7.2	12,59356816	**04.07.2021**	1.5-3	19,8890045
13.07.2021	>7.2	2,611651633	**13.07.2021**	1.5-3	4,97346185
27.08.2021	>7.2	9,339822416	**27.08.2021**	1.5-3	11,85418142
02.09.2021	>7.2	1,327765332	**02.09.2021**	1.5-3	2,061213969
08.09.2021	>7.2	1,262397287	**08.09.2021**	1.5-3	2,52650514
14.09.2021	>7.2	1,281659873	**14.09.2021**	1.5-3	2,672139924
21.09.2021	>7.2	0,922939338	**21.09.2021**	1.5-3	1,617717093
28.09.2021	>7.2	2,007808645	**28.09.2021**	1.5-3	3,546895412
06.10.2021	>7.2	2,261481826	**06.10.2021**	1.5-3	3,382081565
12.10.2021	>7.2	1,621194821	**12.10.2021**	1.5-3	3,206016681
27.10.2021	>7.2	1,202957257	**27.10.2021**	1.5-3	3,867133781
16.11.2021	>7.2	3,109988145	**16.11.2021**	1.5-3	4,52582562
26.11.2021	>7.2	1,290782531	**26.11.2021**	1.5-3	4,32224011
03.12.2021	>7.2	1,498985793	**03.12.2021**	1.5-3	1,656428503
10.12.2021	>7.2	1,353758495	**10.12.2021**	1.5-3	3,834014096
16.12.2021	>7.2	0,235230344	**16.12.2021**	1.5-3	0,937654289
29.12.2021	>7.2	1,552346493	**29.12.2021**	1.5-3	3,082993519
06.01.2022	>7.2	2,061470139	**06.01.2022**	1.5-3	13,96177503
17.01.2022	>7.2	1,13531643	**17.01.2022**	1.5-3	3,105330291

27.01.2022	>7.2	0,877264247	**27.01.2022**	1.5-3	5,253962841
02.02.2022	>7.2	1,406426794	**02.02.2022**	1.5-3	4,135264445
10.02.2022	>7.2	0,080765433	**10.02.2022**	1.5-3	0,381212843
23.02.2022	>7.2	0,976871827	**23.02.2022**	1.5-3	1,975563816
04.03.2022	>7.2		**04.03.2022**	1.5-3	1,358467271
10.03.2022	>7.2	1,095558594	**10.03.2022**	1.5-3	1,33458956
17.02.2021	0.49-0.95	0,08717756	**17.02.2021**	3-7.2	4,087658919
26.02.2021	0.49-0.95	0,558315676	**26.02.2021**	3-7.2	5,212041044
05.03.2021	0.49-0.95	8,636582825	**05.03.2021**	3-7.2	6,101533116
10.03.2021	0.49-0.95	9,184959438	**10.03.2021**	3-7.2	6,953651811
18.03.2021	0.49-0.95	3,18122991	**18.03.2021**	3-7.2	2,219191305
12.04.2021	0.49-0.95	11,2376408	**12.04.2021**	3-7.2	6,903504549
21.04.2021	0.49-0.95	6,521250789	**21.04.2021**	3-7.2	4,391124772
28.04.2021	0.49-0.95	5,002092255	**28.04.2021**	3-7.2	12,67326415
06.05.2021	0.49-0.95	4,927426703	**06.05.2021**	3-7.2	6,025931262
12.05.2021	0.49-0.95	4,747011259	**12.05.2021**	3-7.2	0,240487355
19.05.2021	0.49-0.95	3,1005435	**19.05.2021**	3-7.2	5,050970863
31.05.2021	0.49-0.95	3,782630352	**31.05.2021**	3-7.2	4,162847776
11.06.2021	0.49-0.95	3,906770622	**11.06.2021**	3-7.2	5,231459845
17.06.2021	0.49-0.95	1,729025641	**17.06.2021**	3-7.2	2,165223599
04.07.2021	0.49-0.95	20,54165995	**04.07.2021**	3-7.2	21,42676804
13.07.2021	0.49-0.95	4,436033193	**13.07.2021**	3-7.2	10,80968542
27.08.2021	0.49-0.95	15,30125735	**27.08.2021**	3-7.2	12,54829634
02.09.2021	0.49-0.95	2,057778612	**02.09.2021**	3-7.2	4,567306619
08.09.2021	0.49-0.95	3,255206013	**08.09.2021**	3-7.2	6,07079671
14.09.2021	0.49-0.95	4,858907309	**14.09.2021**	3-7.2	5,815833953
21.09.2021	0.49-0.95	2,365675367	**21.09.2021**	3-7.2	3,883893423
28.09.2021	0.49-0.95	2,933009667	**28.09.2021**	3-7.2	9,033389942
06.10.2021	0.49-0.95	6,290908338	**06.10.2021**	3-7.2	7,994625588
12.10.2021	0.49-0.95	4,297205503	**12.10.2021**	3-7.2	7,889468387
27.10.2021	0.49-0.95	10,96424178	**27.10.2021**	3-7.2	7,880389489
16.11.2021	0.49-0.95	12,76357257	**16.11.2021**	3-7.2	8,211857355
26.11.2021	0.49-0.95	1,220435701	**26.11.2021**	3-7.2	5,398710205
03.12.2021	0.49-0.95	11,4834776	**03.12.2021**	3-7.2	5,863100888
10.12.2021	0.49-0.95	3,860173681	**10.12.2021**	3-7.2	5,603055995
16.12.2021	0.49-0.95	3,652604514	**16.12.2021**	3-7.2	1,535531415
29.12.2021	0.49-0.95	9,516050921	**29.12.2021**	3-7.2	6,30119141
06.01.2022	0.49-0.95	10,5047967	**06.01.2022**	3-7.2	6,848699091
17.01.2022	0.49-0.95	11,20925095	**17.01.2022**	3-7.2	2,00519268
27.01.2022	0.49-0.95	16,55415276	**27.01.2022**	3-7.2	2,739245584
02.02.2022	0.49-0.95	20,95693545	**02.02.2022**	3-7.2	3,463136945
10.02.2022	0.49-0.95	1,385934827	**10.02.2022**	3-7.2	0,306908645
23.02.2022	0.49-0.95	7,712587708	**23.02.2022**	3-7.2	2,712413871
04.03.2022	0.49-0.95	7,386461196	**04.03.2022**	3-7.2	3,435449158
10.03.2022	0.49-0.95	6,832301775	**10.03.2022**	3-7.2	

Table 2.2 OC, EC, TC fractionated concentrations data

Date	Fraction	OC (µg/m^3)	EC (µg/m^3)	TC (µg/m^3)	Date	Fraction	OC (µg/m^3)	EC (µg/m^3)	TC (µg/m^3)
17.02.2021	<0.49	2,67	0,38	3,05419718	**17.02.2021**	1.5-3	5,12	0,13	5,25114532
26.02.2021	<0.49	5,39	0,07	5,46266211	**26.02.2021**	1.5-3	0,89	0,02	0,91392608
03.12.2021	<0.49	2,65	1,06	3,70606229	**03.12.2021**	1.5-3	0,49	0,03	0,51808717
10.12.2021	<0.49	2,83	1,08	3,90980712	**10.12.2021**	1.5-3	0,44	0,03	0,46995584
16.12.2021	<0.49	2,26	1,06	3,31545549	**16.12.2021**	1.5-3	0,23	0,02	0,25187128
29.12.2021	<0.49	5,09	1,13	6,22186376	**29.12.2021**	1.5-3	0,78	0,06	0,84395318
06.01.2022	<0.49	6,19	1,75	7,93417087	**06.01.2022**	1.5-3	1,00	0,05	1,05235556
17.01.2022	<0.49	5,39	1,45	6,84217118	**17.01.2022**	1.5-3	0,89	0,04	0,92445274
27.01.2022	<0.49	5,19	1,74	6,93083859	**27.01.2022**	1.5-3	1,08	0,07	1,1490825
02.02.2022	<0.49	5,71	2,28	7,99075023	**02.02.2022**	1.5-3	1,13	0,05	1,17565132
10.02.2022	<0.49	0,83	0,33	1,16671644	**10.02.2022**	1.5-3	0,15	0,01	0,16223912
23.02.2022	<0.49	3,31	0,96	4,27081804	**23.02.2022**	1.5-3	0,43	0,03	0,46265141
05.03.2021	<0.49	5,16	1,00	6,16298544	**05.03.2021**	1.5-3	1,00	0,02	1,0154712
10.03.2021	<0.49	4,85	0,38	5,23875733	**10.03.2021**	1.5-3	0,62	0,02	0,63764206
18.03.2021	<0.49	1,55	0,23	1,7862632	**18.03.2021**	1.5-3	0,17	0,01	0,21787539
12.04.2021	<0.49	2,55	0,40	2,94517635	**12.04.2021**	1.5-3	0,35	0,01	0,35904145
21.04.2021	<0.49	3,37	0,31	3,67224789	**21.04.2021**	1.5-3	0,08	0,00	0,0842698
28.04.2021	<0.49	3,83	0,43	4,26162598	**28.04.2021**	1.5-3	0,52	0,02	0,66791881
06.05.2021	<0.49	2,78	0,17	2,95002897	**06.05.2021**	1.5-3	0,35	0,02	0,42309144
12.05.2021	<0.49	5,91	0,82	6,73510238	**12.05.2021**	1.5-3	0,60	0,03	0,76207928
19.05.2021	<0.49	2,33	0,36	2,69104856	**19.05.2021**	1.5-3	0,35	0,01	0,40779501
31.05.2021	<0.49	1,42	0,38	1,80492429	**31.05.2021**	1.5-3	0,23	0,02	0,26253241

04.03.2022	<0.49	3,10	1,05	4,14889213	**04.03.2022**	1.5-3	0,54	0,03	0,56036075
10.03.2022	<0.49	2,86	0,67	3,53114096	**10.03.2022**	1.5-3	0,34	0,02	0,36395497
11.06.2021	<0.49	2,34	0,49	2,82378081	**17.06.2021**	1.5-3	0,26	0,01	0,28917257
17.06.2021	<0.49	0,94	0,25	1,19053385	**04.07.2021**	1.5-3	0,54	0,02	0,55272842
04.07.2021	<0.49	2,01	0,41	2,41307824	**27.08.2021**	1.5-3	0,66	0,02	0,73072329
27.08.2021	<0.49	5,63	0,18	5,81014127	**02.09.2021**	1.5-3	0,29	0,01	0,3476027
02.09.2021	<0.49	1,06	0,50	1,56299288	**08.09.2021**	1.5-3	0,32	0,01	0,3949924
08.09.2021	<0.49	1,83	0,51	2,34286852	**14.09.2021**	1.5-3	0,41	0,01	0,44915027
14.09.2021	<0.49	2,37	0,69	3,06921998	**21.09.2021**	1.5-3	1,11	0,02	1,1288442
21.09.2021	<0.49	1,51	0,64	2,15024704	**28.09.2021**	1.5-3	0,31	0,01	0,36753555
28.09.2021	<0.49	1,66	0,50	2,165567	**12.10.2021**	1.5-3	0,25	0,02	0,32616431
12.10.2021	<0.49	3,69	1,42	5,10965436	**27.10.2021**	1.5-3	1,05	0,02	1,06192671
27.10.2021	<0.49	5,30	1,11	6,41811208	**16.11.2021**	1.5-3	0,63	0,05	0,67840694
16.11.2021	<0.49	4,79	1,12	5,91037042	**26.11.2021**	1.5-3	0,59	0,07	0,6554551
26.11.2021	<0.49	0,98	0,57	1,55229053	**17.02.2021**	3-7.2	1,14	0,04	1,17577229
17.02.2021	0.49-0.95	6,35	0,38	6,72441766	**26.02.2021**	3-7.2	0,48	0,01	0,59757896
26.02.2021	0.49-0.95	4,34	0,02	4,36787839	**03.12.2021**	3-7.2	0,65	0,03	0,91509641
03.12.2021	0.49-0.95	1,35	0,10	1,44414751	**10.12.2021**	3-7.2	0,43	0,03	0,60496158
10.12.2021	0.49-0.95	1,61	0,15	1,7592639	**16.12.2021**	3-7.2	0,30	0,02	0,31619078
16.12.2021	0.49-0.95	1,70	0,12	1,82110005	**29.12.2021**	3-7.2	1,01	0,07	1,18167142
29.12.2021	0.49-0.95	3,30	0,31	3,61946164	**06.01.2022**	3-7.2	0,89	0,05	1,1680021
06.01.2022	0.49-0.95	3,86	0,26	4,11914199	**17.01.2022**	3-7.2	0,44	0,05	0,48138557
17.01.2022	0.49-0.95	3,25	0,37	3,61799637	**27.01.2022**	3-7.2	0,52	0,05	0,56708537
27.01.2022	0.49-0.95	26,21	8,66	34,8681313	**02.02.2022**	3-7.2	0,73	0,05	0,90177836
02.02.2022	0.49-0.95	4,32	1,00	5,32580959	**10.02.2022**	3-7.2	0,10	0,01	0,10904121

10.02.2022	0.49-0.95	0,79	0,08	0,8701536	**23.02.2022**	3-7.2	0,38	0,02	0,50791533
23.02.2022	0.49-0.95	2,46	0,15	2,61042836	**05.03.2021**	3-7.2	0,58	0,01	0,59368469
10.03.2021	0.49-0.95	3,40	0,05	3,44903173	**10.03.2021**	3-7.2	0,62	0,02	0,78226482
18.03.2021	0.49-0.95	0,88	0,01	0,88633315	**18.03.2021**	3-7.2	0,21	0,01	0,2710618
12.04.2021	0.49-0.95	1,57	0,13	1,69789781	**12.04.2021**	3-7.2	0,43	0,02	0,60328542
21.04.2021	0.49-0.95	1,32	0,02	1,34240548	**21.04.2021**	3-7.2	0,37	0,02	0,53039268
28.04.2021	0.49-0.95	1,65	0,03	1,6783443	**28.04.2021**	3-7.2	0,82	0,04	1,24821669
06.05.2021	0.49-0.95	10,82	1,06	11,8768121	**06.05.2021**	3-7.2	0,62	0,02	0,7630167
12.05.2021	0.49-0.95	1,59	0,02	1,60718056	**12.05.2021**	3-7.2	0,51	0,02	0,71752533
19.05.2021	0.49-0.95	0,82	0,02	0,83966869	**19.05.2021**	3-7.2	0,66	0,02	0,78111111
31.05.2021	0.49-0.95	0,79	0,02	0,81072514	**31.05.2021**	3-7.2	0,67	0,02	0,83940781
04.03.2022	0.49-0.95	7,65	2,19	9,83951216	**04.03.2022**	3-7.2	0,46	0,03	0,69814515
10.03.2022	0.49-0.95	1,85	0,09	1,93479945	**10.03.2022**	3-7.2	0,34	0,02	0,49585296
11.06.2021	0.49-0.95	1,11	0,02	1,13372528	**17.06.2021**	3-7.2	0,41	0,01	0,50383514
17.06.2021	0.49-0.95	0,49	0,01	0,49608172	**04.07.2021**	3-7.2	1,47	0,02	1,49834944
04.07.2021	0.49-0.95	0,88	0,03	0,91596537	**27.08.2021**	3-7.2	0,62	0,02	0,9109559
27.08.2021	0.49-0.95	3,50	0,04	3,54601558	**02.09.2021**	3-7.2	0,56	0,01	0,74234686
02.09.2021	0.49-0.95	0,52	0,02	0,53770624	**08.09.2021**	3-7.2	0,56	0,02	0,74111868
08.09.2021	0.49-0.95	0,77	0,01	0,78013561	**14.09.2021**	3-7.2	0,85	0,03	1,03995525
14.09.2021	0.49-0.95	1,18	0,02	1,19761116	**21.09.2021**	3-7.2	0,51	0,01	0,62216729
21.09.2021	0.49-0.95	0,93	0,02	0,95523084	**28.09.2021**	3-7.2	0,57	0,01	0,73780507
28.09.2021	0.49-0.95	0,86	0,01	0,8759872	**12.10.2021**	3-7.2	0,61	0,03	0,76995274
12.10.2021	0.49-0.95	1,35	0,08	1,42564248	**27.10.2021**	3-7.2	0,85	0,05	1,05239485
27.10.2021	0.49-0.95	3,11	0,16	3,27463401	**16.11.2021**	3-7.2	0,45	0,03	0,61950746
16.11.2021	0.49-0.95	2,96	0,16	3,11951149	**26.11.2021**	3-7.2	0,15	0,01	0,22244276

26.11.2021	0.49-0.95	0,53	0,06	0,59017081	**17.02.2021**	>7.2	0,38	0,03	0,41096497
17.02.2021	0.95-1.5	4,40	0,13	4,52691738	**26.02.2021**	>7.2	0,30	0,01	0,40110991
26.02.2021	0.95-1.5	2,94	0,03	2,97248445	**03.12.2021**	>7.2	0,16	0,01	0,17242524
03.12.2021	0.95-1.5	0,78	0,04	0,81575626	**10.12.2021**	>7.2	0,28	0,02	0,41680684
10.12.2021	0.95-1.5	1,02	0,08	1,10157771	**16.12.2021**	>7.2	0,09	0,01	0,09605568
16.12.2021	0.95-1.5	0,90	0,05	0,94979973	**29.12.2021**	>7.2	0,23	0,02	0,32875547
29.12.2021	0.95-1.5	1,90	0,19	2,09167509	**06.01.2022**	>7.2	0,23	0,02	0,33354041
06.01.2022	0.95-1.5	2,53	0,15	2,67863806	**17.01.2022**	>7.2	0,17	0,01	0,18456629
17.01.2022	0.95-1.5	2,34	0,20	2,54558126	**27.01.2022**	>7.2	0,17	0,02	0,19793564
27.01.2022	0.95-1.5	3,14	0,30	3,4440365	**02.02.2022**	>7.2	0,22	0,02	0,29217493
02.02.2022	0.95-1.5	3,57	0,51	4,07824763	**10.02.2022**	>7.2	0,05	0,00	0,04834798
10.02.2022	0.95-1.5	0,44	0,02	0,46398727	**23.02.2022**	>7.2	0,10	0,01	0,15445806
23.02.2022	0.95-1.5	1,49	0,07	1,55945024	**05.03.2021**	>7.2	0,24	0,02	0,3257235
05.03.2021	0.95-1.5	2,80	0,03	2,83062599	**10.03.2021**	>7.2	0,22	0,01	0,28523623
10.03.2021	0.95-1.5	1,65	0,03	1,67113898	**18.03.2021**	>7.2	0,11	0,00	0,13057188
18.03.2021	0.95-1.5	0,46	0,01	0,4712053	**12.04.2021**	>7.2	0,18	0,01	0,21957533
12.04.2021	0.95-1.5	0,94	0,03	0,96451048	**21.04.2021**	>7.2	0,24	0,01	0,26080415
21.04.2021	0.95-1.5	0,81	0,02	0,82967122	**28.04.2021**	>7.2	0,22	0,01	0,31130043
28.04.2021	0.95-1.5	0,86	0,03	0,89709863	**06.05.2021**	>7.2	0,20	0,01	0,27256945
06.05.2021	0.95-1.5	0,60	0,02	0,61420645	**12.05.2021**	>7.2	0,24	0,01	0,31802546
12.05.2021	0.95-1.5	0,82	0,02	0,84195628	**19.05.2021**	>7.2	0,19	0,01	0,24542129
19.05.2021	0.95-1.5	0,53	0,02	0,54483831	**31.05.2021**	>7.2	0,12	0,01	0,15435693
31.05.2021	0.95-1.5	0,39	0,02	0,40124229	**04.03.2022**	>7.2	0,15	0,01	0,25661752
04.03.2022	0.95-1.5	1,21	0,05	1,26505807	**10.03.2022**	>7.2	0,11	0,01	0,17382021
10.03.2022	0.95-1.5	0,82	0,03	0,84804603	**17.06.2021**	>7.2	0,07	0,00	0,0950544

11.06.2021	0.95-1.5	0,65	0,02	0,66775097	**04.07.2021**	>7.2	0,15	0,00	0,15673105
17.06.2021	0.95-1.5	0,26	0,01	0,2659376	**27.08.2021**	>7.2	0,21	0,02	0,33722492
04.07.2021	0.95-1.5	0,67	0,02	0,68422931	**02.09.2021**	>7.2	0,13	0,00	0,16775806
27.08.2021	0.95-1.5	0,13	0,00	0,13533	**08.09.2021**	>7.2	0,15	0,01	0,20190011
02.09.2021	0.95-1.5	0,29	0,02	0,30955868	**14.09.2021**	>7.2	0,23	0,01	0,31224698
08.09.2021	0.95-1.5	0,39	0,02	0,40719593	**21.09.2021**	>7.2	0,10	0,00	0,13418785
14.09.2021	0.95-1.5	0,59	0,02	0,60780956	**28.09.2021**	>7.2	0,16	0,01	0,21184603
21.09.2021	0.95-1.5	0,49	0,02	0,51135429	**12.10.2021**	>7.2	0,29	0,02	0,44091524
28.09.2021	0.95-1.5	0,46	0,01	0,46599588	**27.10.2021**	>7.2	0,44	0,04	0,65107335
12.10.2021	0.95-1.5	0,63	0,04	0,67777528	**16.11.2021**	>7.2	0,28	0,02	0,48871169
27.10.2021	0.95-1.5	2,03	0,11	2,14489126	**26.11.2021**	>7.2	0,06	0,00	0,066548
16.11.2021	0.95-1.5	2,37	0,16	2,52254507					
26.11.2021	0.95-1.5	0,05	0,00	0,05347884					

Table 3.3 OC, EC, TC fractionated concentrations data

Date	**Fraction**	**CC (µg/m^3)**	**Date**	**Fraction**	**CC (µg/m^3)**	**Date**	**Fraction**	**CC (µg/m^3)**
17.02.2021	1.5-3	0	**26.02.2021**	3-7.2	0,104163215	**17.02.2021**	>7.2	0
26.02.2021	1.5-3	0	**05.03.2021**	3-7.2	0	**26.02.2021**	>7.2	0,10274465
05.03.2021	1.5-3	0	**10.03.2021**	3-7.2	0,143614751	**05.03.2021**	>7.2	0,071496874
10.03.2021	1.5-3	0	**18.03.2021**	3-7.2	0,062140391	**10.03.2021**	>7.2	0,041835601
18.03.2021	1.5-3	0,032510536	**12.04.2021**	3-7.2	0,032616893	**18.03.2021**	>7.2	0,024485783
12.04.2021	1.5-3	0	**21.04.2021**	3-7.2	0,146209095	**12.04.2021**	>7.2	0,041700078
21.04.2021	1.5-3	0	**28.04.2021**	3-7.2	0,412120895	**21.04.2021**	>7.2	0,017426084
28.04.2021	1.5-3	0,132716898	**06.05.2021**	3-7.2	0,14012878	**28.04.2021**	>7.2	0,092989143
06.05.2021	1.5-3	0,060613844	**12.05.2021**	3-7.2	0,203233511	**06.05.2021**	>7.2	0,070607525
12.05.2021	1.5-3	0,123660602	**19.05.2021**	3-7.2	0,116862682	**12.05.2021**	>7.2	0,076777104
19.05.2021	1.5-3	0,052762629	**31.05.2021**	3-7.2	0,14515319	**19.05.2021**	>7.2	0,058213314
31.05.2021	1.5-3	0,021926464	**11.06.2021**	3-7.2	0	**31.05.2021**	>7.2	0,035082342
11.06.2021	1.5-3	0	**17.06.2021**	3-7.2	0,091015787	**11.06.2021**	>7.2	0
17.06.2021	1.5-3	0,025294174	**04.07.2021**	3-7.2	0	**17.06.2021**	>7.2	0,020970383
04.07.2021	1.5-3	0	**27.08.2021**	3-7.2	0,274828152	**04.07.2021**	>7.2	0
27.08.2021	1.5-3	0,04461496	**02.09.2021**	3-7.2	0,182089686	**27.08.2021**	>7.2	0,110868175
02.09.2021	1.5-3	0,047483224	**08.09.2021**	3-7.2	0,173313822	**02.09.2021**	>7.2	0,042183757
08.09.2021	1.5-3	0,060585952	**14.09.2021**	3-7.2	0,183962808	**08.09.2021**	>7.2	0,054675128

14.09.2021	1.5-3	0,040075328	**21.09.2021**	3-7.2	0,107336936	**14.09.2021**	>7.2	0,080363822
21.09.2021	1.5-3	0	**28.09.2021**	3-7.2	0,163390448	**21.09.2021**	>7.2	0,03006281
28.09.2021	1.5-3	0,051801463	**12.10.2021**	3-7.2	0,159886321	**28.09.2021**	>7.2	0,053744018
12.10.2021	1.5-3	0,063911778	**27.10.2021**	3-7.2	0,189135838	**12.10.2021**	>7.2	0,141503669
27.10.2021	1.5-3	0	**16.11.2021**	3-7.2	0,155957669	**27.10.2021**	>7.2	0,191861743
16.11.2021	1.5-3	0	**26.11.2021**	3-7.2	0,067433064	**16.11.2021**	>7.2	0,191901818
26.11.2021	1.5-3	0	**03.12.2021**	3-7.2	0,245101414	**26.11.2021**	>7.2	0
03.12.2021	1.5-3	0	**10.12.2021**	3-7.2	0,173524045	**03.12.2021**	>7.2	0
10.12.2021	1.5-3	0	**16.12.2021**	3-7.2	0	**10.12.2021**	>7.2	0,126107591
16.12.2021	1.5-3	0	**29.12.2021**	3-7.2	0,148522186	**16.12.2021**	>7.2	0
29.12.2021	1.5-3	0	**06.01.2022**	3-7.2	0,255851519	**29.12.2021**	>7.2	0,08528181
06.01.2022	1.5-3	0	**17.01.2022**	3-7.2	0	**06.01.2022**	>7.2	0,0904463
17.01.2022	1.5-3	0	**27.01.2022**	3-7.2	0	**17.01.2022**	>7.2	0
27.01.2022	1.5-3	0	**02.02.2022**	3-7.2	0,154489262	**27.01.2022**	>7.2	0
02.02.2022	1.5-3	0	**10.02.2022**	3-7.2	0	**02.02.2022**	>7.2	0,056611501
10.02.2022	1.5-3	0	**23.02.2022**	3-7.2	0,116827224	**10.02.2022**	>7.2	0
23.02.2022	1.5-3	0	**04.03.2022**	3-7.2	0,221578729	**23.02.2022**	>7.2	0,046606605
04.03.2022	1.5-3	0	**10.03.2022**	3-7.2	0,150157145	**04.03.2022**	>7.2	0,094125513
10.03.2022	1.5-3	0				**10.03.2022**	>7.2	0,059202476